LANDSAT-4 Science Investigations Summary

Including December 1983 Workshop Results

Volume II

REFERENCE

NOT TO BE TAKEN FROM THIS ROOM

NASA

LANDSAT-4 Science
Investigations Summary

Including December 1983
Workshop Results

Volume II

John Barker, *Editor*
NASA Goddard Space Flight Center

Proceedings of the Landsat-4 Early
Results Symposium, February 22-24, 1983,
and the Landsat Science Characterization
Workshop, December 6, 1983, and held at
NASA Goddard Space Flight Center
Greenbelt, Maryland

Page intentionally left blank

The Landsat Science Office at Goddard Space Flight Center
(GSFC) is charged with the responsibility of characterizing the
quality of Landsat-4 image data and, through data analysis, the
performance of the Landsat system. It has enlisted the participa-
tion of recognized and experienced members of the Landsat community
(private, acadmic and government, U.S. and International) in in-
vestigating various aspects of this multifaceted topic. The Landsat
Science Investigations Program provides the framework within which
the individual investigations are taking place. One feature of the
Program is to provide in-progress exchange of observations and
findings among individual investigators, especially through an
ongoing series of Investigations Workshops. Release of information
resulting from the investigations is via public symposia. The
Landsat-4 Early Results Symposium (so named since most investigators
had had access to Landsat data for only a brief period) was held
on February 22-24, 1983. A second public symposium is planned for
late 1984.

The present document is the first to be published con-
taining collected results of the Investigations Program. It was
originally intended as an Executive Summary companion volume to
the Proceedings of the Landsat-4 Early Results Symposium, presenting
abstracts of papers included in the proceedings. However, since
publication has been delayed, it was decided that this summary
volume should encompass results reached during post-symposium
investigations wherever possible. Thus, results summarized herein
range in date reported from February 22, 1983 (in a few cases) to
December 6, 1983 (in most cases) on which date was held the most
recent Investigations Workshop.

This document is arranged to follow the organization of
the Early Results Symposium. It includes introductory papers
(Landsat program and system descriptions) in their entirety
followed by summaries of results of each individual investigation
in the order in which they were reported at the symposium (even
though most contain more recent data). The symposium proceedings,

to be published in the near future, will contain investigations papers in this same order.

The papers delivered at the symposium were divided into three major sessions: one on Multispectral Scanner (MSS) Investigations, one on Thematic Mapper (TM) Investigations and one on Applications Investigations. The MSS and TM sessions progressed topically from radiometry to geometry; the Applications session progressed through the various disciplines of application. Although the focus of some investigations shifted from one topic to another during the period since the symposium, the summaries of results of such investigations are, nonetheless, retained in the original presentation order in these summary volumes.

LANDSAT-4 INVESTIGATION SUMMARY
VOLUME I

LANDSAT-4 INVESTIGATION SUMMARY
VOLUME II

LANDSAT-4 MSS AND TM SPECTRAL CLASS COMPARISON AND COHERENT NOISE ANALYSIS

P. ANUTA, L. BARTOLUCCI, E. DEAN, F. LOZANO
E. MALARET, C. MCGILLEM, J. VALDES, AND C. VALENZUELA
PURDUE UNIVERSITY

SUMMARY

Landsat-4 MSS and TM data quality and information content were
evaluated and reported previously[1]. These results included geometric,
radiometric, and dimensionality evaluations. Recent results have been
obtained which evaluate the separability of spectral classes in TM and MSS
data and analyze coherent noise in the data. These results are summarized
here.

A detailed spectral analysis was conducted of thematic mapper and MSS
data for an area near Des Moines, Iowa from the September 3, 1982 data set.
Data were utilized from 7 blocks distributed throughout the area which
included agricultural, forest, suburban, urban, and water scene types. The
blocks were processed using a clustering algorithm to produce up to 18 cluster
groupings for each block. Each cluster class was then identified with a
ground-cover class using aerial photography and maps of the area. The
clusters from each of the 7 blocks were inspected with regard to separability,
means, and variances and were either deleted or pooled with spectrally similar
clusters. The separability measure used in the transformed divergence
function or processor [2] measures the statistical distance between classes
based on class means and covariance matrices. The measure has a maximum value
of 2,000 and the minimum of 0. Spectrally, very close classes will typically
have values as low as 50 to 500.

TABLE 1

SPECTRALLY SEPARABLE CLASSES IN TM AND MSS DATA
OF DES MOINES, IOWA AREA

CLASS NUMBER	TM CLASS NAME	EXISTS IN MSS	CLASS NAME	TM CLASS NAME	EXISTS IN MSS
1	Forest1	x	22	Substation	
2	Forest2	x	23	Quarry	
3	Corn1	x	24	Concrete	x
4	Corn2		25	Sludge	x
5	Soy1	x	26	Industrial1	
6	Soy2	x	27	Industrial2	
7	Soy3	x	28	Urban/Hiway	x
8	Soy4	x	29	Soil/Hiway	
9	Soy5	x	30	Residential1	x
10	Soy6	x	31	Residential2	x
11	Wheat Residue	x	32	Beach1	
12	Grass1	x	33	Beach2	
13	Grass2		34	Beach3	
14	Grass3		35	Soilwet1	
15	Soil/Veg1		36	Soilwet2	
16	Soil/Veg2		37	Marsh	
17	Soil/Veg3		38	Water1	x
18	Farm/Grass		39	Water2	x
19	Road/Farm		40	Water3	x
20	Baresoil1	x	41	Water4	x
21	Baresoil2		42	Water5	

TABLE 2

SEPARABILITY (TRANSFORMED DIVERGENCE) FOR 42 CLASSES
IN THEMATIC MAPPER DATA

CHANNEL COM-BINATIONS	DIVERGENCE		BEST CHANNELS*
	MIN.	AVE.	
1	1	1574	5
2	210	1880	4 5
3	522	1949	3 4 5
4	1090	1973	3 4 5 7
5	1356	1979	3 4 5 6 7
6	1405	1983	2 3 4 5 6 7
7	1553	1986	1 2 3 4 5 6 7

For the TM data, initial 94 classes were defined and the pooling and deleting process reduced these to 42 final spectrally separable classes. Table 1 lists these classes. The MSS data were then analyzed using the same clustering and merging sequence. The number of separable classes in the MSS is 21, half of the TM result. This result is considered to be a very significant indicator of the dimensionality of TM relative to MSS. The MSS class occurrences are indicated in Table 1. The minimum divergence values of any one class with respect to all others also were much less for the MSS classes relative to TM. Table 2 contains the minimum and average transformed divergence values for the 42 spectral classes and for the best subsets of TM spectral bands. It should be noted that the best spectral band for any combination of Bands 1 through 7 is the first middle IR band (1.55-1.75μm). The next best band is the near IR (0.76-0.90μm), followed by the red band and then the thermal IR. The best combination of four bands includes one from each of the four regions of the spectrum (visible, near IR, middle IR, and thermal IR). Table 3 contains the minimum and average transformed divergence values for the best combination of MSS bands.

---

* Channel 6 is the second middle IR band and Channel 7 is the thermal IR band.

TABLE 3

SEPARABILITY FOR 21 CLASSES IN MSS DATA

| CHANNEL | DIVERGENCE | |
COMBINATIONS	MINIMUM	AVERAGE
3	32	1842
2 3	730	1957
2 3 4	1032	1968
1 2 3 4	1112	1973

The high average divergence indicates that the 21 spectral classes found in the MSS were about as separable as the TM classes. However, there was twice the number of equally separable TM classes. This is considered to be the most significant result of the spectral analysis.

A final test was carried out in the comparison using the small amount of ground truth available. A set of 5,615 TM and 1,376 MSS pixels containing forest, corn, soybean, soil, water, and urban classes was extracted from the TM and MSS data where the cover classes were known or could be inferred from aerial photography. The overall correct recognition for the seven-band TM classification was 95.7% and 67.4% for the MSS. The results are listed in Table 4. A TM classification was run using four TM bands (2,4,5,7)** as determined from the separability analysis and the overall result was 92.6%. The four-band classification takes only one-third the computer time as for seven bands. The result is included in Table 4 and it can be seen that the corn class is the one most affected by the reduction in bands.

The "test" fields are limited in number of pixels and so are not really evaluating how representative the final spectral classes are of the

---

**This combination was used rather than 3,4,5,7 as it had a higher minimum divergence with only a slight reduction in the average.

entire scene but rather how separable the classes are. Deletion of certain spectral classes (e.g., Corn2), due to low separability, resulted in much confusion of corn with trees in the MSS but not the TM. Also, the resolution of TM actually allowed "purer" cluster classes to be defined since smaller areas (e.g., beaches, roads) were distinct.

TABLE 4

CLASSIFICATION ACCURACY FOR TEST DATA IN
THE DES MOINES, IOWA AREA
SCENE ID: 40049-16264

CLASS	TM PER POINT CLASSIFIER (ALL 7 BANDS) %CORRECT	TM PER POINT CLASSIFIER (BEST 4 BANDS) %CORRECT	MSS PER POINT CLASSIFIER (ALL 4 BANDS) %CORRECT
Forest	99.0	97.1	91.2
Corn	92.0	76.8	30.8
Soybeans	100.0	99.8	99.3
Bare Soil	99.7	99.0	55.6
Grass	96.8	87.6	1.9
Water	100.0	96.8	98.9
Urban	91.7	99.9	50.2
Overall	95.7	92.6	67.4

MSS and TM data were analyzed for the presence of any coherent noise sources which could potentially affect data utility. The MSS data visually demonstrated significant wavelike noise patterns in low level imagery, such as Lake Michigan. The period of these signals is nominally 15 pixels with a higher frequency component in the 3-pixel range. Fourier analysis revealed several coherent peaks and substantiated the visually-determined results. The TM data did not visually suggest similar noise. However, Fourier spectral analysis revealed two coherent peaks at wavelengths of 3.12 and 17 pixels. These frequencies are similar to the ones found in the MSS. The amplitude of the noise is very low having a standard deviation of .6 digital count, so it should not significantly affect numberical classification of visual analysis. The cause of the noise signals in the MSS and TM is not known. These results further verify the high quality and increased utility of the TM data and promise significant increase in the usefulness of these data in earth resources applications.

REFERENCES

1.   Bartolucci, L.A., M.E. Dean, P.E. Anuta, "Evaluation of the Radiometric Quality of the TM Using Clustering and Multispectral Distance Measures," Proc. Landsat-4 Scientific Characterization Early Results Symposium, NASA Goddard Space Flight Center, Greenbelt, MD, Feb. 22-24, 1983. To be published.

2.   Swain, P.H., T. V. Robertson, A. G. Wacker, "Comparison of the Divergence and B-Distance in Feature Selection", LARS/Purdue University. LARS Information Note 020871, 1971.

TM FAILED DETECTORS DATA REPLACEMENT

L. FUSCO, D. TREVESE
EUROPEAN SPACE AGENCY/EPO

As known, some of the Landsat-4 Thematic Mapper detectors (band 2 detector 4 and band 5 detector 3) have inadequate performances. The operational system correction processing will disregard the data sensed by the failed detectors and replace them by data coming from the neighbour detectors of the same spectral band.

Some studies have already been carried out by Bernstein et al. [1] in algorithms to compensate for the failed detectors. The present paper describes the analysis performed by ESA-Earthnet and attempts to suggest an operational failed detector replacement algorithm.

The following considerations were applied in the study definition:

- the algorithm to replace a failed detector pixel should use, at the maximum, the 3 x 3 neighbour pixels in not more than 2 spectral bands

- the algorithm performance should be assessed not only by visual inspection of specific ground features, but also using objective and quantitative measurements on the reconstructed pixels.

- simple fast processing algorithms should be proposed. Intuitively, linear regression expressions are adequate to estimate a missing element in the 3 x 3 pixel domain, i.e., the probability that more than two clusters are present in any 3 x 3 pixel domain is negligible.

Two subscenes were selected for the present investigation; they were extracted from track 23, frame 33, acquired on 22.08.82 (Arkansas) and track 191, frame 31, acquired at Fucino on 23.01.83 (Rome, Italy).

To properly analyze the chosen candidates algorithms, each processing consisted in generating a synthetic image where each pixel was computed by applying the algorithms described below to all original good pixels.

Each synthetic image was compared with the original image and the following objective quality measurements were extracted:

- correlation coefficient between the original and synthetic images
- rms value (E) of the difference image
- histogram of the difference image
- two-dimensional spread function between the original and synthetic images

The following algorithms were considered:

A1 : <u>Neighbour line replacement</u> : the generic pixel in the band d with failed detector i are replaced by previous detector i-1 :

$$(1) \qquad d_i = d_{i-1}$$

In this case the synthetic image corresponds to the original image shifted by one line.

A2 : <u>Adjacent line interpolation</u> : expressed by,

$$(2) \qquad d_i = \frac{d_{i+1} + d_{i-1}}{2}$$

A3 : Reconstruction with two bands image data and fixed parameters :
expressed by,

$$(3) \quad d_i = M \left(c_i - \frac{c_{i+1} + c_{i-1}}{2} \right) + \frac{d_{i+1} + d_{i-1}}{2}$$

where c indicates the co-located generic pixel radiance in a second (not necessary highly correlated) band and M is a fixed parameter. The case with M $= \sigma_d / \sigma_c$, i.e. defined by the ratio of the two standard deviations, is reported in (1). Note that if (3) is written as :

$$(3') \quad d_i = M (c_i - \mu_c) + \mu_d$$

where μ_c and μ_d are the full scene means for the two bands, then :

$$(3'') \quad M = \rho_{ac} \, \sigma_d / \sigma_c$$

with ρ_{dc} being the correlation coefficient, will minimize the rms value in the full scene difference image.

A4 : Reconstruction with two bands image data and local determined parameters : expressed by,

$$(4) \quad d_i = m (c_i - \mu_c) + \mu_d$$

where μ_c and μ_d are the means and M is the slope of the linear repression for d over c estimated in a local neighbour of d_i and c_i. Typically, the neighbourhood is chosen, being the six nearest (3 above, 3 below) pixels to d_i and c_i.

In the case for which the slop M in (4) diverges (the local variance in c is close to 0), M is computed by 3". Note that the most expensive element to compute in (4) is M. If a threshold is defined for the local variance of c under which M = M (e.g., is computed by 3") then the computing effort may be limited. This threshold is a function of the chosen band c.

The overall results show that :

- the change from algorithm A1 to A2 improves the rms error substantially. However the visual inspection of local structures show some important distortions.

- both algorithms A3 and A4 have a good performance in maintaining local structures and with a proper setting of parameters have better rms errors than A1 and A2. Visually no major differences may be assessed between A3 and A4.

Some detailed results are shown in the following:

Figure 1, 2 illustrate the histogram of the difference (synthetic - original) images and Figure 3, 4 illustrate the spread function of synthetic versus original images for the processing of Band 5 using algorithm A1 and A4 (in this case, band 7 was chosen as the second correlated band). To compare algorithm A3 and A4 an heuristic approach was taken in the sense that different synthetic images were generated forging different values for the M in (3) and (4). An example of the comparison is shown in Figure 5. The abscissa indicates the value of M scaled by the full scene $\sigma d/\sigma c$.

The ordinate indicates the rms error of the synthetic-original image and the correlation coefficient between the two images for algorithm A3 and A4. For algorithm A4 the threshold on the local variance was set by $c_{i-1} = c_{i+1}$.

The following remarks apply :

- the algorithm A4 has always a smaller rms error and a higher correlation coefficient than A3. We have also achieved this result in cases of poorly correlated bands (i.e., 5 and 3), and different types of ground structures.

10

-   the value $\rho d c \sigma d / \sigma c$ instead of $\sigma d / \sigma c$ for M in all cases shows an improvement in the error measurements, but does not always correspond to the optimal slope.

-   varying M, algorithm A4 is more stable than A3 as it uses M only for a fraction of the total number of pixels; therefore the choice of M is less critical.

We are considering using this algorithm in the TM EPO operational system correction processing and we are now investigating the computing performances.

References :   R. Bernstein, J. Lotspiech: Analysis and evaluation of the Landsat-4 MSS and TM sensors and Ground Data Processing System. Early Results.
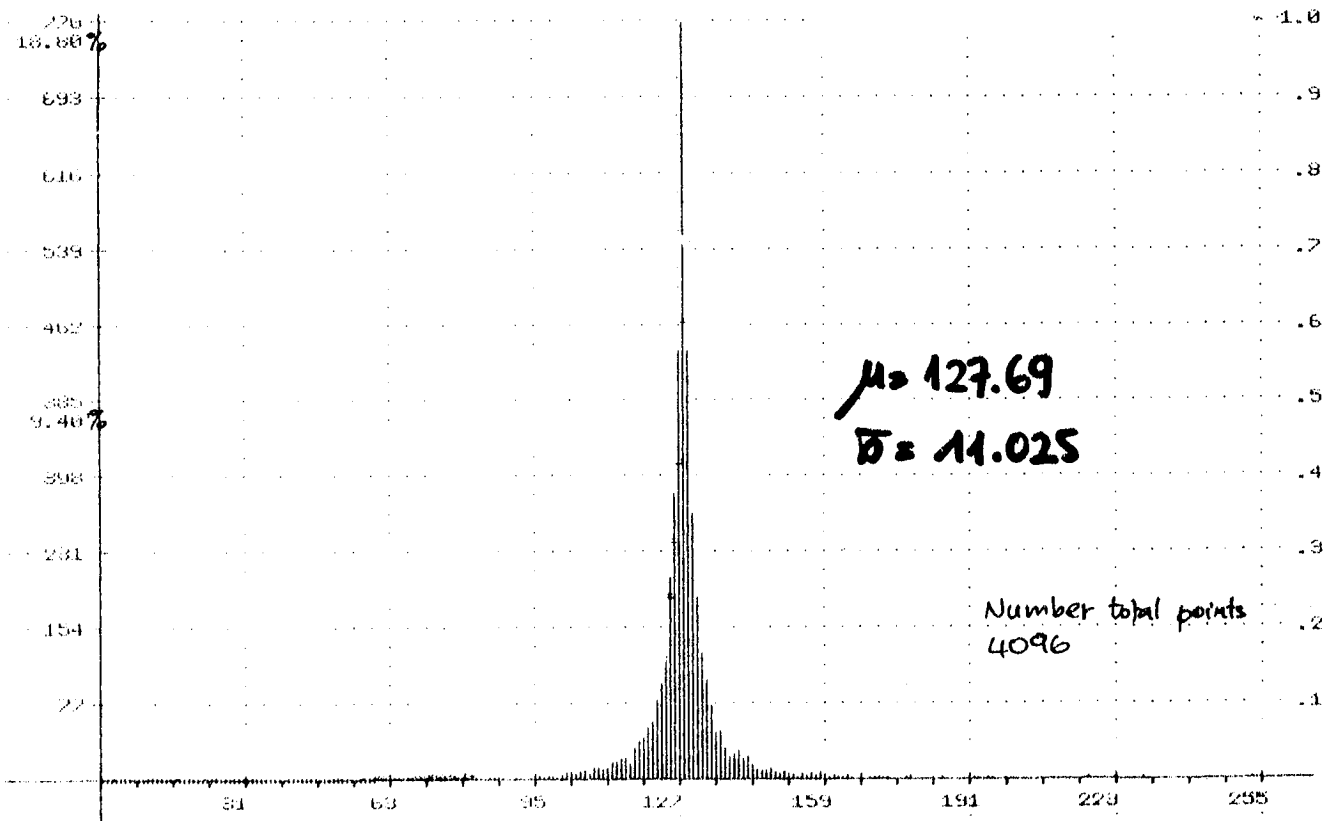
FIGURE 1. HISTOGRAM OF DIFFERENCE IMAGE (SYNTETIC-ORIGINAL)+128 PROCESSED
WITH ALGORITHM A1. BAND 5 ARKANSAS - 22.08.82

$\mu = 127.69$
$\sigma = 11.025$

Number total points
4096
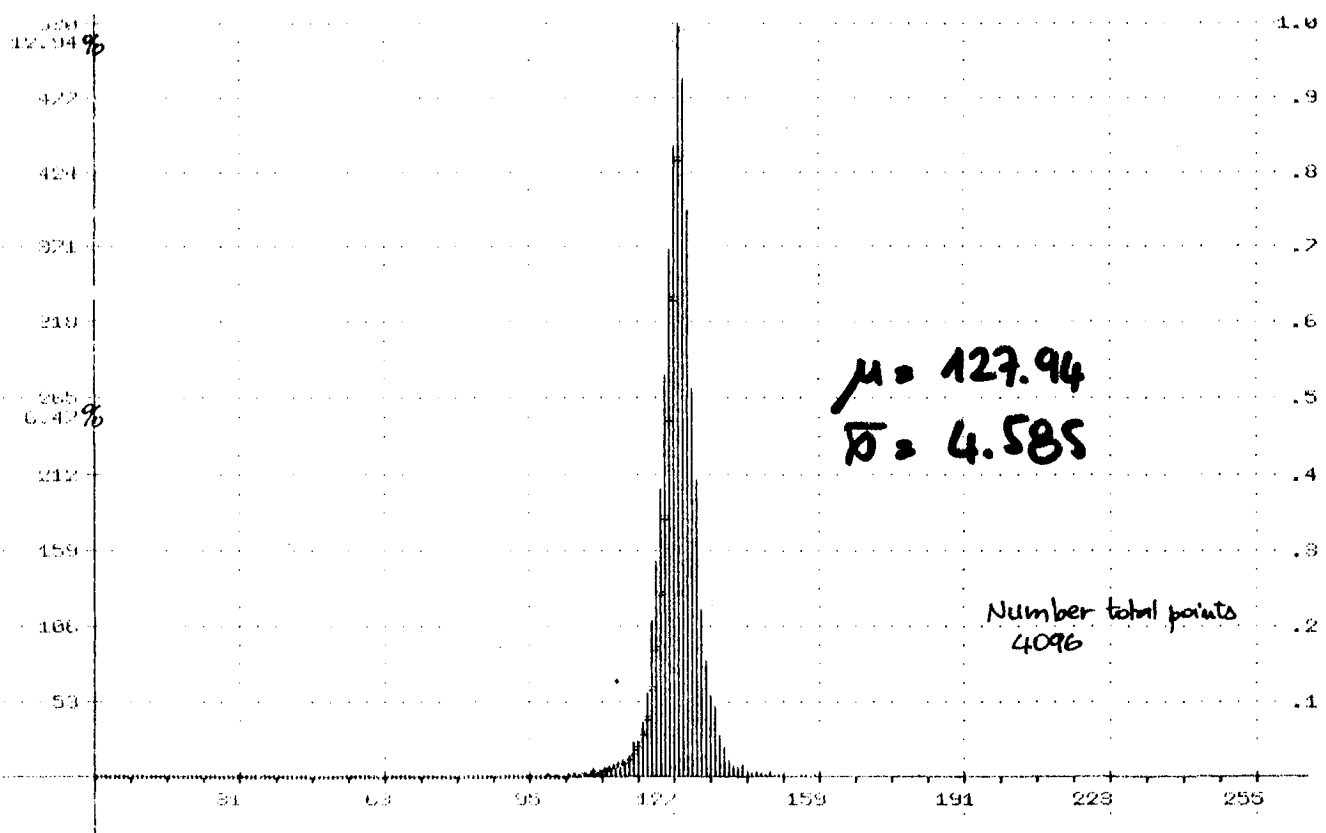
FIGURE 2. HISTOGRAM OF DIFFERENCE IMAGE (SYNTETIC-ORIGINAL)+128 PROCESSED
WITH ALGORITHM A4. BAND 5 ARKANSAS - 22.08.82

$\mu = 127.94$
$\sigma = 4.585$

Number total points
4096

12
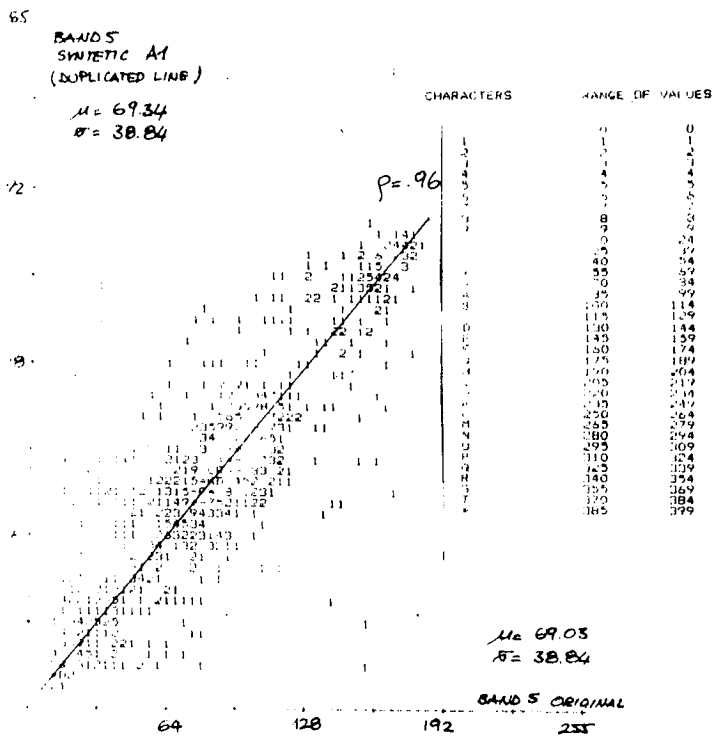
FIGURE 3. SPREAD FUNCTION OF ORIGINAL VS. SYNTHETIC IMAGE
GENERATED WITH ALGORITHM A1. BAND 5 ARKANSAS - 22.08.82.
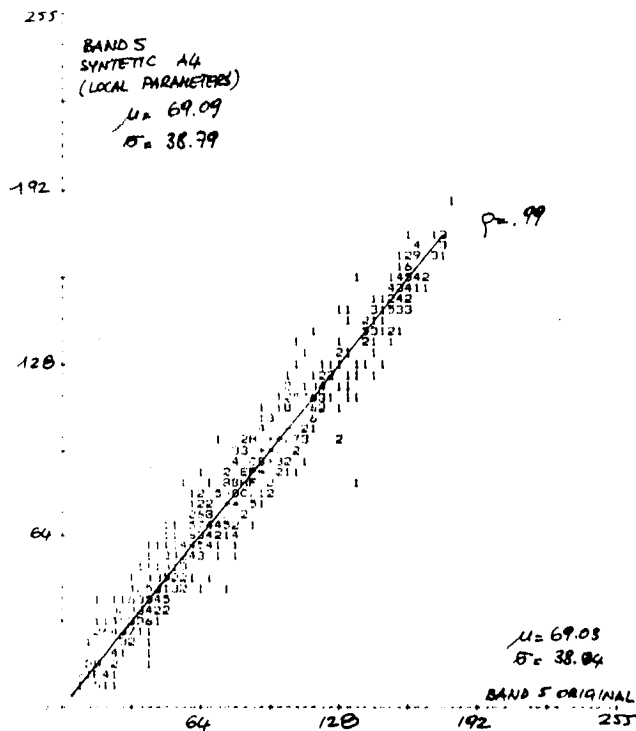
FIGURE 4. SPREAD FUNCTION OF ORIGINAL VS. SYNTHETIC IMAGE
GENERATED WITH ALGORITHM A4. BAND 5 ARKANSAS - 22.08.82

13
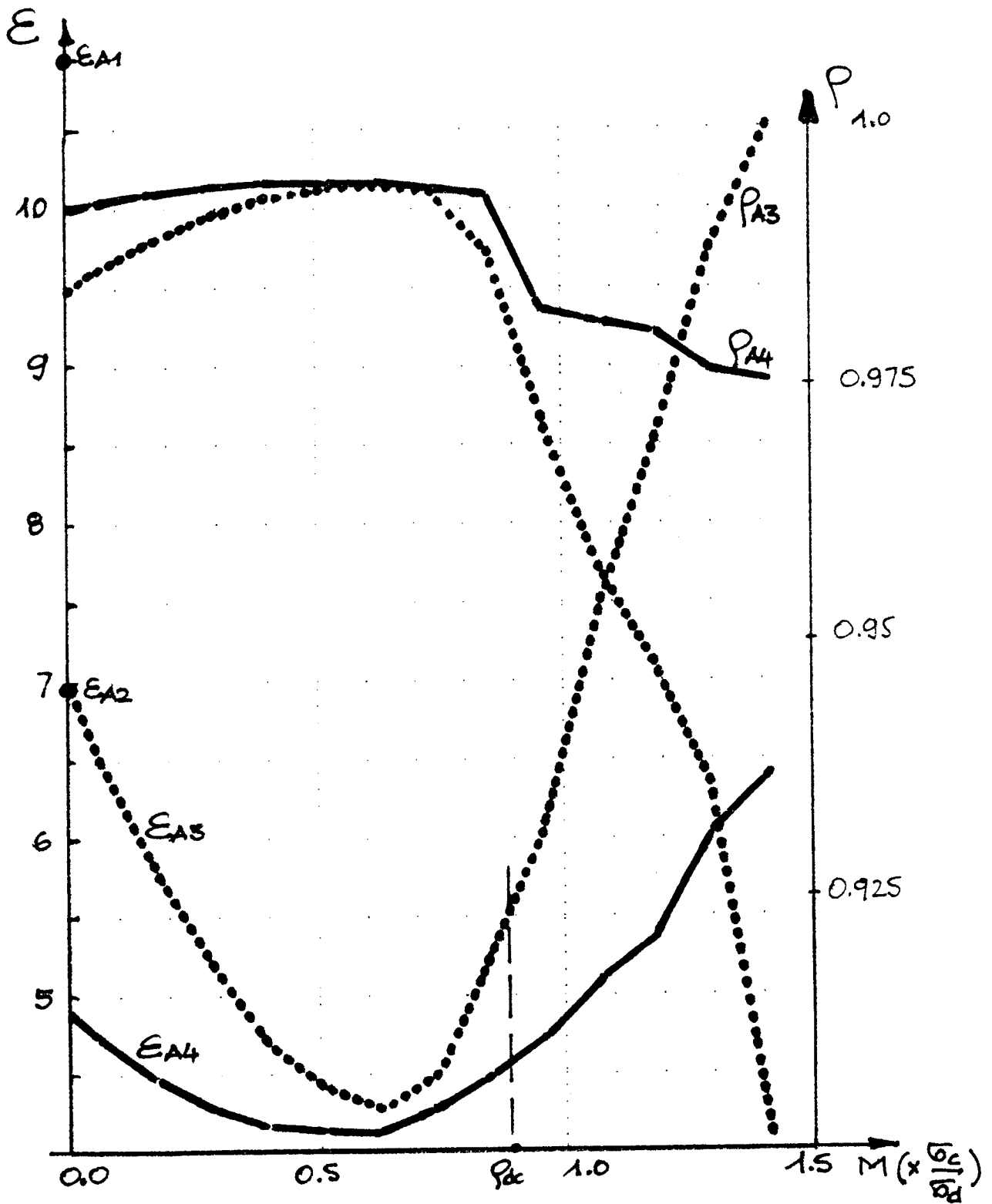
FIGURE 5. PERFORMANCE COMPARISON BETWEEN

A 3 AND A4 ALGORITHMS

$\mathcal{E}$ IS THE RMS OF (SYNTHETIC-ORIGINAL) IMAGE,

ρ IS THE CORRELATION COEFFICIENT, VARYING THE SLOPE

M. FOR THE SAME DATA SET

$\mathcal{E}_{A1} = 11.02$ AND $\mathcal{E}_{A2} = 6.9$.

IN-FLIGHT ABSOLUTE RADIOMETRIC CALIBRATION OF THE
THEMATIC MAPPER

K. R. CASTLE, R. G. HOLM, C. J. KASTNER, J. M. PALMER AND
P. N. SLATER
UNIVERSITY OF ARIZONA

M. DINGUIRARD
CENTRE D'ETUDES ET DE RECHERCHES DE TOULOUSE

C. E. EZRA AND R. D. JACKSON
U. S. DEPARTMENT OF AGRICULTURE

R. K. SAVAGE
ATMOSPHERIC SCIENCES LABORATORY

The Thematic Mapper (TM) multispectral scanner system was placed into earth orbit on July 16, 1982, as part of NASA's Landsat-4 payload. The entire system had been calibrated in an absolute sense at Santa Barbara Research Center before launch. During flight, an internal calibration system monitors the calibration of the focal plane. To determine temporal changes of the absolute radiometric calibration of the entire system in flight, we initiated a program at White Sands, New Mexico, on January 3, 1983, to make spectroradiometric measurements of the ground and the atmosphere simultaneously with TM image acquisitions over that area. By entering our measured values into an atmospheric radiative transfer program, we determined the radiance levels at the entrance pupil of the TM in four of the TM spectral bands (full width at half maximum: band 1, 0.45-0.52µm; band 2, 0.53-0.61µm; band 3, 0.62-0.69µm; and band 4, 0.78-0.91µm). These levels were compared to the output digital counts from the detectors that sampled the radiometrically measured ground area, thus providing an absolute radiometric calibration of the entire TM system utilizing those detectors. Then, by reference to an adjacent, larger uniform area, the calibration was extended to all 16 detectors in each of the three bands.

On January 3, 1983, an 80-mm layer of two-day-old snow covered the flat gypsum surface at the White Sands Missile Range. The reflectance of the snow was measured by reference to a 1.2 x 1.2-m barium sulfate panel using a Barnes Modular Multispectral 8-Channel Radiometer (Model 12-1000), which collected radiant flux simultaneously in all the TM spectral bands over a total field angle of 15°. The instrument was mounted on a rotatable boom 2.5 m above the snow to allow an average radiance value to be determined for an area of about 0.5 x 5 m. The measurements were made at 1708 GMT, coinciding with the overpass of the TM. The solar zenith angle was 62.8°. With the radiance of the barium sulfate panel at 62.8° as a reference, the reflectance of the snow in TM bands 1 to 4 was found to be 0.769, 0.761, 0.756 and 0.732 respectively, with an rms uncertainty of ± 0.02 in all cases.

Using the ground reflectance data and optical depth data, determined using a solar radiometer, as input to an atmospheric radiative transfer program, the following quantities were calculated. Their values are listed in Table 1.

$E_{D,Dir}$: The downward direct solar irradiance at the ground is $E_0 \cos\theta_z \exp(-\tau'_{ext} \sec\theta_z)$ where E_0 is the exoatmospheric solar irradiance and θ_z is the solar zenith angle

$E_{D,Dif}$: The downward diffuse solar irradiance at the ground

$L_{U,Dir}$: The upward direct radiance at the TM due to $E_{D,Dir}$ and $E_{D,Dif}$

$L_{U,P}$: The upward path radiance at the TM is

$$L_T - (E_{D,Dir} + E_{D,Dif}) \frac{\rho}{\pi} \exp(-\tau'_{ext} \sec 5^\circ)$$

L_T: The total radiance at the TM at a 5° nadir angle.

TABLE 1. IRRADIANCES AND RADIANCES (NORMALIZED TO UNITY SOLAR EXOATMOSPHERIC IRRADIANCE).

BAND	SOLAR ZENITH ANGLE	$\dfrac{E_{D,Dir}}{E_0}$	$\dfrac{E_{D,Dif}}{E_0}$	$\dfrac{L_{U,Dir}}{E_0}$	$\dfrac{L_{U,P}}{E_0}$	$\dfrac{L_T}{E_0}$
1	55°	0.345	0.185	0.097	0.033	0.130
	65°	0.212	0.152	0.067	0.025	0.092
2	55°	0.392	0.145	0.105	0.024	0.129
	65°	0.253	0.122	0.073	0.019	0.092
3	55°	0.425	0.122	0.111	0.019	0.130
	65°	0.282	0.104	0.078	0.015	0.093
4	55°	0.454	0.095	0.112	0.014	0.126
	65°	0.308	0.082	0.079	0.011	0.090

Further calculations allowed the values in Table 2 to be determined.

TABLE 2. EXOATMOSPHERIC IRRADIANCES AND THE RADIANCES AT THE TM IN THE TM PASSBANDS AS DETERMINED FROM SITE MEASUREMENTS AT WHITE SANDS.

BAND	EQUIVALENT TM BANDWIDTH in μm	WAVELENGTH LIMITS IN μm	$E_\bullet$ in $mWcm^{-2}$	L_T in $mWcm^{-2}sr^{-1}$
1	0.0715	0.4503-0.5218	14.4	1.45
2	0.0887	0.5269-0.6156	16.6	1.66
3	0.0771	0.6213-0.6984	12.3	1.25
4	0.1349	0.7719-0.9068	14.7	1.44

We next describe how we determined corresponding sets of L_T values from pre-flight and in-flight internal calibration data. By identifying our site on the raw image data, we determined which detectors scanned the area and in what order, and how many samples each collected. The site was scanned from north to south by detector numbers 3, 2, 1, 16 and 15, in that order. They collected 1, 3, 5, 4 and 2 samples respectively. We found the average digital count for each detector, using offset and gain values reported by Barker et al., then calculated the average spectral radiance, L_T, from L_T = (average count-offset)/gain. (Throughout this paper, spectral radiances are referred to the entrance pupil). These spectral radiances were multiplied by the number of samples for each detector. The resultant products were added and then divided by the total number of samples, 15. Thus we derived a value for the average spectral radiance of our site as measured by the TM, proportionally weighted according to the number of samples per detector. These values are listed in Table 3.

TABLE 3. AVERAGE COUNTS AND SPECTRAL RADIANCES (in $mWcm^{-2}sr^{-1}$ $μm^{-1}$) FOR FIVE DETECTORS IN TM BANDS 2, 3 AND 4 AS CALCULATED FROM PRE-FLIGHT CALIBRATION DATA.

DETECTOR	BAND 2 AVERAGE COUNT	BAND 2 AVERAGE SPECTRAL RADIANCE	BAND 3 AVERAGE COUNT	BAND 3 AVERAGE SPECTRAL RADIANCE	BAND 4 AVERAGE COUNT	BAND 4 AVERAGE SPECTRAL RADIANCE
3	139.0	17.04	165.0	15.40	133.0	11.89
2	143.7	17.42	169.7	15.86	132.0	12.02
1	146.2	17.52	171.6	15.73	134.2	12.00
16	141.5	17.43	167.8	15.85	132.0	12.01
15	147.5	17.65	172.5	15.88	131.5	12.05
WEIGHTED AVERAGE		17.46		15.78		12.01

Then the average spectral radiance per band was multiplied by the equivalent bandwidth to provide the weighted average radiance in each band. (These values are listed in column B of Table 4.)

Barker et al. have reported that the TM internal calibrator, used in flight, indicates that the response of TM bands 1 through 4 has slowly decreased with time during the period July-December 1982. We have used the Barker et al. data to change the pre-launch calibration data. The changed values are listed in column C of Table 4. With respect to this decrease in response, we note, first, that the internal calibrator compares the response of only the TM filters, detectors, and electronics to seven different irradiance levels; it does not measure any change in transmittance of the image-forming system. Second, it is possible that the decrease in response is wholly or partly due to a change in the output of the internal calibrator.

Table 4 summarizes our results based on measurements at White Sands and compares them to pre-flight calibration and in-flight calibration data from the TM internal calibrator. The estimated uncertainty in our results is 5%; the estimated uncertainty in the pre-flight calibration is no better than 6%.

TABLE 4. COMPARISON OF RADIANCES ($mWcm^{-2}sr^{-1}$) IN TM BANDS 2, 3 AND 4.

BAND	COLUMN A	COLUMN B	COLUMN C	$(\frac{A-B}{A})\%$	$(\frac{A-C}{A})\%$
2	1.66	1.55	1.50	6.6	9.8
3	1.25	1.22	1.16	2.4	7.2
4	1.44	1.62	1.57	-12.9	-9.6

COLUMN A GIVES THE RADIANCE LEVELS AT THE TM AS DERIVED FROM GROUND AND ATMOSPHERIC MEASUREMENTS AT WHITE SANDS ON JANUARY 3, 1983, AND THE USE OF AN ATMOSPHERIC RADIATIVE TRANSFER PROGRAM (SEE TABLE 3).

COLUMN B GIVES THE WEIGHTED AVERAGE RADIANCE IN EACH PASSBAND ($mWcm^{-2}sr^{-1}$) AS DETERMINED FROM TM IMAGE DATA OF OUR WHITE SANDS SITE IN CONJUNCTION WITH PRE-FLIGHT CALIBRATION DATA.

COLUMN C GIVES THE VALUES IN COLUMN B AS MODIFIED BY THE CHANGE IN RESPONSE SUGGESTED BY THE INTERNAL CALIBRATOR DATA OF DECEMBER 8, 1982.

Band 1 saturated over the snowfield at White Sands. Pre-flight data indicates that a saturation level of 255 counts corresponds to a radiance at the sensor of 1.14 mWcm^{-2}sr^{-1} in TM band 1. We estimate that the snowfield provided a radiance levelof 1.45 mWcm^{-2}sr^{-1} at the sensor.

We are presently fabricating field equipment to provide more detailed and accurate measurements of the surface and atmosphere at White Sands. Our goal is to reduce the uncertainty in sensor absolute calibration to less than $\pm$3%.

We plan to continue the work described here to include the in-flight absolute radiometric calibration of the Landsat-5 Multispectral Scanner System and TM and the Systeme Probatoire d'Observation de la Terre, Haute Resolution Visible (SPOT/HRV) systems.

LANDSAT-4 THEMATIC MAPPER CALIBRATION
AND ATMOSPHERIC CORRECTION

WARREN A. HOVIS
NOAA/NATIONAL ENVIRONMENTAL SATELLITE, DATA,
AND INFORMATION SERVICE

The Landsat-4 Thematic Mapper, with its wide spectral coverage and digitization to 8 bits per word, is a large step forward in the direction of quantitative radiometry from the Multispectral Scanner (MSS). In order to utilize the quantitative accuracy built into the Thematic Mapper effectively, more attention must be paid to calibration before launch, changes of calibration with time in orbit, and atmospheric interference with the measurements, especially in the 450 to 520 nanometer band. All of these factors are important if we are to determine the upwelled radiance that would be measured at the surface. Recent experience with the Coastal Zone Color Scanner (CZCS) program has led to procedures wherein Rayleigh correction factors can be generated utilizing simultaneous surface truth data that empirically give correct upwelled surface radiances, despite errors in sensor calibration, solar spectral irradiance measurements, and reported values of Rayleigh optical depth. These techniques offer sensitive tests for change in calibration, especially at shorter wavelengths. Instruments, such as the CZCS, have shown that calibration changes first, and to the largest degree, at the shorter wave lengths, with lesser changes as wave length increases. These techniques are utilized to calculate a Rayleigh correction factor that, together with geometric terms, will give an accurate correction for this portion of the atmospheric contribution to the signal. Long term observation of the Rayleigh corrected radiance over clear water will be a sensitive indicator of any change in claibration as the sensor ages in orbit.

CALIBRATION OF TM DATA FROM
GROUND-BASED MEASUREMENTS

S. I. RASOOL
LABORATOIRE DE METEOROLOGIE DYNAMIQUE, PARIS

P. Y. DESCHAMPS
DEPARTMENT ETUDES THEMATIQUES, CNES, TOULOUSE

WHY:

To be able to derive physical properties of the earth's surface.

For Climate Applications:

- Spectral reflectance/albedo of the surface
- Aerosol loading of the atmosphere.

For Quantitative Use in Remote Sensing:

- Ocean Color (phytoplancton and sediments)
- Multitemporal Analysis of Vegetation, Snow Cover.

METHOD:

- Ground-Based Measurements:
  - Surface Reflectance
  - Atmospheric Optical Properties.

- Radiative Transfer Model:
  - To compute the signal at the top of the atmosphere and compare to TM data.

21

GROUND-BASED MEASUREMENTS

- **Surface Reflectance:**
    - Broadband radiometers: development of a radiometer at 1.6 and 2.2 μm
    - spectrometer (0.4-1.1 μm).

- **Atmospheric Properties:**
    - Downward global and diffuse solar radiation (pyronometer)
    - Direct solar radiation (pyroheliometer)
    - (Aerosol) optical thickness and its spectral dependence (0.4-1.6 μm) (sun radiometer)
    - Water vapor content.

SCAN-ANGLE AND DETECTOR EFFECTS IN THEMATIC MAPPER RADIOMETRY

MICHAEL D. METZLER AND WILLIAM A. MALILA
ENVIRONMENTAL RESEARCH INSTITUTE OF MICHIGAN

Objective

The objective of our investigation is to quantify the performance of the Thematic Mapper (TM) as manifested by the quality of its image data, in order to suggest possible improvements for data production and assess the effects of data quality on its utility for land resources applications. The major emphasis of our work has been on the radiometric characteristics of TM data, with some attention to spatial and spectral characteristics.

Approach

Computer-compatible tapes of raw data (CCT-BT), radiometrically corrected data (CCT-AT), and geometrically corrected data (CCT-PT) were initially examined for two frames, 40049-16262 (Iowa) and 40037-16031 (Arkansas), with concentration on the CCT-BT and CCT-AT data. Histograms, scan-line (across-track) and along-track averages, Fourier transformations, and gray maps were produced and analyzed, for each band, each detector and each scan direction. Since February, four additional frames have been examined, plus calibration data from CCT-ADDS tapes. Also reflective data from nighttime scenes have been analyzed to characterize noise.

Initial Findings

Initial examination of Thematic Mapper data yielded an overall positive reaction to its quality and information content. We did, however, observe and quantify some relatively low-level artifacts relatable to the

23

sensor and data processing stages. We also have noted and quantified scene-related scan-angle effects that could be important in analysis of full scenes and in comparing data from different portions of a scene.

Horizontal stripes and discernable banding are common artifacts in image data from sensors that scan arrays of detectors. We found evidence of striping in corrected TM data due to residual between-detector calibration differences and quantization effects like those found in MSS data. Figure 1 illustrates one pattern of differences found in Band 2 between averages of successive scan line across a homogeneous scene. Effects of unequal analog-to-digital conversion bin sizes in CCT-BT data and empty quantization levels in CCT-AT data are largely masked by the interpolation process used to produce CCT-PT data.

In addition, we detected a new type of banding caused by the combination of bidirectional scanning by the 16-detector arrays and a systematic droop of signal values during the active portion of each scan. The resulting differences between forward and reverse scans are illustrated in Figure 2, as a function of scan angle for TM Band 1. This effect produces swaths or bands of differing signal levels that are most pronounced near the frame edges and minimal at the frame center. Similar behavior was detected in Bands 2, 3 and 4, relatively little effect in Bands 5 and 7, and a substantially different behavior in the thermal band (Band 6). The markedly different full-frame averages for forward and reverse scans in the thermal band are shown in Figure 3.

The scan-related banding in the reflective bands was superimposed on substantial scene-related scan-angle effects in the data. Again for Band 1, the full-frame averages for forward and reverse scans are presented in Figure 4. The dominant scan-angle effect here is due to differential backscattering by the atmosphere, differing path lengths, and bidirectional reflectance effects on the ground. It was expected to be greater than seen before in Landsat MSS data due to the larger scan angles for all bands and the shorter wavelength of Band 1. Differences were observed between bands due to spectal phenomena.

An empirical first-order model to correct for the scan-direction banding effect was derived for the Band 1. Refinement of the model awaits further understanding of the sensor phenomena driving the effect and other scene data for validation. We also recommend that procedures be investigated to normalize the scene-related scan-angle effects, as has been done previously for aircraft and Landsat MSS data.

In the time since the first presentation of this work in February 1983, our effort has been directed at characterization of another radiometric anomaly which we first described there. This artifact appears in two forms of level shifts, where the affected detectors have their mean output signal raised (or lowered) for one or more scans. All detectors in the reflective bands demonstrate this effect to some degree, although for most detectors, the magnitude of the shift is 0.5 signal counts. Band 1 Detectors 4, 12, 10 and 8 show the greatest amounts of Form #1 noise with level shifts of 2.2, 1.8, 1.0 and 0.75 counts, respectively, as shown in the down-track profile of Figure 5. A second, more regular pattern of level shifts is exemplified by Band 7 Detector 7 (Figure 6). Each detector exists in one of four noise states representing the combinations of these two forms of level shift and their phases.

A procedure to remove most of the effect of these level shifts has been developed which uses the dark level presented to each detector by the calibration shutter just after DC restore. A simulation of this procedure appeared promising and further evaluation has been recommended.

Spatial and spectral characteristics of coincident TM and MSS were compared for an agricultural scene. High correlations were found between similar spectral bands and transformed variables. The improved spatial resolution of TM was also evident.

CCT-AT 4-0049-16-262 TM P027 R030 BAND 2
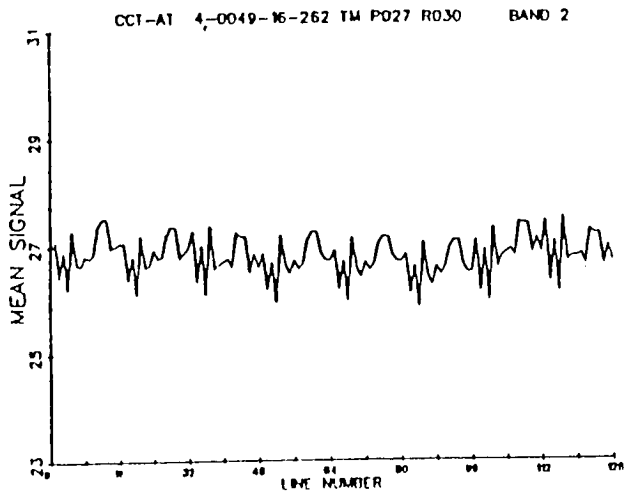
FIGURE 1. DOWN-TRACK MEAN SIGNAL, BAND 2, ILLUSTRATING DETECTOR CALIBRATION DIFFERENCES

CCT-AT 4-0049-16-262 TM P027 R030 BAND 1 DETECTOR 4
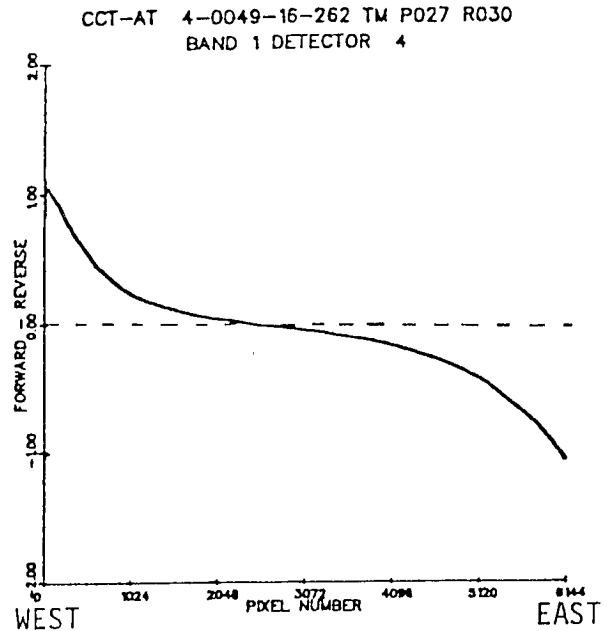
FIGURE 2. DIFFERENCE IN CROSS-TRACK MEAN SIGNAL BETWEEN FORWARD AND REVERSE SCANS, BAND 1

CCT-AT 4-0049-16-262 TM P027 R030 BAND 6 DETECTOR 4
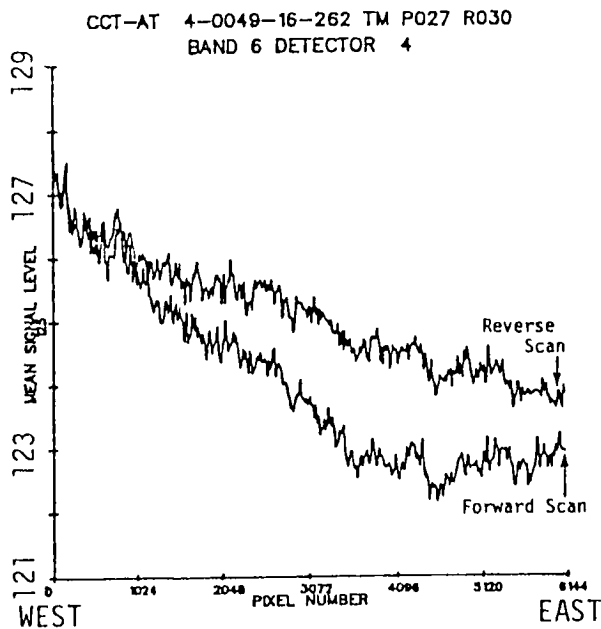
FIGURE 3. CROSS-TRACK MEAN SIGNAL, BAND 6, ILLUSTRATING SCAN DIRECTION EFFECT

CCT-AT 4-0049-16-262 TM P027 R030 BAND 1 DETECTOR 4
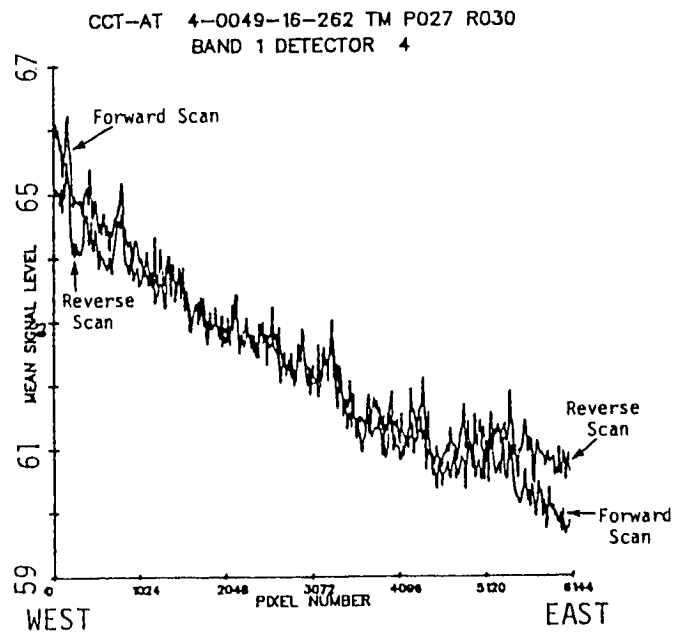
FIGURE 4. ILLUSTRATION OF SCAN-ANGLE EFFECT, ACROSS A FRAME (BAND 1)

26

MEAN VALUE OF EACH SCAN BY DETECTOR
CCT-BT   4016102481   D11620783180   BAND 1

MEAN VALUE OF EACH SCAN BY DETECTOR
CCT-BT   4016102481   D11620783180   BAND 7
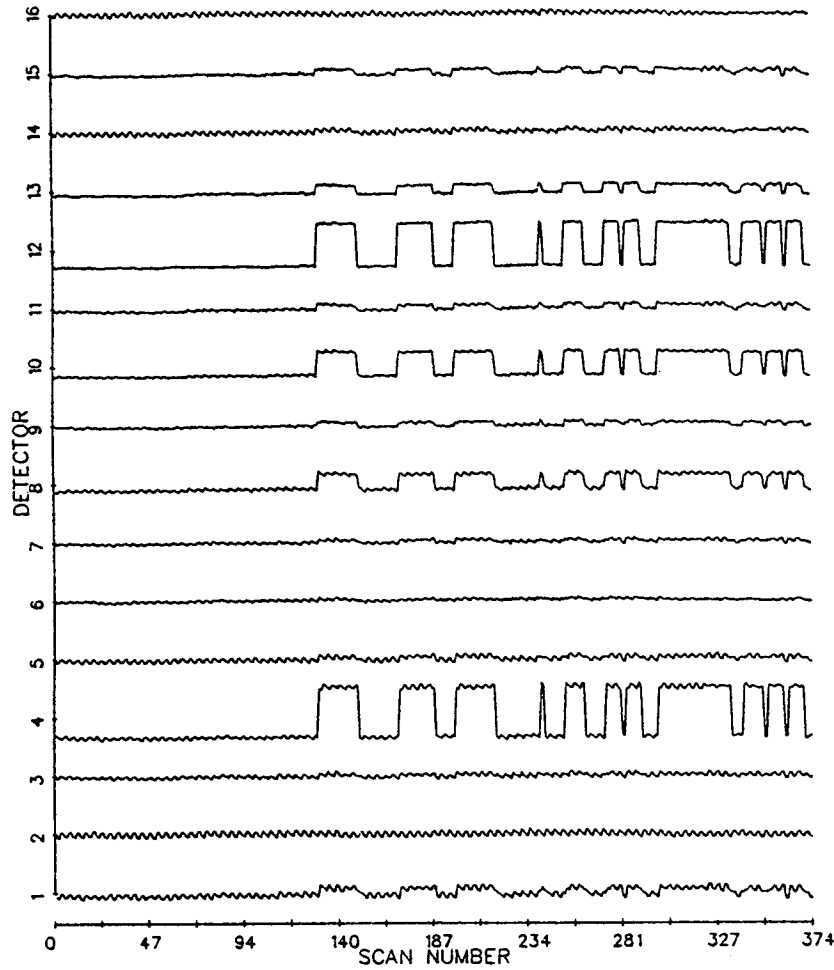
FIGURE 5.   SCAN AVERAGES (BY DETECTOR)
            OF NIGHTTIME SCENE DATA, BAND 1
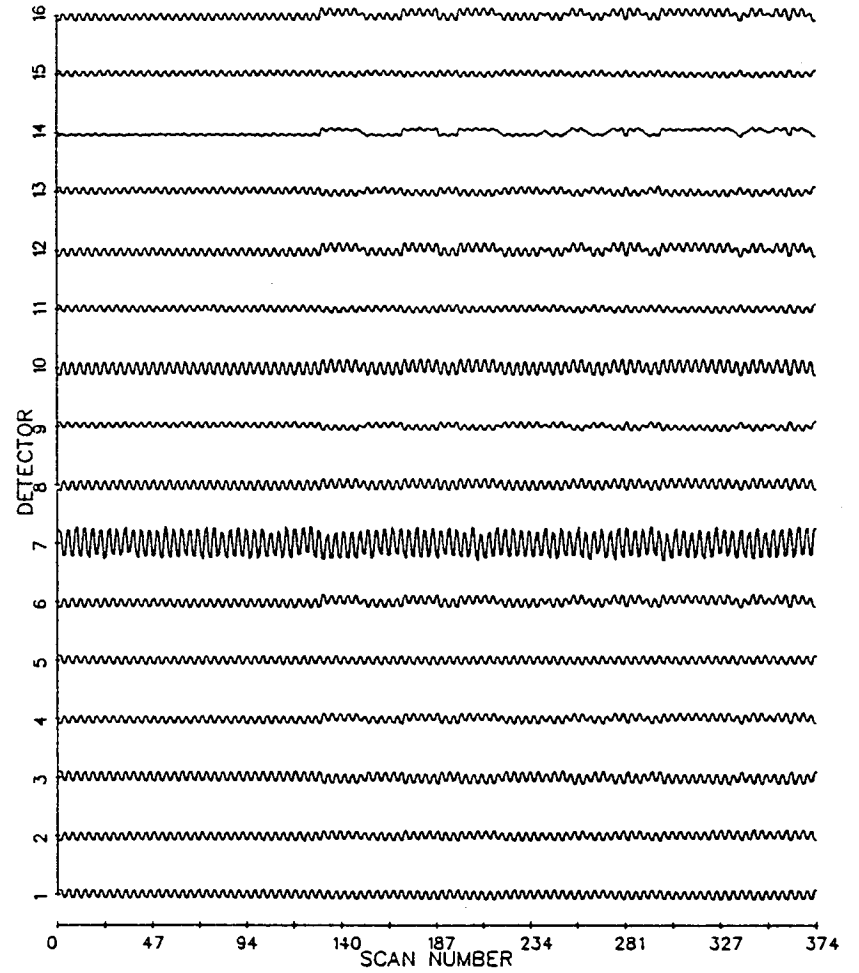
FIGURE 6.   SCAN AVERAGES (BY DETECTOR)
            OF NIGHTTIME SCENE DATA, BAND 7

27

THEMATIC MAPPER SPECTRAL DIMENSIONALITY AND DATA STRUCTURE

E. P. CRIST AND R. C. CICONE
ENVIRONMENTAL RESEARCH INSTITUTE OF MICHIGAN

Thematic Mapper data, simulated from field and laboratory
spectrometer measurements of a variety of agricultural crops and a wide range
of soils, are analyzed to determine their dispersion in the six-space defined
by the reflective TM bands (i.e., excluding the thermal band). While similar
analyses of MSS data from agricultural scenes have found that the vast
majority of the MSS data occupy a single plane, the simulated TM data are
shown to primarily occupy three dimensions, defining two intersecting planes
and a zone of transition between the two (see Figure 1). Viewing the "Plane
of Vegetation" head-on provides a projection comparable to the single plane of
MSS data. The "Plane of Soils" and transition zone represent new information
made available largely as a result of the longer infrared bands included in
the Thematic Mapper. A transformation, named the Thematic Mapper Tasseled
Cap, is presented which rotates the TM data such that the described data
structure is most readily accessible to view.

Subsequent analysis has resulted in an equivalent transformation for
actual TM data. Figure 2 shows an example of the data distributions in TM
Tasseled Cap space for an agricultural scene. The associated transformation
matrix is presented in Table 1.

The first three features of the transformation, which define the two
planes and account for more than 95% of the total data variability, are named
Brightness, Greenness, and Wetness. Brightness, a weighted sum of all six

bands, responds to changes in albedo. Greenness, a weighted contrast between the sum of the visible bands and the near-infrared band, responds to the presence of green vegetation. Wetness, a weighted contrast between the sum of the visible and near-infrared bands and the sum of the longer infrared bands, responds to soil moisture status (for bare soils data). The added dimension in the TM data, represented by the Wetness feature, provides improved information with regard to both vegetation and soil classes.

The TM Tasseled Cap transformation of actual data, and our current understanding of vegetation and soil characteristics in this feature space, are detailed in the reference cited below.

REFERENCE

Crist, E.P. and R. C. Cicone. 1984. A physically-based transformation of Thematic Mapper data - the TM Tasseled Cap. IEEE Transactions on Geoscience and Remote Sensing (submitted).

TABLE 1.   THEMATIC MAPPER TASSELED CAP COEFFICIENTS - ACTUAL DATA

TM BAND

Feature	1	2	3	4	5	7
Brightness	.3037	.2793	.4743	.5585	.5082	.1863
Greenness	-.2848	-.2435	-.5436	.7243	.0840	-.1800
Wetness	.1509	.1973	.3279	.3406	-.7112	-.4572
Fourth	-.8242	.0849	.4392	-.0580	.2012	-.2768
Fifth	-.3280	.0549	.1075	.1855	-.4357	.8085
Sixth	.1084	-.9022	.4120	.0573	-.0251	.0238
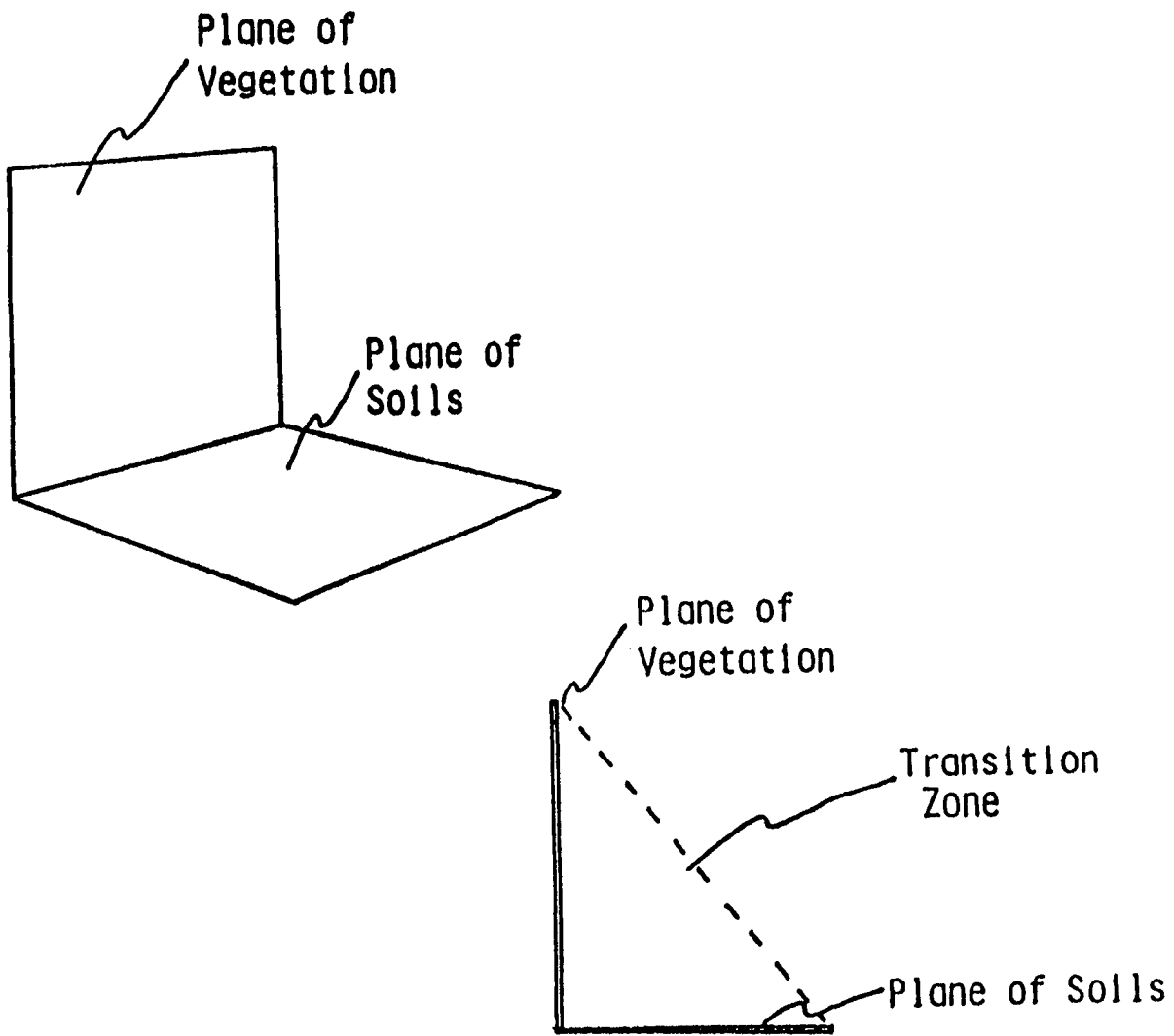
FIGURE 1. DIMENSIONAL RELATIONSHIPS IN 6-BAND THEMATIC MAPPER DATA
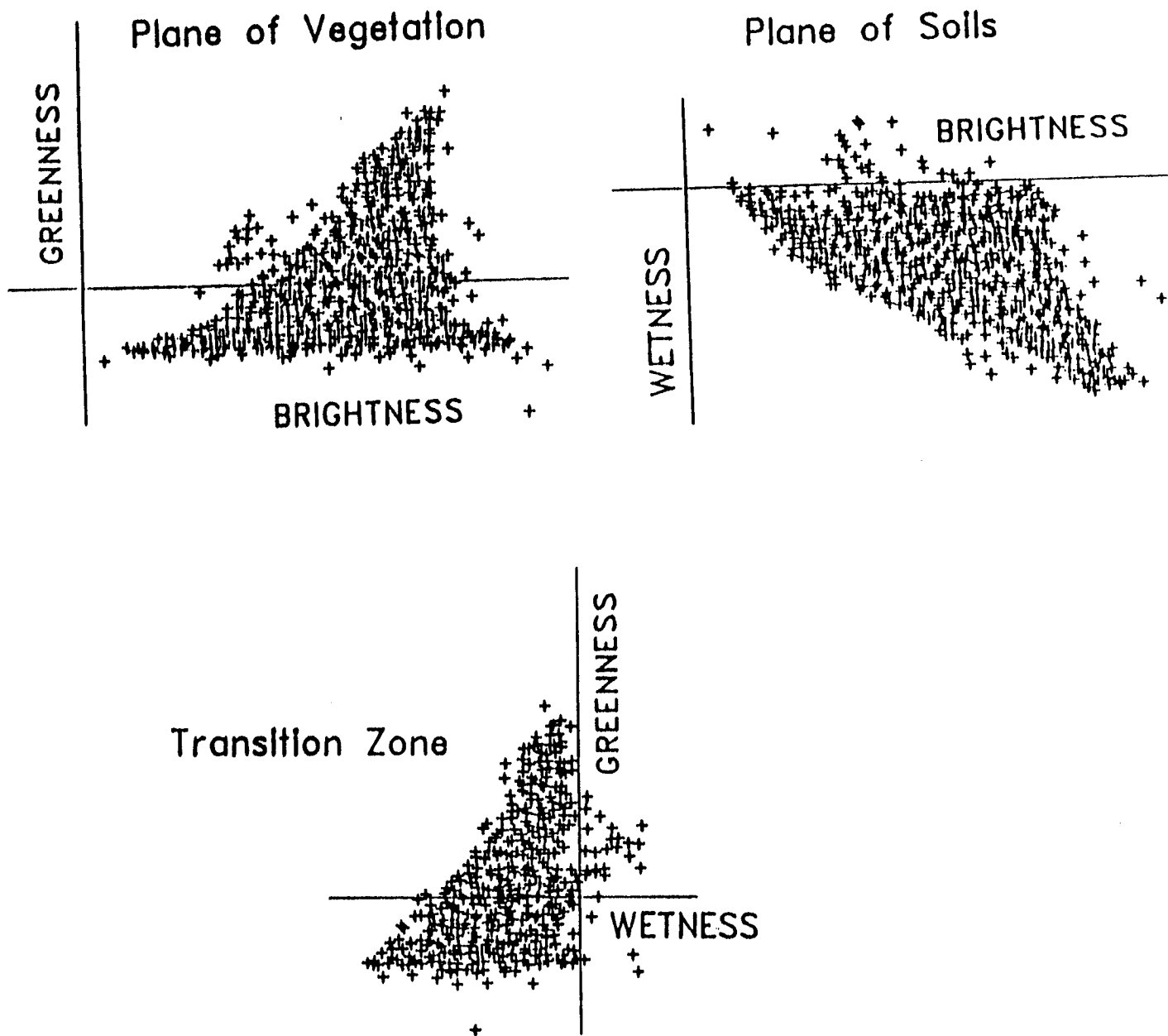
FIGURE 2. THEMATIC MAPPER TASSELED CAP ACTUAL DATA DISTRIBUTION

MTF ANALYSIS OF LANDSAT-4 THEMATIC MAPPER

ROBERT SCHOWENGERDT
UNIVERSITY OF ARIZONA

A research program to measure the Landsat-4 Thematic Mapper (TM) modulation transfer function (MTF) is described. The research is being conducted by the University of Arizona and NASA/Ames Research Center under the contract "An Investigation of Several Aspects of Landsat-D Data Quality" (Robert C. Wrigley, Principal Investigator).

Measurement of a satellite sensor's MTF requires the use of a calibrated ground target, i.e., the spatial radiance distribution of the target must be known to a resolution at least four to five times greater than that of the system under test. Any radiance structure smaller than this will have a small effect on the calculated MTF. Calibration of the target requires either the use of man-made special purpose targets with known properties, e.g., a small reflective mirror or a dark-light linear pattern such as line or edge, or use of relatively high resolution underflight imagery to calibrate an arbitrary ground scene. Both approaches will be used in this program; in addition a technique that utilizes an analytical model for the scene spatial frequency power spectrum will be investigated as an alternative to calibration of the scene. The test sites and analysis techniques to be used in this program are described in this paper.

INTRABAND RADIOMETRIC PERFORMANCE OF THE
LANDSAT-4 THEMATIC MAPPER

HUGH H. KIEFFER, ERIC M. ELIASON, PAT S. CHAVEZ, JR.
U.S. GEOLOGICAL SURVEY, FLAGSTAFF

ABSTRACT

This preliminary report examines those radiometric characteristics of the Landsat-4 Thematic Mapper (TM) that can be established without absolute calibration of spectral data. Our analysis is based largely on radiometrically raw (B type) data of three daytime and two nighttime scenes; in most scenes, a set of 512 lines were examined on an individual-detector basis. Subscenes selected for uniform-radiance were used to characterize subtle radiometric differences and noise problems. We have discovered various anomalies with a magnitude of a few digital levels or less. Virtually all of this nonideal performance is incorporated into the fully processed (P type) images, but disguised by the geometric resampling technique.

The effective resolution in radiance is degraded by a factor of about 2 by the irregular width of the digital levels. Underpopulated levels are consistent over all bands and detectors, and are spaced an average of 4 digital numbers (DN) apart. In band 6, level 127 is avoided by a factor of 30. This behavior is masked by resampling in the P data. In the radiometrically corrected (A type) data, small differences--typically, 0.8 DN--exist between the average DN for the 16 detectors in each band; the standard deviations also differ, typically by 0.4 DN.

Several detectors exhibit a change of gain with a period of several scans; the largest effect is about 4%. These detectors appear to switch between two response levels during scan-direction reversal; all the affected detectors switch simultaneously. There is no apparent periodicity to these changes. This behavior can cause small apparent differences between forward and reverse scans for parts of an individual image.

33

The magnitude of interdetector variation is readily seen by making an image of the first derivative in the vertical (line) direction of a flat field and stretching progressively wider ranges to gray; most detectors differ from their neighbors by 1 or 2 DN.

At high-contrast boundaries, some of the detectors in band 5 commonly overshoot by several DN and require about 30 samples to recover; this behavior occurs erratically. A small asymptotic decrease in response occurs along scanlines.

The high-frequency noise level of each detector was characterized by the standard deviation of the first derivative in the sample direction across a flat field. By this measure, the noise level is: 1.6 to 2.5 DN in band 1, 0.3 to 1.6 DN in band 2, 0.5 to 1.4 DN in band 3, 0.4 to 0.8 DN in band 4, 1.3 to 1.8 DN in band 5, and 1.3 to 2.8 DN in band 7.

A coherent-sinusoidal-noise pattern is evident in detector 1 of band 3. One-dimensional Fourier transforms show that this "stitching" pattern has a period of 13.8 samples, with a peak-to-peak amplitude ranging from 1 to 5 DN. Oscillations of the same frequency but of less than half this amplitude also occur for two other detectors in this band. Noise with a period of 3.24 samples is pronounced for most of the detectors in band 1; to a lesser extent in bands 2, 3, and 4; and at or below background-noise levels in bands 5, 6, and 7. We have adapted and applied a noise-removal algorithm that tracks the varying-amplitude periodic noise to reduce the conherent-noise of detector 1 in band 3; this algorithm appears to work quite well.

For two areas, we determined the correlation between the six reflective bands and used it to select three groups of bands whose aggregate first principal-components contain the greatest total information. A composite of the first components of bands 1, 2, and 3, bands 5 and 7, and band 4, together containing 98% of the information in the reflectance bands, has reduced the effect of noise.

ANALYSIS OF LANDSAT-4 TM DATA FOR LITHOLOGIC AND IMAGE MAPPING PURPOSES

M. H. PODWYSOCKI, J. W. SALISBURY, L. V. BENDER, O. D. JONES AND
D. L. MIMMS
U. S. GEOLOGICAL SURVEY, RESTON

The principal progress to report since the last Landsat-4 Thematic Mapper (TM) Workshop is in the area of lithologic mapping, making particular use of the new near-infrared bands available for the first time on the Thematic Mapper.

Lithologic mapping techniques used band ratios combined with digital masking to test the capability of mapping geologic materials based on specific absorption features which lie within the bandpass of TM bands. Limonitic minerals, such as hematite, goethite, jarosite, and lepidocrocite, among others, which contain ferric iron oxides, oxyhydrides, and sulfates, display marked decreases in reflectance from the near-infrared (TM band 4) to the visible part of the spectrum (TM bands 1, 2, 3). Limonite also is detectable in Landsat MSS data. Of more interest to the geologist participating in a mineral-resource analysis or exploration program are the parts of the spectrum sensed by TM bands 5 and 7. Many minerals containing AL-O-H and Mg-O-H chemical bonds in their lattice structures, as well as carbonate minerals, often display characteristic absorption bands in the 2.1- to 2.4-μm region (TM band 7). The O-H-bearing minerals include clays, some micas, and hydrated aluminous sulfates, all of which are potential indicators of mineralized rocks. For all these materials, reflectance in the 1.6-μm region (TM band 5) is greater than in the 2.1- to 2.4-μm region. Hence, a TM 5/7 band ratio can be used to distinguish between materials having or lacking absorption bands in the 2.1-2.4-μm region.

Because of the low solar energy levels in the 1.5- to 2.4-μm region, the performance of TM bands 5 and 7 is most crucial. We have examined TM data for several regions in the United States under medium to low sun-angle illumination conditions to determine the limits under which materials with absorption features can be detected. We have found that under low sun-angle

conditions ambiguities result between low reflectance targets such as shadows and water bodies and certain geologic materials which have absorption features in the 2.1- to 2.4-μm regions. We proposed data-processing techniques to resolve some of these ambiguities.

A mid-September scene of Macon, Georgia (ID 40050-15333) was analyzed to determine the detectability of kaolinite, a mineral having intense absorption bands in the 2.2-μm region. The Macon area is known for its quarries, which produce nearly pure kaolin for industrial applications. Examination of a color-ratio-composite (CRC) image composed of a 5/7 ratio for detection of absorption bands in the 2.1- m to 2.4- m region, a 5/2 ratio for detection of limonite, and a 3/4 ratio for detection of vegetation, revealed that the kaolin quarries could be readily distinguished from other quarries in gravel and granitic rocks. Furthermore, the kaolin quarries could be subdivided into two groups, based on the presence or absence of limonite staining of the kaolinite. No ambiguities between the kaolinite and water bodies were detected, presumably because the high sun elevation (52 degrees above the horizon) resulted in sufficiently high reflectance from water bodies to avoid the problem described below. Perceptible shadows were not observed, because of the high sun elevation and the low relief terrain.

A late-December scene of an area along the Atlantic coast, centered on Fort Pierce, Florida (ID 40157-15174) was examined to determine the capability of distinguishing beach sands containing varying amounts of carbonate materials. The carbonate materials are primarily in the form of shell fragments, and are mixed in varying proportions with quartz sand, depending upon their position with respect to the source areas for the shell fragments and quartz. The 5/7 band ratio was used to detect the carbonate minerals, a 3/1 ratio was used for detection of limonite and a 2/4 ratio was used for vegetation detection. A CRC image created from these ratios showed that scattered pixels in ocean waters displayed the same response as that expected for carbonate sands which lack limonite. This source of confusion was caused by the relatively low digital response values (DNs) for the water in TM bands 5 and 7, due to the relatively low sun angle (31 degrees above the horizon) of this late December scene. Low DNs on the order of 5-10 in band 5 and 3-6 in band 7, coupled with a superposed random noise variation of 2-3 DNs, leads to relatively large changes in the 5/7 ratio values for water.

Consequently, some pixels over water bodies may display ratio values greater than those for carbonate-bearing sands. These low response values can be attributed to the low levels of solar energy in this part of the spectrum due to the low elevation of the winter sun, coupled with the intrinsically low reflectance of water in the near-infrared compared with the visible part of the spectrum. This source of confusion was eliminated by digitally masking out water bodies based on their low reflectance in TM band 5 before additional image analysis was attempted.

TM 5/7 ratios of vegetation will be similar to or greater than, those for carbonate minerals because water present in plant-leaf structures lowers the overall reflectance in the 1.6-μm region and more so in the 2.2-μm region. Hence, digital masking using the low values of vegetation in the TM 2/4 band ratio is required before detailed analysis of the intensity of the carbonate absorption band can be determined from the 5/7 ratio data.

A final problem was posed by bright fringes that appeared at the shorelines of water bodies. These are apparently due to ringing or overshoot resulting from the resampling algorithm used in the NASA SCROUNGE facility for correcting these data. The bright fringes made the TM 5/7 band ratio images appear noisy and made interpretation more difficult. We found that the 3/1 band ratio could be used to generate a third mask to eliminate this problem. After the vegetation and bright fringing masks were applied to the 5/7 band ratio data, the 5/7 ratio values could be related to the intensity of the carbonate absorption band centered at 2.33μm.

Besides the calcareous sands, it was found that metal-roofed buildings (usually mobile homes) displayed strong carbonate bands. These structures are painted with a special rubberized latex paint that is designed to withstand the thermal expansion and contraction of metal roofs without cracking. One of the whiteners in this paint is calcite, which results in a very strong carbonate absorption band for this paint. The extremely flat spectral response for this paint in the visible, however, easily served to distinguish it from natural carbonate sands, the reflectance of which falls off from the red to the blue region of the spectrum. Interestingly, a similar false target problem was encountered in the Las Vegas, Nevada, scene described below, so such anomalous painted surfaces are not confined to Florida.

37

Part of a mid-December scene centered on Las Vegas, Nevada (ID 40149-17440), was analyzed to determine the capability of mapping hydrothermally altered rocks, based on their high content of clay, mica, and hydrated aluminum sulfate minerals. The area selected is in a high-relief terrain (600 m, 2000 ft) which has several known gold- and silver-mining districts. Band ratios examined included 5/7 for the O-H-bearing minerals, 5/2 and 3/1 for limonite, and 3/4 for vegetation detection. Because of the high-relief terrain and low solar illumination angle (25 degrees above the horizon), shadows were extensive. An examination of a CRC image revealed that both shadows and water bodies were confused with bleached hydrothermally altered rocks and other rocks having 2.2-μm abosrption features. Digital masking of low-reflectance materials such as water bodies and shadow areas alleviated some of the problem, but edges of shadow areas and water bodies still created ambiguities. These could be recognized readily by photointerpretive techniques. An apparent mixed-pixel problem also has been encountered for mixtures of vegetation and desert soil. Mixtures of these two materials produce 5/7, 3/4 and 5/2 and 3/1 ratios similar to those of hydrothermally altered rocks. Examination of a standard false-color infrared (CIR) image composed of TM bands 2, 3, and 4, which shows vegetation as red, indicated that the CIR was a sensitive indicator of vegetation, even in the mixed-pixel areas, where vegetation appeared as a slight "blush" of red in the image. The CIR image was converted to Munsell color space (Hue-Saturation-Value) and all red hues were digitally masked out. This mask was digitally overlayed on the CRC image and most of the ambiguity between mixed pixels of vegetation and soils with hydrothermally altered rocks was eliminated. In addition to identifying hydrothermally altered rocks in the digitally masked image, surfaces covered with thin coatings of desert varnish, could be distinguished, because of their extremely low reflectance in the visible part of the spectrum, and their increasing reflectance toward longer wavelengths in the infrared. Rooftops of buildings coated with calcite-bearing paint also were noted, and care had to be exercised so that these isolated occurrences were not mistaken for bleached hydrothermally altered rocks.

In addition to the lithologic mapping reported above, U.S. Geological Survey personnel in the National Mapping Division are working on the production of an image map from TM data, which will be reported on fully at the

next workshop. Briefly, a map accurate to National Map accuracy standards at 1:100,000 is being produced from a Washington, D.C. scene. The map design has been completed and TM bands 1, 3 and 5 have been digitally enhanced and produced as film separates. The films have been screened so that they are suitable for standard lithographic printing, and will be available for distribution January 30, 1984. The following are the basic specifications of the map.

Name: Washington, D.C. and Vicinity
                         Landsat Image Map

Scale: 1:100,000

Sheet   38 30'N to 39 15'N;
Boundaries: 76 22'30"W to 77 37'30"W

Composition: TM Band 1 - Yellow
                         TM Band 3 - Magenta
                         TM Band 5 - Cyan

Projection   UTM with 10,000 meter grid spacing;
and Grid: State Plane Coordinate Systems ticks
                         with 25,000 foot tick spacing

Source Data: Landsat-4 TM image 40109-15140,
                         November 2, 1982
                         Geometric control derived from 7.5
                         minute quadrangles

In addition to the map publication discussed above, a U.S. Geological Survey I-series report on the Washington, D.C. image map is being prepared for publication by early summer, 1984. This map will include black-and-white prints of the six visible and near-infrared bands for the full map at an approximate scale of 1:550,000 and an array of approximately 25 color composite images. Approximately five color composite images will be made at the full 1:100,000 scale for the corridor between the Dulles Airport area and the District of Columbia city center.

STATUS OF THE ESA-EARTHNET LANDSAT-4 TM GROUND PROCESSING CHAIN

L. FUSCO
EUROPEAN SPACE AGENCY/EPO

KEYWORDS: Landsat-4, Thematic Mapper, System Corrections, Acquisition, Data Recording

The European programme of the European Space Agency received a mandate to upgrade the two existing Landsat stations operating in Europe, Kiruna in Sweden and Fucino in Italy, to acquire and process TM data. This project is in the process of being brought to completion. It is the intention of this paper to summarize the salient features of the TM systems, and to review the preliminary results of the acceptance tests being carried out using the TM passes acquired in Fucino between December 1982 and February 1983, before the X band downlink anomaly of Landsat-4.

Table 1 lists the requirements on TM acquisition, recording and preprocessing systems for the Earthnet Landsat stations. It should be noted that the TM processing chain was specified to generate only digital data products, since film product generation would be jointly carried out on the photographic system shared between MSS and TM. The throughput requirements were tailored to the expected volume of data which could be acquired in Europe; however the production capability can be increased in the first instance by augmenting the number of shifts (hours of operation) without system modifications.

Only Fucino was ready to acquire TM data before the failure of the Landsat-4 X-band downlink; therefore the only operational experience in acquiring data in X-band refers to this station. The overall system performance was well within specifications. The tracking system in both S and X band was essential; particularly during the acceptance phase, it was found that switching between S and X band tracking was required up to two/three times per pass.

TABLE 1. LANDSAT-4 TM ACQUISITION AND PROCESSING REQUIREMENTS

1.	Acquisition	: G/T	31 dB/K at X Band
		G/T	21 dB/K at S Band

2.	Tracking	: Velocity AZ 12 DEG/sec. Acceleration AZ/EL 10 DEG/sec.
		EL 10 DEG/sec.

3. Recording : Input bit rate 20 to 120 Mbps
Recommended packing density 25 kbpi
Read/Reproduce speed IRG standards 120 ips to 3.75
Throughput BER better than 10^{-6} (10^{-8} with Error
Detect/Correct Code)

4. On-line monitoring: R/T data visualization via moving window display of a selectable band

5. Out put product:

- Quick look CCT covering up to 24 scenes (full pass) selectable band radiometric corrected and annotated

- Full resolution, all band, full scene raw data

- As above system corrected data

- Full resolution, all band, quarter scene, raw data

- As above system corrected data

- Full resolution, single band, full scene, raw data

- As above system corrected data

6. Standard quality control and data management aids.

The experience with the 42 track HDTR has been very favorable both in terms of S/N of the recording and of cross compatability between units. Based on operational experience, it has been decided to operate at constant speed rather than at constant packing density, since in this way we could use the R/T moving window display unit. What proved to be more complex than expected was the selection of the High Density Digital Tapes (HDDTs) after several benchmark tests, video tape type SONY VI6.188 has been selected. This appears to have the best cost performance ratio, although tests are continuing with other brands in order to keep abreast of developments in the field.

The synchronization and preprocessing chain interfaces the HDTR and performs the following tasks:

- on line data visualization on the moving window display
- data demultiplexing
- data buffering and preprocessing
- digital product generation
- quality checking on products generated
- reporting on housekeeping

The selected design makes use of standard off the shelf equipment for nearly all the system, while Figure 1 shows the configuration layout.

When full resolution products are to be generated, the playback takes place at 8 times real-time. The generation of a full scene entails typically three steps, i.e.:

- the transfer from HDTR to the format synchronizer to the DEMUX down to the GPIOP, the AP 120B, the second GPIOP, the computer memory and finally to a disk file. During this phase, PCD data are selected from the data flow and transferred to the Perkin Elmer for the calculation of the geometric correction tables.

- At the same time, the AP120B performs the extraction of histograms for the different channels and forwards them to the Perkin Elmer for the calculation of the radiometric

42

FIGURE 1. LAYOUT OF EPO TM PROCESSING CHAIN

43
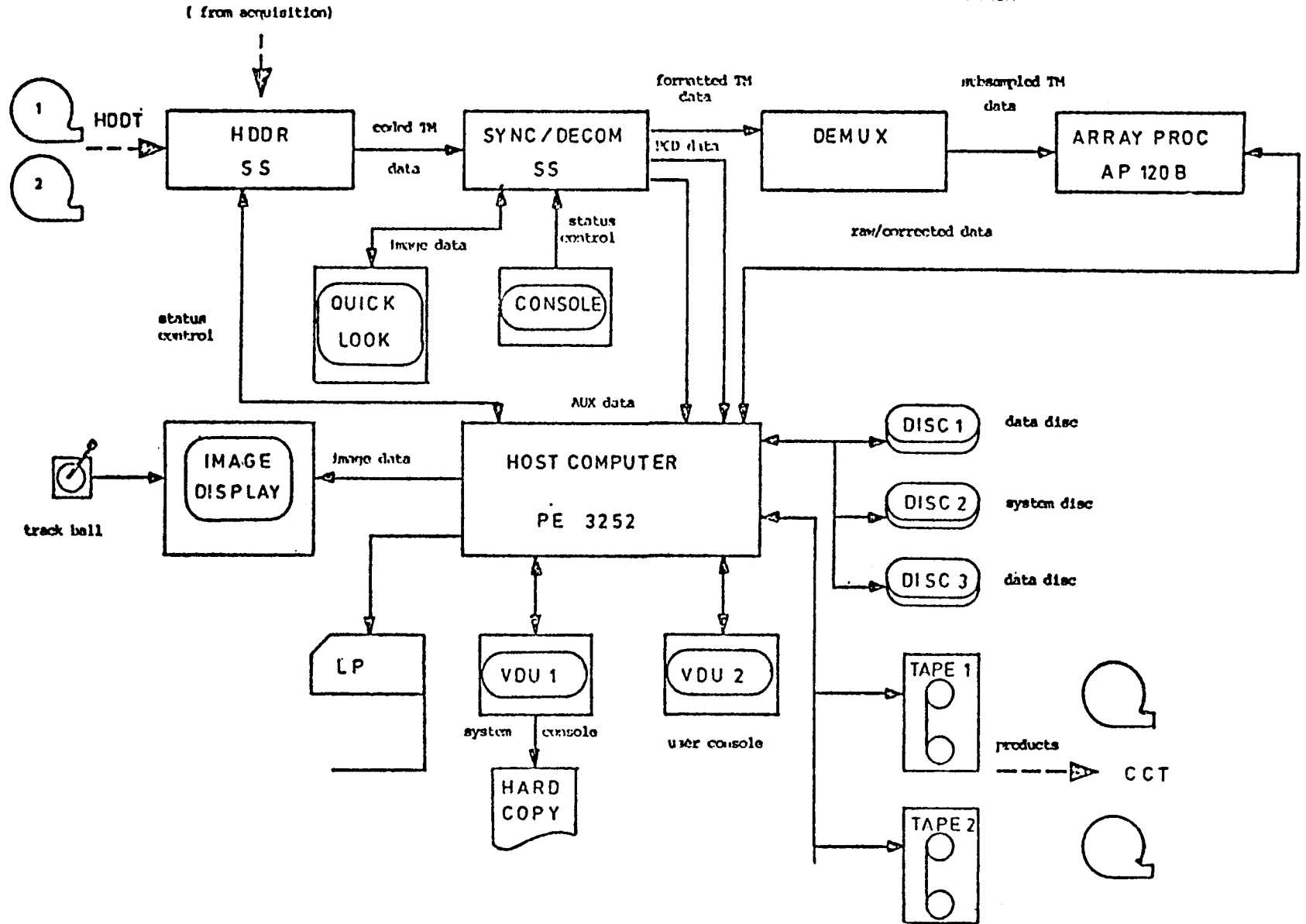
correction tables based upon sensor statistics. Obviously this phase involves a data formatting as well, performed on the fly on the AP and GPIOP's.

- the second step starts when the Perkin Elmer has computed the geometric and radiometric correction look-up tables and transfers them to the Array Processor. At this point, data are read back from disk to the Array Processor where the corrections are applied.

- the last step involves the transfer of corrected data from the AP to the PE memory and from there to the output tape. During this phase, quality checks on data are performed.

Since the standard bulk corrected product is only corrected with the Nearest Neighbor method, the data flow can be kept balanced in all three steps without identifiable bottlenecks.

The acceptance test specifications of the TM preprocessing chain called for system performance assessment over a significant sample of data; this task is on-going at present, therefore only partial results can currently be provided.

Table 2 summarizes preliminary system performance figures versus requirements on throughput. Figures on radiometric and geometric accuracy achieved are not yet available but the initial tests shows that the target performance figures are met. Due to operational problems, nearly half of the Earthnet TM holdings are without PCD. The TM chain can cater for those data but with degraded geometric accuracy. The quality of bulk corrected products generated from this data set are being assessed.

TABLE 2. TM CHAIN - THROUGHPUT REQUIREMENT VS. ACTUAL PERFORMANCE

Product	Target Production time	Preliminary Performance results
1. Quick-look CCT, 1 band, 24 scenes max.	60 MN	40'
2. Raw data full frame, all bands	45 MN	60'
3. Raw data quarter frame, all bands	15 MN	40'
4. Raw data full frame, 1 band	10 MN	30'
5. System corrected data, full frame, all bands	60 MN	60'
6. System corrected data, quarter frame, all bands	25 MN	40'
7. System corrected data, full frame, one data	15 MN	30'

Note: Actual Production Times to be confirmed at the end of acceptance tests.

AN ANALYSIS OF LANDSAT-4 THEMATIC MAPPER
GEOMETRIC PROPERTIES

R. E. WALKER, A. L. ZOBRIST, N. A. BRYANT,
B. GOKHMAN, S. Z. FRIEDMAN, AND T. L. LOGAN
JET PROPULSION LABORATORY

Landsat Thematic Mapper P-data of Washington, D. C., Harrisburg, PA,
and Salton Sea, CA were analyzed to determine magnitudes and causes of error
in the geometric conformity of the data to known earth-surface geometry.
Several tests of data geometry were performed. Intra-band and inter-band
correlation and registration were investigated, exclusive of map-based ground
truth. Specifically, the magnitudes and statistical trends of pixel offsets
between a single band's mirror scans (due to processing procedures) were
computed, and the inter-band integrity of registration was analyzed. A
line-to-line correlation analysis was done at one hundred pixel spacings using
Kuglin and Hine's phase correlation image alignment adapted to a one
dimensional FFT correlation technique. This analysis for single bands
revealed the following: aside from two swath border areas where vaguely
coherent patterns of offset existed, there appeared to be no predictable,
systematic offsets between scans in any of the scenes. In the Salton Sea
scene, offsets of a given sample in a given set of adjacent near swath border
scan lines (i.e., lines 41-45) were more often of the same sign (+/-) than of
different signs, and the magnitudes of the offsets tended to be similar for
that sample. The offsets varied between $\pm.5$ pixels in 93% of the sample
matches performed, and in the remaining 7%, the offset generally were close to
the $\pm.5$ marks (within ± 8). The 93 percent figure was true in all scenes
studied.

Inter-band misregistration of the P-tapes was not significant between bands of the primary focal plane (bands 1-4). In these, misregistration varied between +.25 pixels 96% of the time, and most frequently was within the +.15 pixel offset range. Between bands of the primary focal plane and bands of the secondary focal plane, pixel offsets were consistently negative and often in the range between -.75 and -1.25 pixels in the P-tape. A-tape inter-band misregistration was comparable to that of the P-tape in most respects. One notable exception was that bands 5 and 7 showed much improved registration between them in the P-tapes over the A-tapes.

Two TM scenes were tested for their conformity to the Space Oblique Mercator (SOM) projection. A total of 394 control points were found by comparing 1:24000 series topographic maps and the scenes. Least squares fits were performed between the pairs of points (line-sample vs. latitude-longitude), using first and second order linear equations. Both of these yielded large residual offsets, suggesting that a third order or higher equation would be needed to effectively project the latitudes and longitudes into the SOM. With the acquisition of new SOM software from NCIC, and its subsequent implementation into an IBIS routine, the lat-longs were projected into SOM x's and y's. Final least-squares fits were done between these x-y's and their respective line-samples. The resulting residuals were quite small: for the Harrisburg scene the mean of all residuals was 26.95 meters (.90 pixels assuming 30 m per pixel) and the sigma was 128.69 m (.62 pixels). The numbers for the Salton Sea scene were slightly higher; mean = 38.32 m (1.28 pixels), sigma = 29.23 m (.97 pixels). These figures are quite small relative to measurement errors inherent in the methods used here. Ongoing research will attempt to analyze systematic factors contributing to the small residuals still left, including modelling and removing the effects of elevation in each scene and improving the accuracy of our methods. In addition, some tests can be easily repeated for scenes processed through the modified (post January 1983) version of the Scrounge, as well as the TIPS, processing systems.
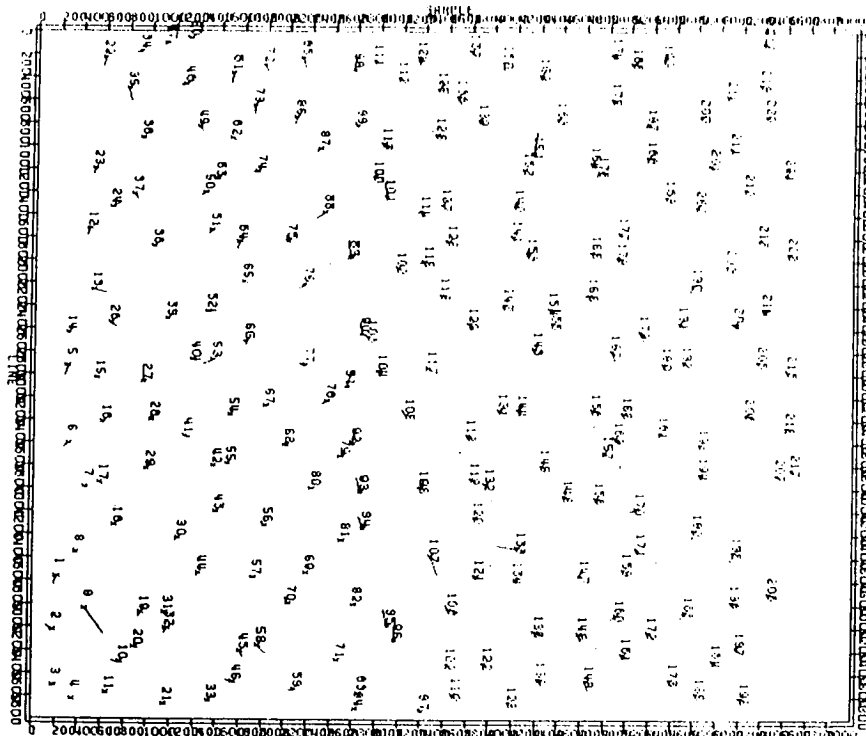
Figure 1a: 2-D Plot of residuals between GCP line-samples and SOM XY's
for Harrisburg, PA TM scene (magnification factor 60).
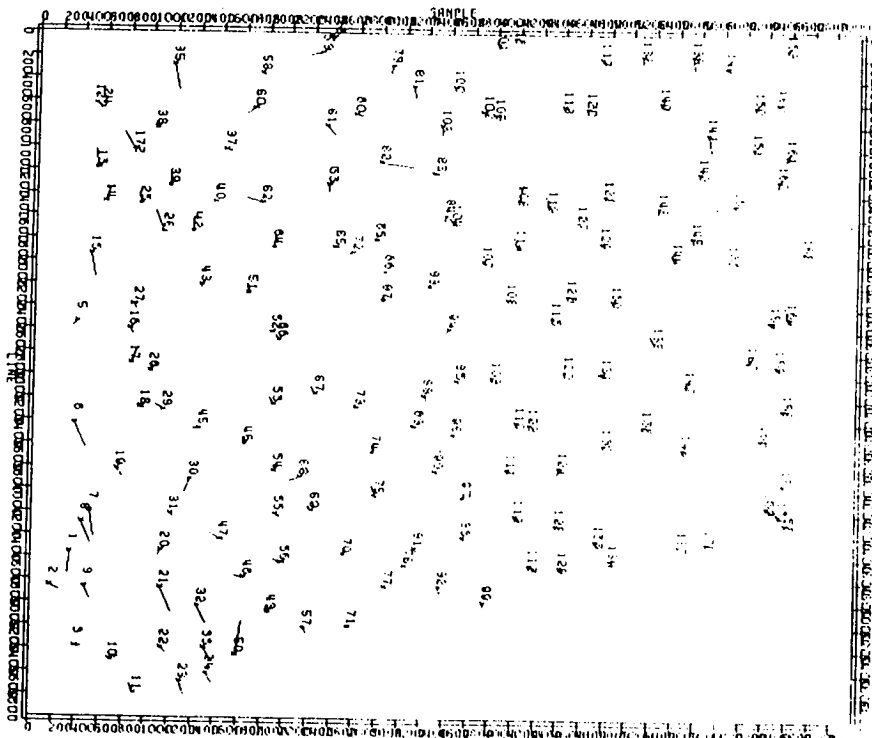
Figure 1b: 2-D Plot of residuals for Salton Sea, CA TM scene.
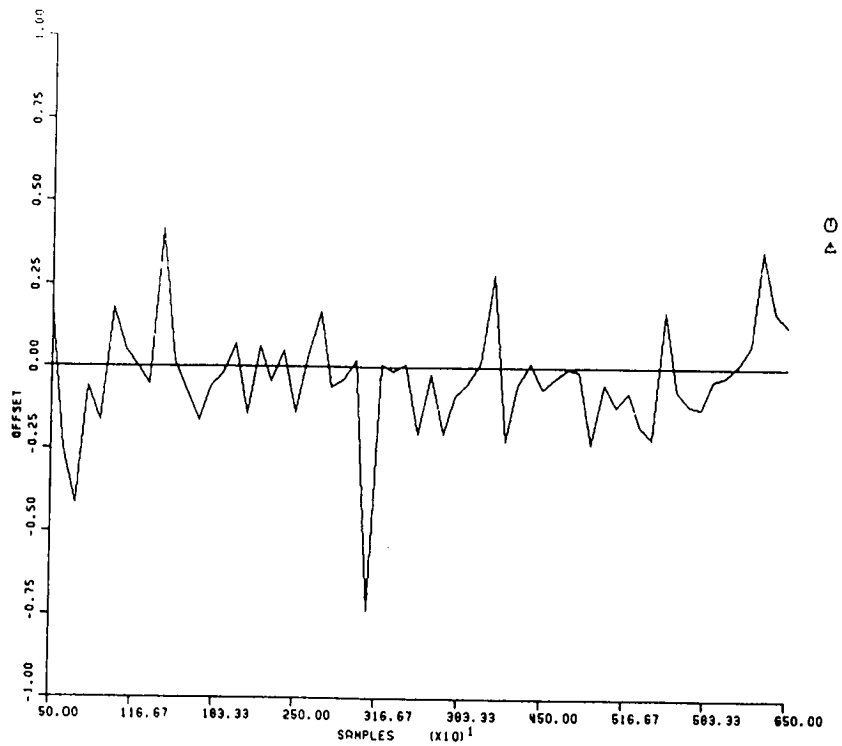
LINE MATCH FOR BANDS 1 AND 3. LINE 7. LANDSAT TM

Figure 2a: Interband linematch correlation between bands 1 and 3 (both primary focal plane) for line 7 of Harrisburg PA TM P-tape.
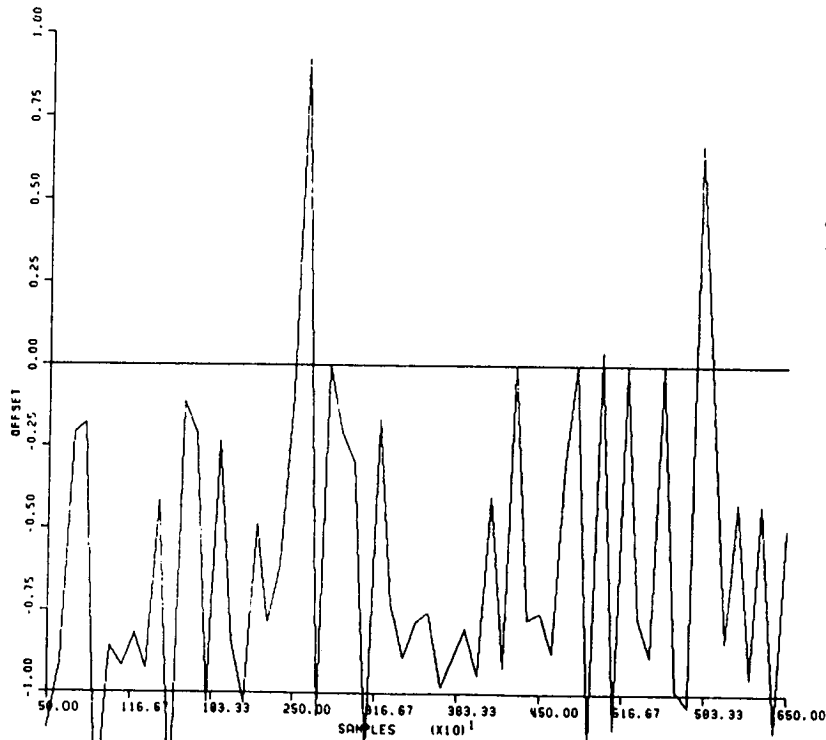
LINE MATCH FOR BANDS 1 AND 5. LINE 6. LANDSAT TM

Figure 2b: Interband linematch correlation between bands 1 (primary focal plane) and 5 (secondary focal plane) for Harrisburg P-tape.

49

THE USE OF LINEAR FEATURE DETECTION TO INVESTIGATE
THEMATIC MAPPER DATA PERFORMANCE AND PROCESSING

CHARLOTTE M. GURNEY

SYSTEMS AND APPLIED SCIENCES CORPORATION

Geometric and radiometric characteristics of Thematic Mapper data are investigated through analysis of linear features in the data. A linear feature is defined as two close, parallel and opposite edges. Examples in remotely sensed data are such features as rivers and roads.

Linear features are detected using a local operator which considers the arrangement of grey levels in a 5 by 5 pixel array. Results depend upon the contrast between line and background material, feature width, feature alignment with the pixel boundaries, and the detector threshold. The detector threshold refers to the degree of difference which must exist between line and background before a pixel is accepted as being part of a linear feature. At low thresholds all of a feature may be detected, as the threshold is increased less of the feature will be detected.

If it is assumed that the percent material in a pixel is linearly proportional to its contribution to the reflectance, and that every alignment of the feature with the pixel boundaries is equally probable then a set of expressions may be derived relating the model parameters.

For lines up to 1 pixel wide:

$$T = 3bW - (3bW - bW/2)A \tag{1}$$

where

T = detector threshold

A = % accuracy / 100

b = contrast = $(|\text{background mean} - \text{line mean}|)/100$

W = line width as a % of pixel width

Similarly for lines 1-2 pixels wide:

$$T = 300b - \left[\frac{3b(100-W)}{2} \right] \quad \left[1 + A \right] \qquad (2)$$

Contrast measurements may be made by selecting training areas corresponding to known linear and background materials and using the mean grey level in these areas. Since the contrast is based on the mean values it is apparent that high variances within a training area will lead to results which conform less closely to the theoretical expectations of the model.

Using TM data for Iowa, containing a uniform grid network of roads, the linear feature detection procedure was applied at the same threshold for all bands. Variations in results therefore reflected differences in scene contrast and variance from band to band. Band 6 failed to detect any linear features. For bright linear features bands 1 and 3 gave the best results, but bands 2, 5 and 7 also performed well. Band 4 was distinctive in that field boundaries were detected in preference to the road network. For dark linear features both bands 4 and 5 gave good results.

The model described above was used to estimate the widths of linear features in two highly contrasting areas. This was undertaken in order to establish the utility of the model for this purpose and to ensure that the ground IFOV meets pre-launch specifications.

The first test area was taken from TM data of North Carolina in an area with a homogeneous, flat background traversed by narrow gravel roads. The second area was from TM data northwest of Washington, D. C. containing the Washington beltway (width approximately 50m) against a heterogeneous background. For each test area sites were selected to establish line: background contrast. The detection procedure was then applied at at least three different thresholds. The resulting detection accuracies were computed and results substituted in the equations given above. The feature width as a percent of the pixel width was then estimated.

For the North Carolina data band 6 results were too poor to use and were discarded. With the exception of band 4 all the other bands gave very similar results leading to a road width estimate of 6 metres assuming a 28.5 by 28.5m pixel. Band 4 gave a larger width estimate; this band also had a relatively high variance of line and background materials.

Bands 6 and 4 were discarded from the Washington, D. C. results since they had such poor contrasts. Of the remaining bands, bands 1-3 gave closely corresponding results with a width estimate of 50 metres. However bands 5 and 7 both over-estimated the width by about 6 metres. This mis-estimate is tentatively attributed to the relatively poor contrast for these bands, or to a mis-estimation of the contrast.

Linear feature detection was also used to investigate band : band registration by superimposing detection results from different bands. Shifts of less than 1 pixel in both x and y directions between primary and cold focal planes were observed.

It is concluded that the geometric and radiometric precision of TM data is sufficiently good to allow accurate measurement of linear feature widths. Results also confirm a 28.5m ground IFOV as specified prior to launch. The increase dimensionality of the TM data as compared with MSS data allows the possibility of independent verification of results by using data from several bands. Under good conditions features as narrow as one quarter of a pixel in width may be accurately measured. These results have considerable potential for applications and in hydrology or topographic mapping.

SPATIAL RESOLUTION ESTIMATION OF LANDSAT-4 TM DATA

CLARE D. MCGILLEM, PAUL E. ANUTA AND ERICK MALARET
PURDUE UNIVERSITY

KAI-BOR YU
VIRGINIA POLYTECHNIC INSTITUTE

Satellite-based multispectral imaging systems have been in operation since 1972 and the latest in the Landsat series of sensors was launched in July 1982. One system parameter of interest is resolution and this paper discusses experiments to determine the actual overall resolutions after launch. Atmospheric effects and post processing effects add to the prelaunch optical resolution. Scene structures, such as roads and field edges, were used with numerical estimation procedures to predict resolution in Landsat-4 Thematic Mapper imagery. A nominal resolution of 39 meters was determined as compared to the predicted 30m prelaunch value.

AN ANALYSIS OF THE HIGH FREQUENCY VIBRATIONS
IN EARLY THEMATIC MAPPER SCENES

JOHN KOGUT AND ELAINE LARDUINAT
RESEARCH AND DATA SYSTEMS, INC.

The potential effects of high frequency vibrations on the final Thematic Mapper (TM) image have been evaluated for 26 scenes between day 4 and day 50 after LANDSAT-4 launch. The angular displacements of the TM detectors from their nominal pointing directions as measured by the TM Angular Displacement Sensor (ADS) and the spacecraft Dry Rotor Inertial Reference Unit (DRIRU) give data on the along scan and cross scan high frequency vibrations present in each scan of a scene. These measurements were used to find the maximum overlap and underlap between successive scans, and to analyze the spectrum of the high frequency vibrations acting on the detectors.

The history of the scan overlap and underlap for this time period shows that a consistent underlap which was present immediately after launch disappeared after day 10. The maximum overlap/underlap within a scene stabilized after day 15 from launch to an average of -0.337 pixels / +0.358 pixels for the reflective bands, and -0.034 pixels / +0.141 pixels for band 6.

The Fourier spectrum of the along scan and cross scan vibrations for each scene was also evaluated. In the scenes analyzed, the along scan high frequency vibrations were strongly concentrated at 7 Hz and had amplitudes of about 80 microradians. Additional vibration peaks were present in the 56 Hz to 77 Hz range. Cross scan vibrations were also concentrated at 7 Hz and had amplitudes near 7 microradians. For the cross scan data additional spectral peaks occurred at 21 Hz and in the 56 Hz to 67 Hz range. The spectra of the scenes examined indicate that the high frequency vibrations arise primarily from the motion of the TM and MSS mirrors, and that their amplitudes are well within expected ranges.

ASSESSMENT OF THEMATIC MAPPER BAND-TO-BAND REGISTRATION
BY THE BLOCK CORRELATION METHOD

DON H. CARD AND ROBERT C. WRIGLEY
NASA/AMES RESEARCH CENTER

FREDERICK C. MERTZ AND JEFF R. HALL
TECHNICOLOR GOVERNMENT SERVICES, INC.
AMES RESEARCH CENTER

The design of the Thematic Mapper (TM) multispectral radiometer makes it susceptible to band-to-band misregistration. The non-cooled detectors of the visible and near-infrared bands (TM bands 1-4) and the cooled detectors of the middle and thermal-infrared bands (TM bands 5-7) are located on separate focal planes in the sensor. In addition, there are several compensation devices in effect, such as the Scan Line Corrector (SLC), and the Attitude Displacement Sensor. This creates the potential for inter-band misregistration, and could have serious consequences for the use of TM data in applications that rely on simultaneous observations. To estimate band-to-band misregistration a block correlation method was employed. This method was chosen over other possible techniques (band differencing and flickering) because quantitative results are produced. The method used correlates rectangular blocks of pixels from one band against blocks centered on identical pixels from a second band. The block pairs are shifted in pixel increments both vertically and horizontally with respect to each other and the correlation coefficient for each shift position is computed. The displacement corresponding to the maximum correlation is taken as the best estimate of registration error for each block pair. Subpixel shifts were estimated by a bi-quadratic interpolation of the correlation values surrounding the maximum correlation. To obtain statistical summaries for each band combination post-processing of the block correlation results was performed. Editing of the data consisted of deleting blocks that had low correlation values. This procedure tended to eliminate blocks having obviously high positive or negative shifts. However, not all outliers were eliminated, therefore a further step was to discard high shift values by keeping only those shifts within a specified threshold.

TABLE 1

Descriptive statistics for band-to-band misregistration for selected Thematic Mapper band combinations (Arkansas scene - August 22, 1982). The first band listed in each set is the primary band for the correlations, and all correlation blocks having the correlation coefficient $<.6$ were discarded. (Unit of misregistration (shift) is in pixels).

TM Bands	Shift Direction	Number of Blocks	Mean Shift	S.D.	Min Shift	Max Shift	95% Conf. Int. for Mean Shift
3 vs 1	Across-scan	256	-.04	.06	-.2	.2	(-.05,-.03)
	Along-scan	256	-.03	.06	-.4	.1	(-.04,-.02)
3 vs 4	Across-scan	44	-.03	.33	-1.0	1.1	(-.13,.07)
	Along-scan	44	.10	.38	-.4	1.9	(-.02,.22)
3 vs 5	Across-scan	217	.22	.73	-9.3	3.3	(.12,.32)
	Along-scan	217	.49	.41	-2.7	4.0	(.44,.54)
3 vs 7	Across-scan	264	.16	.20	-.4	2.2	(.14,.18)
	Along-scan	264	.49	.18	-.4	1.1	(.47,.51)
7 vs 5	Across-scan	280	.06	.09	-.5	.6	(.05,.07)
	Along-scan	280	-.01	.07	-.4	.3	(-.02,.0)
6 vs 7	Across-scan	4	-3.50	1.04	-4.7	-2.2	(-5.2,-1.8)
	Along-scan	4	-3.20	2.31	-4.9	.2	(-6.9,.48)

The fundamental results of the block correlation analysis for selected TM band combinations are displayed in Table 1. The table shows the results of editing the shift data by discarding all shift values having corresponding correlations less than 0.6. In order to show that this editing procedure is reasonable, band pairs 3 vs. 5 and 6 vs. 7 were subjected to further editing. These pairs were selected because they showed the largest

outliers in Table 1. Band pair 3 vs. 5 was edited by discarding blocks that either had shifts outside the range -3 to 3 pixels or had correlations <0.6. Similarly, band pair 6 vs. 7 was edited by discarding blocks that either had shifts outside the range -10 to 10 or had correlations <0.3. The results, show that the mean shift values are quite robust to the editing procedure (discarding shifts based on correlation thresholds and shift values). Additionally, Table 1 shows that the target specification for TM band-to-band registration of 0.2 pixels is easily achieved for those band combinations within the same focal plane (bands 1 vs. 3 and 3 vs. 4 in the non-cooled focal plane, and bands 5 vs. 7 in the cooled focal plane), with the exception of bands 6 vs. 7. Band 6 presents special problems, which will be discussed below. Although the shift for bands 3 vs. 4 was within the 0.2 pixel specification, the standard deviations of across-scan and along-scan shifts were higher than the 1-3 and 5-7 band pairs, and far fewer blocks were retained after editing (44 out of 297). The relatively poor performance for bands 3 and 4 is apparently due to the inverse correlation between spectral responses in the visible and near IR bands.

A relatively large and consistent shift between bands in different focal planes (bands 3 vs. 5 and 3 vs. 7) is evident in Table 1; the along-scan shift is larger than the permitted 0.3 pixel misregistration specification. This result confirmed an earlier visual assessment using the flickering method, in which an approximate shift of a half pixel was noted in the along-scan direction (band 3 vs. 5). Given that the GSFC TM data processing software can correct sub-pixel misregistrations, we suggest that the appropriate shifts reported here be implemented to correct the misregistration between the uncooled and cooled focal planes. For the TM scene analyzed, the recommended shift corrections should be 0.5 pixels along-scan and 0.2 pixels across-scan.

Band 6 presents a special problem, in that it had a very low correlation with band 7, and therefore editing was much more difficult as evidenced in Table 1 (only 4 blocks with correlations above 0.6 were retained). Flickering between bands 6 and 7 indicated a poor visual correlation but verified an approximate 4 pixel shift. As noted earlier, the shift estimates for band 6 vs. band 7 seem to be quite robust to the editing

procedure. Based on these results, we suggest correcting the band 6 misregistration by shifts of 3 pixels (28.5 meters) in both the along-scan and the across-scan directions.

In summary it can be stated that the block correlation method is a reasonable approach to the quantitative assessment of band-to-band misregistration. It is quite robust to the method of editing outliers and seems to result in estimates of registration error that are consistent with expectations. For the band combinations studied the following conclusions can be drawn:

1. The misregistration of TM spectral bands within the non-cooled focal plane lie well within the 0.2 pixel target specification (TM Bands 3 vs. 1 and 3 vs. 4).

2. The misregistration between the middle IR bands (TM Bands 5 and 7) is well within the 0.2 pixel specification.

3. The thermal IR band has an apparent misregistration with TM Band 7 of approximately 3 pixels in each direction.

4. TM Band 3 has a misregistration of approximately 0.2 pixel in the across-scan direction and 0.5 pixel in the along-scan direction, with both TM Bands 5 and 7.

TESTS OF LOW-FREQUENCY GEOMETRIC DISTORTIONS IN LANDSAT-4 IMAGES

R. M. BATSON AND W. T. BORGESON
U. S. GEOLOGICAL SURVEY, FLAGSTAFF

ABSTRACT

The geometric fidelity of the GSFC filmwriter used for Thematic Mapper (TM) images was assessed by measurement with accuracy better than three micrometers of a test grid. A set of 55 control points with known UTM coordinates was measured on a digital display of part of band 5 of the TM image of the Washington, D. C. area and fitted to the control points. The tests indicate that the geometric fidelity of TM images is likely to be higher than the ability of film recorders to reproduce the images.

INVESTIGATION OF TM BAND-TO-BAND REGISTRATION USING
THE JSC REGISTRATION PROCESSOR

S. S. YAO AND M. L. AMIS
LOCKHEED ENGINEERING AND MANAGEMENT SERVICES COMPANY, INC.

Several Thematic Mapper (TM) scenes from the Goddard Space Flight Center (GSFC) SCROUNGE processing system were available at the Johnson Space Center (JSC) for preliminary investigation. One area of interest to the investigators is the accuracy of the TM band-to-band registration. The detectors for the seven-band TM system are placed in two groups aboard the spacecraft: located at the primary focal plane are detector arrays for bands 1 to 4, while the remaining detectors are placed on the cold focal plane.

Software in the SCROUNGE system is used to register the bands together to an accuracy of less than 0.3 pixel, or approximately 9 meters on the ground. Given this level of accuracy, it is expected that the data from the first four bands would register to each other better than those between band 4 and band 5, for example. In the current investigation, the JSC registration processor is used to study the registration between TM bands, with special attention given to band 6, the thermal band. Band 6 has a resolution four times coarser than the other bands.

The JSC registration processor performs scene-to-scene (or band-to-band) correlation based on edge images. The edge images are derived from a percentage of the edge pixels calculated from the raw scene data, excluding clouds and other extraneous data in the scene. Correlations are performed on patches (blocks) of the edge images, and the correlation peak location in each patch is estimated iteratively to fractional pixel location accuracy. Peak offset locations from all patches over the scene are then considered together, and a variety of tests are made to weed out outliers and other inconsistencies before a distortion model is assumed. Thus, the correlation peak offset locations in each patch indicate quantitatively how well the two TM bands register to each other over that patch of scene data. The average of these offsets indicate the overall accuracies of the band-to-band registration. For registration between band 3 to band 4 from

the same focal plane, for example, the root-mean-square (rms) error of registration was shown to meet the specification of 0.3 pixel. Between band 4 and band 5 from two different focal planes, the rms error was larger. Band 6, the thermal band, was shown to be misregistered to band 4 by as much as 3.73 pixels rms.

The JSC registration processor was also used to register one acquisition to another acquisition of multitemporal TM data acquired over the same ground track. Band 4 images from both acquisitions were correlated and an rms error of a fraction of a pixel was routinely obtained.

GEODETIC ACCURACY OF LANDSAT-4 MULTISPECTRAL SCANNER AND THEMATIC MAPPER DATA

J. M. THORMODSGARD AND D. J. DEVRIES

U. S. GEOLOGICAL SURVEY, EROS DATA CENTER

ABSTRACT

EROS Data Center is evaluating the geodetic accuracy of Landsat-4 data from both the Multispectral Scanner (MSS) and Thematic Mapper (TM) processing systems. Geodetic accuracy of Landsat data is a measure of the precise registration to the Earth's figure.

Standard geometrically corrected Landsat-4 digital products are either system-corrected or ground control point (GCP) corrected. System-corrected data are processed to remove the geometric distortions caused by the sensor, the spacecraft platform, and terrestrial effects. GCP-corrected data have ground control points applied to further adjust the data to the Earth's surface. Geodetic accuracy of both system- and GCP-corrected MSS data and system-corrected TM data was measured.

The geometric processing of Landsat data includes mapping or registering a portion of the Earth's spherical surface on to a flat image plane creating a map projection. For every geodetic (latitude and longitude) location within the image, map projection coordinates can be computed. The standard Landsat-4 MSS and TM digital tapes contain information which relates the applied map projection coordinate system to the image coordinate (line and sample) system. By converting the latitude and longitude of a given location to the map projection coordinates, the image coordinate location can be calculated.

An assessment of geodetic accuracy of an MSS or TM scene is accomplished using a minicomputer and appropriate software, digitizer, and an image display device. The calculated image location of a selected feature is compared with the actual image location obtained through visual inspection of

the image on the display. Measurements of 15 to 20 features evenly distributed throughout the image provide an estimate of the geodetic accuracy of the scene.

Tests of two system-corrected MSS scenes measured geodetic registration root-mean-square (RMS) errors of approximately 3,200m or 57 pixels. Tests of two TM system-corrected scenes measured RMS errors of approximately 1,250 and 1,000m, or 44 and 35 pixels, respectively. All errors were primarily translational, implying good internal scene registration of both MSS and TM data. The one MSS GCP-corrected scene which was evaluated had an RMS error of approximately 325 m or 6 pixels.

THE EFFECT OF POINT-SPREAD FUNCTION INTERACTION WITH RADIANCE FROM HETEROGENEOUS SCENES ON MULTITEMPORAL SIGNATURE ANALYSIS

M. J. DUGGIN AND L. B. SCHOCH

STATE UNIVERSITY OF NEW YORK/SYRACUSE

The purpose of this report is to demonstrate that the point-spread function is an important factor in determining the nature of feature types on the basis of multispectral recorded radiance, particularly from heterogeneous scenes and particularly from scenes which are imaged repetitively, in order to provide thematic characterization by means of multitemporal signature.

Consider a cloud-free image consisting of n different reflecting elements, each occupying a fractional area a_n of the pixel (IFOV). Then the recorded radiance would be, in band r

$$L_r(\theta',\phi') = \frac{\int_{\lambda_1}^{\lambda_2} I(\lambda) \cdot [E(\theta,\phi,\lambda) \cdot \int_0^x \int_0^y \{g_1(x,y) \cdot R_1(\theta,\phi;\theta',\phi',\lambda)P_1(x,y) \\ + g_2(x,y) \cdot R_2(\theta,\phi;\theta',\phi',\lambda)P_2(x,y) \\ + \ldots + g_n(x,y) \cdot R_n(\theta,\phi;\theta',\phi',\lambda)P_n(x,y)\} \cdot \tau(\theta',\phi',\lambda) \cdot dy \cdot dx \\ + L(\theta_1,\phi_1;\theta_1',\phi_1',\lambda)] \, d\lambda}{\int_{\lambda_1}^{\lambda_2} I(\lambda) \cdot d\lambda} \qquad -(1)$$

where $I(\lambda)$ is the spectral response of the sensor and λ_1, λ_2 are the lower and upper zero power bandpass limits of the sensor, respectively

$E(\theta,\phi,\lambda)$ is the scalar global spectral radiance incident on the pixel

(θ',ϕ',λ) is the atmospheric transmission along the path from the pixel to the sensor

$R_n(\theta,\phi; \theta',\phi',\lambda)$ is the spectral hemispherical-conical reflectance factor for scene element n, which occupies fractional area a_n of the heterogeneous pixel

$P_n(x,y)$ is the point-spread function at position x,y in the pixel

$g_n(x,y)$ is a delta function which equals 1 if scene element n is present at (x,y), but is otherwise zero $\int_0^X \int_0^Y g_n(x,y)dydx = a_n$

$L(\theta_1, \phi_1; \theta'_1, \phi'_1, \lambda)$ is the path radiance for the sun-scattering center-sensor geometry defined by $(\theta_1, \phi_1; \theta'_1, \phi'_1)$ which will differ from the sun-target-sensor geometry $(\theta,\phi; \theta', \phi')$.

To demonstrate the effect of the interaction of scene heterogeneity with the point spread function (PSF)[1], we have constructed a template from the line spread function (LSF) data of Schueler[2] for the thematic mapper (TM) photoflight model and have moved this in 0.25 (nominal) pixel increments in the scan line direction across three scenes of different heterogeneity. We have calculated the sensor output by considering the calculated scene radiance from each scene element occuring between the contours of the PSF template, plotted on a movable mylar sheet while it was located at a given position.

Scene 1, shown in Figure 1 consists of two components: Healthy soybeans and soybeans affected by stress (rust) at the 11.5% severity level. The linear boundary between these two scene components, whose spectral reflectance[3] is shown in Figure 2, lies along track and is perpendicular to the scan direction. Figure 3 shows the calculated radiance in TM bands 1 and 4 (half-power bandwidths 0.45-0.52μm and .76-.90μm respectively) and the ratio of the radiance for TM band 4/band 1. While extensive changes are seen in the single band radiance levels (up to ± 20% in TM band 4, but only ± 2% in TM band 1), a large change (approximately ± 20%) is observed in the ratio TM4/TM1. Figure 4 shows a target in which healthy and stressed (11.5% severity level) soybean plots were considered to exist in an alternating fashion, with exactly a one TM pixel size. The TM PSF template is shown overlaid in order to indicate that a considerable degree of radiance from surrounding pixels is recorded by the sensor, even ignoring the atmospheric

modulation transfer function, which must increase forward scattering. Movement of the PSF by 0.25 pixel increments produces the single band radiance values and TM4/TM1 ratio shown in Figure 5; about one half of the change seen in the case of the single boundaries. An even more homogeneous case is shown in Figure 6, where areas of 0%, 4.75% and 11.5% soybean stress severity are shown in alternating 10 m x 10 m square positions (TM pixel size is 30 m x 30 m nominally). Figure 7 shows the variation of TM1, TM4 radiance values and of the radiance ratio TM4/TM1 as the PSF is moved 0.25 pixel at a time across the IFOV: here the changes are on the order of about ± 3%.

Several facts emerge:

(a) The more heterogeneous the target, the larger the amplitude of the variation in the single band radiance as the PSF peak moves across the scene

(b) The amplitude of the variation in radiance discussed in (a) is reduced as the heterogeneity of the pixel decreases

(c) In the event of multitemporal analysis, the study of the temporal change in signature from a given area may be affected by the error in relocating sequential images (i.e. to a fraction of a pixel)

(d) More data is needed on the PSF's of all sensors which are to be used in studying heterogeneous scenes, especially in the multitemporal mode, so that criteria of superposition accuracy may be fully assessed

(e) The further effect on radiometry of pixel and line re-sampling needs to be considered insofar as it affects multitemporal analysis

(f) More work is needed to study the effects on recorded radiance of the relative juxtaposition of scene elements of different optical properties and heterogeneities

(g) More work is needed to study the effects of the atmosphere on the PSF

(h) More work is needed to study the effects of unresolved cloud, which will modify equation (1) by the addition of a term:

$$L_r(\theta',\phi') = \frac{\int_{\lambda_1}^{\lambda_2} I(\lambda).[E(\theta,\phi,\lambda).\int_0^x \int_0^y \{g_1(x,y)R_1(\theta,\phi;\theta',\phi',\lambda).P_1(x,y)}{\int_{\lambda_1}^{\lambda_2} I(\lambda).dx}$$

$$+ g_2(x,y).R_2(\theta,\phi;\theta',\phi',\lambda).P_2(x,y) + \dots$$

$$+ g_n(x,y).R_n(\theta,\phi;\theta',\phi',\lambda).P_n(x,y) + \dots$$

$$+ g_c(x,y).R_c(\lambda)\}.\tau(\theta',\phi',\lambda) \, dy.dx$$

$$+ L(\theta_1,\phi_1;\theta_1',\phi_1',\lambda)] \, d\lambda$$

$$\qquad \qquad \qquad \qquad \qquad \qquad \qquad \qquad \qquad \qquad \qquad -(2)$$

where g_1 is the fractional proportion of the pixel filled by cloud and where $R_c(\lambda)$ is the (nearly Lambertian) reflectance factor of cloud.

REFERENCES

1.   Forshaw, M. R. B.; Haskell, A.; Miller, P. F.; Stanley, D. J. and Townshend, J. R. G. (1983), "Spatial resolution of remotely sensed imagery: a review paper", Int. Jol. Remote Sensing 4, 497.

2.   Schueler, C., (1983), "Thematic mapper protoflight model line spread function". Seventeenth Internat. Symp. on Remote Sensing of Environment, Ann Arbor, Michigan, May 9-13, Proc. in press.

3.   Casey, P. and Duggin, M. J., unpublished data.
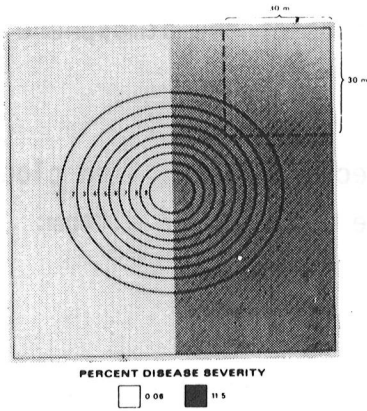
Figure 1
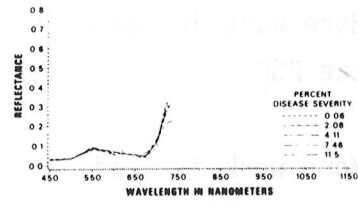
Figure 2
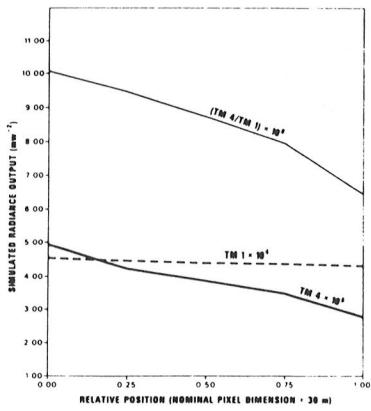
Figure 3
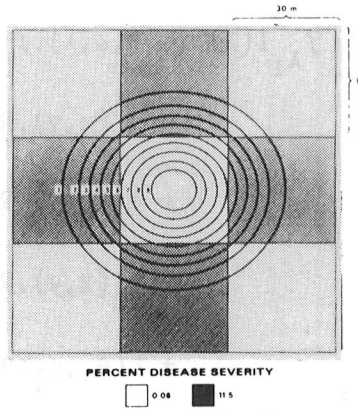
Figure 4
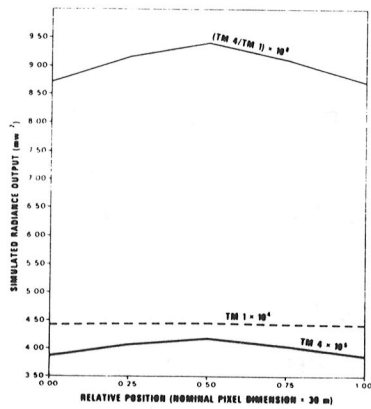
Figure 6
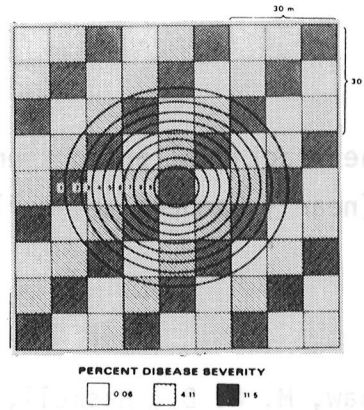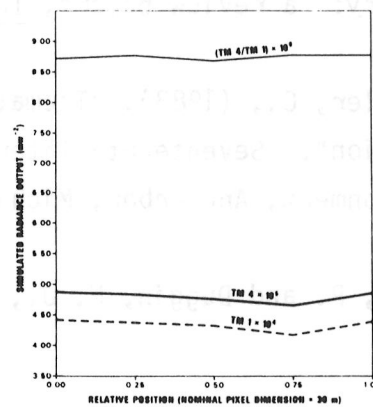
Figure 5

Figure 7

RADIOMETRIC ACCURACY ASSESSMENT OF LANDSAT-4 MULTISPECTRAL SCANNER (MSS) DATA

WILLIAM L. ALFORD
MARC L. IMHOFF
NASA/GODDARD SPACE FLIGHT CENTER

ABSTRACT

The Landsat-4 mission has unique characteristics relative to previous Landsat missions. The spacecraft is new; the orbit is lower with a more frequent repeat cycle; and the ground processing facility consists of new hardware with different algorithms being applied. This study explores how some of these changes have affected the character of the radiometric data quality. Specifically, this paper examines banding effects, radiometric differences between Landsat 3 and 4, and the woodgrain pattern observed visually in the images.

BANDING EFFECTS

Banding effects within each channel were examined using a Landsat-4 image data set calibrated with the old Landsat 2/3 cal-wedge method and with the new histogram method. Data subsets consisting of 400 lines each were created from each of the 24 channels. These were subsequently divided into four 100-line segments. For each segment, the channel means within each band were compared. The improvement in image data quality using histogram calibrations rather than cal-wedge calibrations was clearly demonstrated. The peak to peak range was typically 0.4 with a worst case of 0.62 for the cal-wedge calibrated data, whereas the histogram calibrated data was typically 0.1 peak-to-peak with the worst case being 0.24.

LANDSATS 3 AND 4 RADIOMETRIC COMPARISON

A direct comparison between Landsat-3 and Landsat-4 MSS data was possible with a near simultaneous overpass of both satellites. An area in Vermont was selected where Landsats 3 and 4 passed within two minutes of each

other with scene centers separated by about 10 minutes latitude and 14 minutes longitude. Nine uniform polygonal areas that approximately corresponded to the same ground scene were selected from each image. The means of each area were computed and a linear regression calculated for each band as shown in Table 1.

BANDS	A	B	R^2
1	1.03	0.84	.99
2	0.91	-0.27	.99
3	1.09	0.58	.99
4	0.87	0.42	.99
(Landsat-4 Value) = A x (Landsat-3 Value) + B			

TABLE 1.   RELATIONSHIP BETWEEN THE PIXEL VALUES OF THE LANDSATS 3 AND 4 MSS INSTRUMENTS BASED ON IMAGE DATA VALUES.

Prelaunch calibrations combined with post-launch data were used by the Landsat-D Project to derive values known as R_{max} and R_{min}. These are the radiance values associated with pixel values 127 and 0 respectively. R_{max} and R_{min} values from both the Landsat-3 and 4 MSS's were used also to derive a linear relationship between the two instruments. These coefficients are shown in Table 2. Ideally, the coefficients in both tables should be the same. However, the observed coefficient differences are large enough to cause a 10% difference in some computed quantization levels. Since the residuals in the regression calculations were small and since other data analyzed supported the values of the coefficients in Table 1, we conclude that the coefficients in Table 2 are in error and consequently that some or all of the R_{max} and R_{min} values are in error.

BAND	Landsat-3 (after 5/31/78) R_{min} at 0	Landsat-3 (after 5/31/78) R_{max} at 127	Landsat-4 (after mid Aug 82) R_{min} at 0	Landsat-4 (after mid Aug 82) R_{max} at 127	A	B
1	0.04	2.59	0.02	2.30	1.12	1.11
2	0.03	1.79	0.04	1.80	1.00	-0.72
3	0.03	1.49	0.04	1.30	1.16	-1.01
4	0.03	3.83	0.01	4.00	0.97	-2.28

$$\text{milliwatt cm}^{-2}\ \text{steradian}^{-1}$$

$$(\text{Landsat-4 value}) = A \times (\text{Landsat-3 value}) + B$$

TABLE 2. RELATIONSHIP BETWEEN THE PIXEL VALUES OF THE
LANDSAT 3 AND 4 INSTRUMENTS BASED ON R_{max} AND R_{min} VALUES

WOODGRAIN PATTERN

A woodgrain or diagonal pattern was observed in all of the MSS images. This pattern was especially visible over uniform areas such as water. The pattern appears visually to be the same whether the Thematic Mapper instrument was on or off. This type of pattern or noise is typically caused by one or more spurious sine waves interacting with the analog to digital converter. One assumption fundamental to the analysis is that the noise is the same for all analog channels at the input to the multiplexer/analog-to-digital converter subsystem.

Based on this assumption, pixels from the 24 channels were reordered into a single sequence in the order the pixels were sampled on the spacecraft. An interpolated 25th sample was included in this resequenced data since the format allowed space for thermal band samples. The effect of resequencing was to provide a time sequence that is sampled 25 times higher than any one channel.

Fourier analysis performed on resequenced data of several scenes from Landsat-D, including prelaunch test data, produced similar patterns in the frequency amplitude domain. Most of the frequency components appear to originate from a common source with a fundamental frequency of 114,504 Hz. (A drifting voltage supply oscillator on Landsat-4 operates at about 115 kHz.)

Excepting three frequency components, each component can be accounted for by one of the first 35 harmonics of 114,504 Hz taking into account aliasing effects. However, this may not be the physical source for these frequencies. Two frequencies with inter-modulation products can also account for these components.

We conclude that the Landsat-4 MSS data will have less banding problems than previous MSS data. However, there is an increased noise problem that appears visually as a wood grain pattern. When compared with Landsat-3 data and taking into account the absolute calibration parameters (R_{max} and R_{min}), there are inconsistencies between corresponding data samples. Consequently, absolute calibration cannot be assured at this time.

SPECTRAL CHARACTERIZATION OF THE LANDSAT-4 MSS SENSORS

BRIAN L. MARKHAM AND JOHN L. BARKER
NASA/GODDARD SPACE FLIGHT CENTER

Relative spectral response data for the Landsat-4 and Landsat-4 backup multispectral scanner subsystems (MSS), the protoflight and flight models, respectively, are presented and compared to similar data for the Landsat 1, 2 and 3 scanners. Channel-by-channel (six channels per band) outputs for soil and soybean targets were simulated and compared within each band and between scanners. The two Landsat-4 scanners proved to be nearly identical in mean spectral response, but they exhibited some differences from the previous MSS's (Table 1). Principal differences between the spectral responses of the Landsat-4 scanners and previous scanners were: (1) a mean upper-band edge in the green band of 606 nm compared to previous means of 593 to 598 nm, (2) an average upper-band edge of 697 nm in the red band compared to previous averages of 701 to 710 nm, and (3) an average bandpass for the first near-IR band of 702-814 nm compared to a range of 693-793 to 697-802 nm for previous scanners. These differences caused the simulated Landsat-4 scanner outputs to be 3 to 10 percent lower in the red band and 3 to 11 percent higher in the first near-IR band than previous canners for the soybeans target. Otherwise, outputs from soil and soybean targets were only slightly affected. The Landsat-4 scanners were generally more uniform from channel to channel within bands than previous scanners. One notable case of poor uniformity was the upper-band edge of the red band of the protoflight scanner, where one channel was markedly differently (12 nm) from the rest. For a soybeans target, this nonuniformity resulted in a within-band difference of 6.2 percent in simulated outputs between channels.

Table 1
Spectral Characterization of Landsat MSS'S by Means (Averages of Six Channels)
and Standard Deviations (Each Channel Considered an Observation):
PF (Landsat-4), F (Landsat-4 backup), MSS-1, MSS-2, MSS-3.

a. Band 1 (500-600 nm)

	SCANNER	BAND EDGE (nm) LOWER	UPPER	WIDTH[a] (nm)	SLOPE INTERVAL (nm) LOWER	UPPER	SPECTRAL FLATNESS POSITIVE	NEGATIVE
MEANS	PF	495	605	109	15	23	5.1[b]	8.9[b]
	F	497	607	109	15	21	5.0	11.2[b]
	1[*]	501	599	98	15	27	7.1[b]	16.1[b]
	1[**]	499	597	98	15	27	6.1[b]	14.6[b]
	2	497	598	101	15	22	5.4[b]	14.1[b]
	3	497	593	96	16	22	5.4[b]	19.2[b]
STANDARD DEVIATIONS	PF	0.5	1.2	0.8	0.3	1.0	1.0	2.7
	F	0.8	0.8	0.5	0.6	0.7	0.6	3.4
	1[*]	6.5	4.1	3.5	1.6	5.6	2.4	6.4
	1[**]	5.3	3.0	3.5	1.8	5.4	0.4	5.8
	2	1.4	1.4	1.8	1.2	0.6	2.4	3.5
	3	3.7	2.5	3.8	3.2	3.4	1.5	7.8

[*]WITH OUTLIER CHANNEL INCLUDED a — NO FILTER SPECIFICATION
[**]WITH OUTLIER CHANNEL EXCLUDED b — FAILS TO MEET FILTER SPECIFICATION

BOXES INDICATE CHARACTERISTICS WHERE DIFFERENCES BETWEEN PF OR F AND ALL PREVIOUS
SCANNERS (1,2,3) WERE GREATER THAN DIFFERENCES BETWEEN TWO SETS OF PF MEASUREMENTS.

b. Band 2 (600-700 nm)

	SCANNER	BAND EDGE (nm) LOWER	UPPER	WIDTH[a] (nm)	SLOPE INTERVAL (nm) LOWER	UPPER	SPECTRAL FLATNESS POSITIVE	NEGATIVE
MEANS	PF[*]	603	698	95	12	16	7.0	12.9[b]
	PF[**]	603	696	93	12	16	6.7	12.0[b]
	F	603	697	94	12	15	7.6[b]	11.1[b]
	1	603	701	97	15	26	9.0[b]	13.3[b]
	2[*]	607	710	103	14	30	7.9[b]	18.0[b]
	2[**]	607	710	103	14	29	7.8[b]	16.8[b]
	3	606	705	100	14	31	7.2	17.2[b]
STANDARD DEVIATIONS	PF[*]	0.7	4.7	4.8	0.5	1.9	1.4	2.5
	PF[**]	0.8	0.8	0.6	0.5	1.4	1.5	1.4
	F	0.4	0.6	0.5	0.4	0.9	1.2	3.0
	1	3.5	2.2	2.8	1.7	3.4	3.4	2.8
	2[*]	0.6	0.8	1.0	1.2	3.6	1.1	4.5
	2[**]	0.6	0.9	1.1	1.2	1.0	1.2	3.8
	3	0.9	1.2	0.8	0.8	2.0	2.0	4.8

[*]WITH OUTLIER CHANNEL INCLUDED a — NO FILTER SPECIFICATION
[**]WITH OUTLIER CHANNEL EXCLUDED b — FAILS TO MEET FILTER SPECIFICATION

BOXES INDICATE CHARACTERISTICS WHERE DIFFERENCES BETWEEN PF OR F AND ALL PREVIOUS
SCANNERS (1,2,3) WERE GREATER THAN DIFFERENCES BETWEEN TWO SETS OF PF MEASUREMENTS.

Table 1 continued.

c. Band 3 (700-800 nm)

SCANNER	BAND EDGE (nm) LOWER	UPPER	WIDTH[a] (nm)	SLOPE INTERVAL (nm) LOWER	UPPER	SPECTRAL FLATNESS POSITIVE	NEGATIVE
MEANS							
PF	701	813[b]	112	15	15	13.2[b]	12.8[b]
F	704	814[b]	110	16	14	12.6[b]	9.6[b]
1	694	800	105	19	35	7.2[b]	7.4[b]
2	697	802	106	16	34	8.4[b]	7.9[b]
3	693	793	100	19	32	9.9[b]	22.2[b]
STANDARD DEVIATIONS							
PF	0.7	0.9	1.1	0.3	0.5	2.9*	2.9*
F	0.3	0.2	0.3	1.0	0.3	1.1*	0.8*
1	0.9	1.0	0.9	2.0	3.8	3.2	2.9
2	1.1	2.3	2.1	0.6	2.7	3.0	1.9
3	1.8	1.6	0.8	1.4	1.1	2.7	3.4

*PF, F DIFFERENCE EXCEEDS DIFFERENCE BETWEEN TWO SETS OF PF MEASUREMENTS

a — NO FILTER SPECIFICATION
b — FAILS TO MEET FILTER SPECIFICATION

BOXES INDICATE CHARACTERISTICS WHERE DIFFERENCES BETWEEN PF OR F AND ALL PREVIOUS SCANNERS (1,2,3) WERE GREATER THAN DIFFERENCES BETWEEN TWO SETS OF PF MEASUREMENTS.

d. Band 4 (800-1100 nm)

SCANNER	BAND EDGE (nm) LOWER	UPPER	WIDTH[a] (nm)	SLOPE INTERVAL (nm) LOWER	UPPER[a]	SPECTRAL FLATNESS POSITIVE	NEGATIVE
MEANS							
PF	808	1023	215	23	110	29.8[b]	53.7[b]
F	809	1036	227	23	101	23.0[b]	50.8[b]
1	810	989	179	22	120	46.0[b]	74.5[b]
2	807	990	183	23	118	45.4[b]	75.9[b]
3	812[b]	979	167	24	108	56.4[b]	80.7[b]
STANDARD DEVIATIONS							
PF	0.5	14.9	14.6	0.2	9.2	6.8	6.8*
F	0.1	12.5	12.5	0.4	9.9	6.0	4.1*
1	1.2	3.5	3.7	2.1	7.2	2.3	3.1
2	2.0	4.0	5.3	0.8	2.7	4.7	1.1
3	0.9	7.9	7.6	1.0	3.0	11.7	2.4

*PF, F DIFFERENCE EXCEEDS DIFFERENCE BETWEEN TWO SETS OF PF MEASUREMENTS
BOXES INDICATE CHARACTERISTICS WHERE DIFFERENCES BETWEEN PF OR F AND ALL PREVIOUS SCANNERS (1,2,3) WERE GREATER THAN DIFFERENCES BETWEEN TWO SETS OF PF MEASUREMENTS.
a — NO FILTER SPECIFICATION
b — FAILS TO MEET FILTER SPECIFICATION

INVESTIGATION OF RADIOMETRIC PROPERTIES OF LANDSAT-4 MSS

DANIEL R. RICE AND WILLIAM A. MALILA
ENVIRONMENTAL RESEARCH INSTITUTE OF MICHIGAN

KEYWORDS: Remote Sensing, Landsat-4, Multispectral Scanner, Radiometric
Calibration, Noise, Coherent Noise

OBJECTIVES

The objectives of our investigation are to characterize Landsat-4
multispectral scanner (MSS) image data quality relative to:

a. Detector calibration: Study the calibration of the six
    detectors in each band in order to determine the magnitude of
    any calibration difference that remains after ground processing,
    and, if needed, provide information that would support
    corrective techniques, and

b. Satellite-to-satellite calibration: Study calibration
    differences between Landsat-4 and previous Landsat satellites
    and, as needed, develop a method to adjust Landsat-4
    multispectral scanner (MSS) signals, in all four spectral bands,
    to match the calibration of previous sensors.

GENERAL APPROACH

Two full frames of radiometrically corrected (Type A) Landsat-4 MSS
data were analyzed digitally and visually for evidence of residual calibration
differences between detectors, quantization effects, and other sensor-related
artifacts. Both standard statistical and Fourier analysis technques were
employed.

Opportunities for coincident coverage by Landsats 3 and 4 were identified in the contiguous 48 states. Paired acquisitions for two scenes were obtained and analyzed to establish relationships between signal values from common areas imaged by the two MSS systems. Another pair with coverage by Landsats 2 and 4 was obtained and analyzed.

FINDINGS

General Radiometry

We found that the Landsat-4 MSS produces data of generally good quality with dynamic ranges and target responses similar to those of previous Landsat systems (see Figure 1). Clouds often cause saturation in all bands. The extents of specific system artifacts are discussed individually below.

Detector-to-Detector Differences

Striping caused by residual differences in detector calibration and quantization effects appears to be close to the theoretical minimum of quantization error. The histogram equalization algorithm used to adjust radiometric look-up tables appears to be working as intended. Residual rms differences of 0.3 digital counts or less were measured between detector means from a variety of scene areas. Fourier analysis of a down-track profile obtained by averaging the pixels in each scan line showed amplitudes attributable to the residual detector differences that were also approximately 0.3 digital counts or less. These differences were indicated by disturbances in the transforms at wavelength of two, three, and six scan lines. The effects of such differences could be reduced somewhat (per radiance unit) if signal values were spread over 0-255 counts instead of 0-127.

Coherent Noise

A low-level coherent noise effect was found in all bands, appearing in uniform areas as a diagnoal striping pattern. The principal component of this noise was found by Fourier analysis to be at a consistent wavelength of 3.6 pixels along the scan line (see Figure 2), corresponding to a noise frequency of about 28 KHz. The magnitude vaired from about 0.75 of one count

77

in the worst cases (Band 1) to 0.25 counts in the best case (Band 4). This noise pattern was visually discernable in areas of a Landsat-4 image but not discernable in a simultaneous Landsat-3 image of the same areas.

Line-Length Variation

Scan-line lengths in Type A data were found to vary up to six pixels between scans when TM was operating simultaneously with MSS. These variations should be absent from Type P data and imagery.

Landsat-4 to Landsat-3 Calibration

Regression relationships were computed between average signal amplitudes from a number of areas in common between Landsat-3 and -4 images of the two scenes with paired acquisitions. Linear fits with R^2 values exceeding 0.99 were obtained. Letting

$$\text{Landsat } 3 = \text{Gain} \times (\text{Landsat-4}) + \text{Offset}$$

we computed gains that were higher (by approximately 10% in Bands 1, 2 and 4) than ones based on prelaunch calibration values for the two sensors. Relationships based on 60 data points from a New England scene are presented in Table 1.

Results for the other scene and the Landsat 2/4 pair are presented in the Reference.

REFERENCE

Rice, D. P. and W. A. Malila, Final Report on Investigation of Radiometric Properties of the Landsat-4 Multispectral Scanner, ERIM Report No. 163200-3-F, Environmental Research Institute of Michigan, Ann Arbor, MI 48107, August 1983.
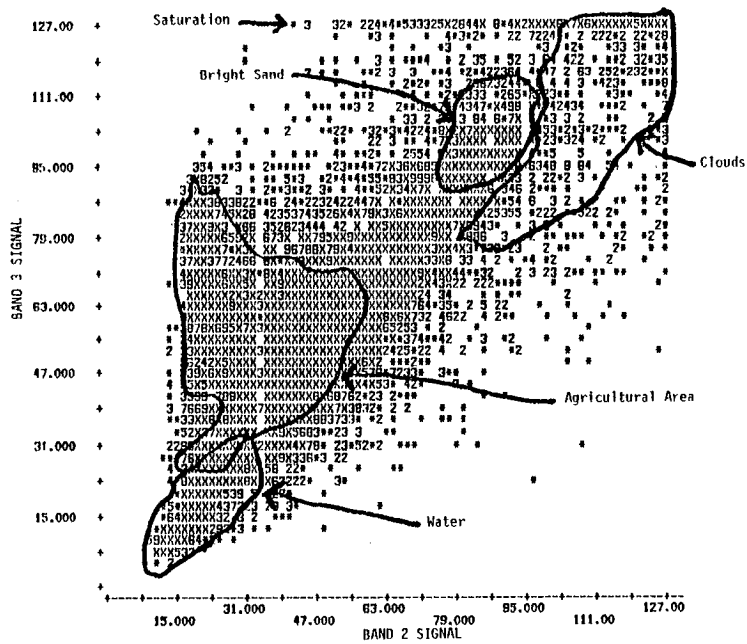
FIGURE 1.   EXAMPLE OF LANDSAT-4 SIGNAL
            DISPERSION FOR A DIVERSE SCENE
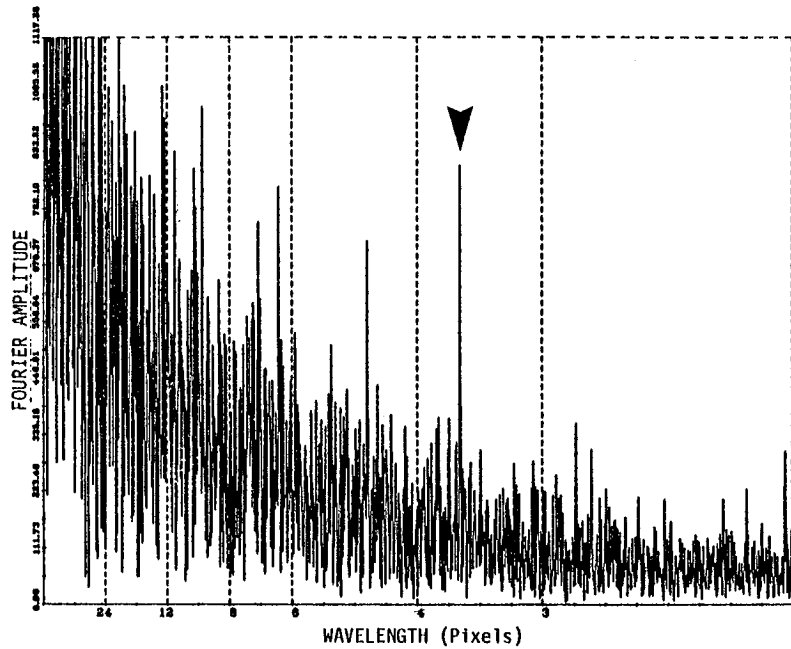
FIGURE 2.   ILLUSTRATION OF THE COHERENT NOISE
            FREQUENCY IN A FOURIER SPECTRUM (BAND 3)

79

TABLE 1
EMPIRICAL LANDSAT -4 TO -3 CALIBRATION COEFFICIENTS

Scene	Band	Gain	Offset	SE*	R^2
New England	1	1.018	-1.614	0.52	0.996
	2	1.112	0.018	0.45	0.999
	3	0.9096	-0.463	0.53	0.999
	4	1.148	-0.421	0.53	0.998
[Prelaunch	1	0.894	-1.00		
Calibration**]	2	1.000	0.722		
	3	0.863	0.870		
	4	1.026	2.34		

*SE = standard error in signal counts

**This information represents carefully conducted ground measurements taken before launch of each satellite, along with a desired scaling of the data.

RELATIONSHIP

Landsat-3 = Gain x (Landsat-4) + Offset

RADIOMETRIC CALIBRATION AND GEOCODED PRECISION PROCESSING OF
LANDSAT-4 MULTISPECTRAL SCANNER PRODUCTS BY THE
CANADA CENTRE FOR REMOTE SENSING

J. MURPHY, D. BENNETT AND F. GUERTIN
CANADA CENTRE FOR REMOTE SENSING

ABSTRACT

The method used by the Canada Centre for Remote Sensing (CCRS) for the radiometric calibration of LANDSAT-4 Multispectral Scanner (MSS) data is reviewed, with reference to the methodology used by the Centre for LANDSAT-1, 2 and 3 MSS data. Inherent in this technique is the possibility for the user to convert the corrected digital values to the absolute scene radiance of the target under observation. The generation of the constants needed for this final conversion requires both the pre-launch and post-launch radiometric calibration constants as supplied by NASA. Results of some preliminary comparative studies of the radiometric properties of the LANDSAT-4 MSS versus earlier satellites in the LANDSAT series are presented. In addition, early observations on the stability of the calibration data, firstly, within one scene, secondly, within one orbit, and thirdly, over a period of several months, are presented. Estimated of residual striping in the corrected products are also presented.

The method used by CCRS, to perform precision processing of LANDSAT MSS data for generating geocoded or map compatible LANDSAT MSS products in the Universal Transverse Mercator projection, is reviewed. LANDSAT-4 MSS precision processed products are evaluated for geodetic accuracy, and are compared to similar products from the previous LANDSAT satellites to assess the orbit independent registration accuracy.

LANDSAT SCENE-TO-SCENE REGISTRATION ACCURACY ASSESSMENT

JAMES E. ANDERSON
NASA/NATIONAL SPACE TECHNOLOGY LABORATORIES

ABSTRACT

This report documents initial results obtained from the registration of Landsat-4 MSS data to Landsat-2 MSS data. A comparison is made with results obtained from a Landsat-2 MSS-to-Landsat-2 MSS scene-to-scene registration (using the same Landsat-2 MSS data as the "base" data set in both procedures). RMS errors calculated on the control points used in the establishment of scene-to-scene mapping equations are compared to error computed from independently chosen verification points. Models developed to estimate actual scene-to-scene registration accuracy based on the use of electrostatic plots are also presented. This project will include analyses of TM data at a later date, and both SCROUNGE and TIPS era products will be evaluated. Analysis or results obtained indicates a statistically significant difference in the RMS errors for the element contribution. Scan line errors were not significantly different. It appears from analysis that a modification to the Landsat-4 MSS scan mirror coefficients is required to correct the situation.

GEOMETRIC ACCURACY OF LANDSAT-4
MSS IMAGE DATA

R. WELCH AND E. LYNN USERY
UNIVERSITY OF GEORGIA, ATHENS

LANDSAT-4 MSS digital data received from the EROS Data Center (EDC) in CCT-P formats are being rectified with the aid of a modified version of the Digital Image Rectification System (DIRS) originally developed at the NASA Goddard Space Flight Center. The rectification procedure involves the digitization of ground control points (GCPs) from U.S. Geological Survey 1:24,000 scale topographic maps and the determination of image locations with the aid of an interactive image processing system. Once the coordinates of the GCPs are determined in both the map (UTM) and image (pixel and line) coordinate systems, these data are transferred to an IBM 370/158 mainframe computer on which the DIRS software is resident. Corrections based on a least-squares fit of polynomials of the 1st to 5th degree are developed and applied to the image coordinates. Accuracy checks are performed by two methods: (1) point pair distance checks involving the comparison of distances computed from the map and image coordinates; and (2) vector plots of the root-mean-square errors ($RMSE_{xy}$) of withheld GCPs to which the least squares polynomial equations have been applied.

Results of analyses of two MSS scenes of the rugged North Georgia area have provided the following results. Distances between point pairs of GCPs computed from the CCT-P data produced errors of approximately $\pm$ 130 m, indicating that the geometric quality of the Landsat-4 MSS data is improved by a factor of two over that of Landsats -1, -2 and -3. However, these data do not meet the pre-launch specifications for geodetic accuracy (i.e., + 0.5 IFOV 90% of the time). Rectification of full scenes using polynomials of the 1st through 5th degree yielded three major conclusions (see Figure 1):

1. $RMSE_{xy}$ values of approximately $\pm$ 80 m are representative of the least-squares fit of a 1st degree polynomial to 10 or more well-distributed GCPs.

2. Rectification to accuracies of ± 1 data pixel (57 m) requires the use of 2nd or 3rd degree polynomials and 20 or more well-distributed GCPs.

3. Rectification accuracies are limited by the resolution of the MSS data, by map and digitizing errors and by displacements due to terrain relief.

$RMSE_{XY}$ AT TEST POINTS
PI9 R36
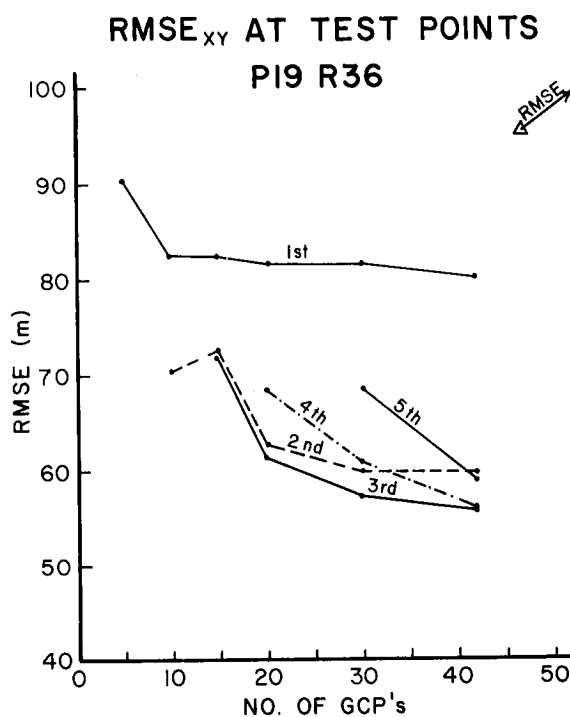
Figure 1. RMSE   as a function of the number of GCPs used to solve polynomials of the 1st through 5th degree.

Subscene areas of 1024 x 1024 and 256 x 256 pixels were rectified with a first order polynomial to produce $RMSE_{xy}$ values of ± 40-45 m. Work to date indicates the geometric quality of Landsat-4 is very good, reflecting the advantages of the improved pointing accuracy and attitude control of the platform.

84

GEOMETRIC ACCURACY ASSESSMENT OF LANDSAT-4
MULTISPECTRAL SCANNER (MSS)

MARC L. IMHOFF AND WILLIAM L. ALFORD
NASA/GODDARD SPACE FLIGHT CENTER

The objectives of this analysis were to analyze standard Landsat-4 MSS digital image data for geometric accuracy. The analysis was performed on 2 P-format (UTM projection), Landsat-4 MSS images of the Washington, D.C. area, scene day 109 (ID number 4010915140) and scene day 125 (ID number 4012515144). The 2 scenes were tested for geodetic registration accuracy (scene-to-map), temporal registration accuracy (scene-to-scene), and band-to-band registration accuracy (within a scene).

Analysis results were compared to the following preflight specification parameters:

- Geodetic accuracy . . . 0.5 sensor pixel (82x82)m or 41m (90% of time)
- Temporal accuracy . . . 0.3 sensor pixel or 24.6m (90% of time)
- Band-to-band accuracy . 0.2 sensor pixel or 16.4m (90% of time)

Twelve geodetic verification points (GVPs) were defined for the area using US Geological Survey (USGS) 7.5 minute topographic quadrangles. Using a zoom transfer scope to overlay the maps with enlarged TV displayed images, the digitized GVP map locations were compared to the TV displayed image locations as defined by the header record information from P-format MSS tapes.

Offsets for each GVP were measured in terms of a 57x57m pixel. Mean offsets for each of the line and sample directions were 0.06 pixel and 0.08 pixel, respectively. The combined RMS error for geodetic registration accuracy was 0.43 pixel (25.51 meters), well within specifications.

Temporal registration and band-to-band registration accuracy analyses were achieved using the cross-correlation method. For both analyses 28 image chips corresponding to map defined GVPs were used for correlation. Temporal

registration accuracy analysis was accomplished using 13 good correlations out of the 28 GVPs to compare scene day 109 to scene day 125 MSS data.

The comparison between the 2 scenes was made on a band-by-band basis. The mean RSS Offset for line and sample for all bands was 0.313 pixel. The offsets were random with a correlation of 0.121 between line and sample offsets. The 90 percent error figure for temporal registration was 0.68 (57x57) pixel (38.8 meters). Although this figure is larger than the specification, it can be considered excellent with respect to user application.

Band-to-band registration accuracy analysis was accomplished using all 28 GVP chips on the day 109 data set. Registration between bands 1 and 2 yielded a combined RMS offset of 0.173 pixel. Registration between bands 3 and 4 yielded a combined RMS offset of 0.167 pixel. Band 2 versus band 3 yielded an RMS offset of 0.464 pixel.

The best case registration errors between bands 1 and 2, and 3 and 4 were 14.2m and 13.7m, respectively, both within specifications. The worst case registration error was 38.0m between bands 2 and 3. The lower statistical correlation between the information content represented by bands 2 and 3 is believed to be the cause of the higher registration error.

IMPACT OF LANDSAT MSS SENSOR DIFFERENCES
ON CHANGE DETECTION ANALYSIS

WILLIAM C. LIKENS AND ROBERT C. WRIGLEY
NASA/AMES RESEARCH CENTER

The work presented has its origins in change detection work carried out at the Ames Research Center in 1981. At that time we co-registered a Landsat-1 and a Landsat-3 scene for the San Bernardino, California area and carried out image differencing as one means of identifying areas of land cover change. It was quickly noted that many spurious or false changes were being delineated in addition to real changes in the scene. These differences were found to be related to differences in the sensors, ground processing, atmosphere, and cover dependent sun angle effects. The data needed to be normalized in some manner to remove these effects. Contingency tables between the images were constructed in order to develop a transfer function relating digital values for individual points in one image to values for those same points in the other image. These functions for each band were used to normalize one date to the other.

In the present study we sought to reverse the above approach by using change detection techniques to pinpoint differences between sensors. Alternately, the use of change detection techniques with Landsat-4 and earlier Landsat MSS sensors can be thought of as a user-oriented test of any insurmountable differences between the sensors when used for change detection. Scattergrams between co-registered scenes (a form of contingency analysis) are used to radiometrically compare data from the various MSS sensors.

Initially, three MSS scenes were acquired and compared for the San Francisco area. These data were not simultaneously imaged; the Landsat-3 scene was acquired four days earlier than the Landsat-4 scene and the Landsat-2 scene was almost exactly a year earlier to minimize cover type and seasonal changes. However, a search of the EROS Data Center's MSS data base

indicated two orbits when data from both Landsat-4 and an earlier Landsat were simultaneously recorded. Three scene pairs of simultaneous coverage were ordered for comparisons. In all cases of same date coverage, the scene pairs were acquired within three minutes or less of each other. Any differences between scenes can then be assumed to be solely a function of sensor differences, as atmospheric effects, sun angle, and scene content will be identical between scenes. This assumption is made, but does not completely hold true in the case of the San Francisco data because the atmosphere is likely to have changed between dates.

The method of analysis was to co-register 512 by 512 pixel subwindows for all data pairs followed by scattergram generation and analysis. In all cases, the Landsat-4 data were used as the base to which other images were registered.

Scattergrams were generated between images for each band. These scattergrams plot the digital number (DN) found for each point in Landsat-4 against the DN recorded for that location in Landsat-2 or -3. Mode (maxima) values were derived from the scattergrams (y-axis modes for fixed x values as well as x-axis modes for fixed y values) and used to visually fit a linear regression (automated regression calculations were distorted by outliers). The regression line represents the relative radiometric transfer function relating Landsat-4 MSS to earlier MSS radiometry. Root mean square (RMS) errors of the registrations varied between .1 and 1.5 pixels. The relatively large errors resulted from a line length error in the Landsat-4 MSS (discussed later).

Radiometric calibration information is also available for each of the MSS sensors. These can be used to predict the relative radiometric transfer functions between sensors.

The relative radiometric differences between Landsats - and -4 appear approximately the same as predicted by the calibration information. Comparisons of Landsats -2 and -3 (Table 4), and -2 and -4 (Table 3), however, show that the actual radiometry of Landsat-2 differs significantly from the calibration specifications. This may reflect drift in sensor sensitivity,

optical degradation of the scan mirror and telescope, or changes in the radiance minimum and maximum constants used in ground processing. Often, changes in sensor calibration are not well disseminated and are thus unavailable to data users.

While radiometric values for Landsats -3 and -4 appear roughly the same as predicted by the calibration specifications, the San Francisco scene pair shows the high degree to which atmosphere can affect relative readings of features on different days. Atmospheric effects (up to 12 digital counts bias added to signal in band 1) in the Landsat-3 scene have caused features to saturate to a much greater degree than in the corresponding Landsat-4 scene, or in other scene pairs.

The saturation of Landsat-4 at relatively low radiance levels (compared to Landsats -1, -2, and -3) in bands 1 and 3 may result in loss of useful information for some data applications, including change detection.

While in the process of generating scattergrams, several geometric artifacts were noted. All bands of each Landsat-4 image contained noise interference patterns. These patterns appeared to have two components: diagonal striping with a period of about 3.5 pixels, and concentric arcs with a period of 10-12 pixels. Over water areas, the noise was noted to have a magnitude of 2 digital counts in band 4.

Sweep offsets were noted in all but the San Francisco Landsat-4 scenes. The San Francisco scene was acquired before Thematic Mapper data acquisition began on the West Coast. All other scenes fall in a time period during which it is probable that TM and MSS were turned on concurrently, indicating the problem may be related to sensor interactions. The offsets result from varying line lengths, and are readily corrected by stretching all lines to a constant length using line length information imbedded in the right edge of the image. The problem occurs only in A-format tapes and is corrected during the geometric processing applied to generate P-tapes.

There appear to be no major problems preventing use of Landsat-4 MSS with previous MSS sensors for change detection, provided the interference

noise can be removed or minimized. This noise may result in detection of spurious changes, as well as affect other uses of the data, including image classification. Analysis of dark (water and forests), rather than light features will be most impacted because the noise will form a higher percentage of the total response at low DN values. The patterns are sweep-dependent, and within a sweep it is not clear that they are completely systematic. The pattern is present even when TM is off. The problem was detected before launch (left uncorrected because of the cost of repair), and is caused by interference between the revised MSS power supply (the power bus on Landsat-4 is different than on previous Landsats) and the sensor's one kilohertz data quantitizer. The frequency of the interference is known to drift because of drift in power supply frequency. The identical problem has been identified in Landsat-D Prime and should be corrected.

Any data normalizations for change detection should be based upon the data, rather than solely upon calibration information. While the observed relative radiometric transfer function between Landsats -3 and -4 was approximately as predicted, there were still significant deviations. Also, actual calibration specifications used in ground processing are not always made widely available, and published figures for Landsat-2 appear incorrect for recent data. Normalizing based upon data content also can have the advantage of allowing simultaneous normalization of the atmosphere as well as the radiometry.

LANDSAT-4 MSS GEOMETRIC CORRECTION:
METHODS AND RESULTS

J. BROOKS, E. KIMMER AND J. SU
GENERAL ELECTRIC SPACE DIVISION

An automated image registration system such as that developed for Landsat-4 can produce all of the information needed to verify and calibrate the software and to evaluate system performance. This paper describes methods and results of the effort that fine-tuned both software and data base and assessed geometric performance of the calibrated Landsat-4 system.

Landsat-4 MSS geometric correction data are generated in a two-step process. The first step utilizes models of the spacecraft-scanner-spinning earth system, with smoothed ephemeris and attitude data as input, to deduce systematic correction data. The systematic correction data, therefore, suffer from random system pointing and spacecraft location errors. If control points are available for the subject scene, the second step - automatic correlation of control point chips to control point neighborhoods - is performed to develop input to the MSS control point location error filter. The output of the filter is the state error vector, which is used to upgrade the systematic correction data to geodetic correction data. This online process is called the MSS Archive Generation process (MAG) because its output is the high density archival tape.

An important offline subsystem of the Landsat-4 MSS Image Generation Facility is the Control Point Library Build (CPLB) subsystem. This hardware and software complex is used to generate control point chips and support data for use in online upgrade of correction data. Control point chips that represent ground truth are called geodetic or supplemental, depending on whether they are used to establish the model surface (with the same filter that is used online) or are selected from the fully corrected imagery. Relative control points are designated in systematically corrected imagery, have no ground truth and can, therefore, be used only for temporal registration.

During the last six weeks before the NASA/NOAA turnover of the system, an extensive effort was carried out to fine-tune both software and data base and to evaluate the geometric performance of the calibrated system. The online processing and the CPLB process provided all the tools necessary for the verification, calibration (including initial scan profile correction) and evaluation of Landsat-4 geometric processing.

The system performance was evaluated for both temporal and geodetic registration. For temporal registration, control points selected from the Washington scene of November 2, 1982 (W1) were used in the correction of the Washington scene of November 18, 1982 (W2). The registration error was determined from the MAG control point residuals (a measure of random error) and a theoretical model bias between the model surface in MAG and CPLB. The 90% errors were computed to be .36 IFOV (Instantaneous Field of View) = 82.7 meters) cross track, and .29 IFOV along track. Also, for actual production runs monitored, the 90% errors were .29 IFOV cross track and .25 IFOV along track. The system specification is .3 IFOV, 90% of the time, both cross and along track.

The geodetic registration performance was evaluated by correcting both scenes W1 and W2 with geodetic control points from W1. Again the registration error was determined from the MAG control point residuals and the model bias. In this case, however, the model bias was measured by designating control points in the geodetically corrected imagery. Because of designation errors, this yields a conservatively high measure of the model bias. With 20 control points used in the MAG correction, and 32 control points designated in CPLB, W1 had 90% errors of .35 IFOV cross track and .26 IFOV along track. Because of cloud cover, only 13 control points were used in MAG to correct W2 and 14 control points designated in CPLB. The 90% errors for W2 were .63 IFOV cross track and .43 IFOV along track. The system specification is .5 IFOV, 90% of the time, both cross and along track.

Based on these evaluations, it appears that the Landsat-4 geometric correction performance is meeting or exceeding its specifications.

IMPACT OF THEMATIC MAPPER SENSOR CHARACTERISTICS
ON CLASSIFICATION ACCURACY

DARREL L. WILLIAMS, JAMES R. IRONS, BRIAN L. MARKHAM,
ROSS F. NELSON AND DAVID L. TOLL
NASA/GODDARD SPACE FLIGHT CENTER

RICHARD S. LATTY
UNIVERSITY OF MARYLAND

MARK L. STAUFFER
COMPUTER SCIENCES CORPORATION

With the launch of Landsat-4 on July 16, 1982, and the successful
operation of its primary payload, the Thematic Mapper (TM), a significantly
new source of data became available to the remote sensing community. Relative
to the familiar Multispectral Scanner (MSS), the TM offers: improved spatial
resolution (30m versus 80m), new and more optimally placed spectral bands, and
improved radiometric sensitivity quantized over eight bits rather than six
bits. All of these improvements in sensor capability were justified from the
standpoint that they would significantly improve data quality and information
content, and, thereby increase digital classification accuracies. The intent
of this study was to determine the extent to which each of these improvements
in sensor performance (TM relative to MSS) would enhance classification
accuracy.

The approach adopted was a three-factor (spectral, spatial, and
radiometric resolution), two-level (TM and MSS) analysis-of-variance (ANOVA).
This approach allowed evaluation of the effects of each factor individually
and in all possible combinations. Digital classification accuracy was used as

the figure of merit. Thematic Mapper data acquired over the Washington, DC area on November 2, 1982, were used to conduct the experiment. The eight data sets required in the ANOVA design (Table 1) were created by applying appropriate degradations to the original TM data (28.5 meter pixel, eight bits, six channels). The spatial degradation consisted of convolution with a 3 x 3 pixel unweighted average filter to simulate the 83 meter IFOV of the MSS, sampled at 2 pixel (57 meters) increments to simulate the 57 meter square pixel of processed MSS data. The spectral degration consisted of a three-band subset of seven TM bands (bands 2, 3 and 4) which are similar to MSS bands 1, 2 and 4. [The thermal data (band 6) were excluded from this study due to the difference in spatial resolution (120 meters)]. The radiometric degradation of TM data to MSS level consisted of an integer division by four.

Nine study sites, each of approximately 256 x 256 TM pixels were randomly selected from the full scene for analysis. Recent aerial photographs of each study site were photointerpreted with 17 land use/land cover categories being identified (later condensed to 5 for comparison). The delineations were digitized and registered to the imagery, and thus, constituted the reference data set.

Random samples within each land cover type were selected for use in training and testing using the digitized reference data. The training pixels were clustered by class, the resulting statistics files merged and the images classified with a per-point Gaussian maximum likelihood classifier using the unedited statistics files. The testing samples were compared point-by-point with the reference data, contingency tables were generated and classification accuracies computed. The computed classification accuracies were analyzed with a three-factor, two-level ANOVA model.

The resulting classification accuracies were low (25-37%) (Table 2). This is the result of: (1) the attempted classification of 17 detailed land-cover categories (a reduction in the number of classes to 5 increased accuracy to 60-72%), (2) the elimination of analyst interaction, which is necessary to optimize classification accuracy, but may introduce biases (when analyst interaction was permitted in the analysis of block A, for the 17 class case, classification accuracy rose from 36.7% to 62%), (3) the inclusion of

94

boundary pixels in the training and test pixels, and (4) the non-optimal time of year of data collection with a low-sun angle and limited vegetative growth.

The ANOVA run on the 17 class case showed significant interaction terms present, necessitating block-to-block comparison of the data. The increase from three to six spectral bands increased classification accuracy from 3% to 8% depending on the levels of the other factors, and all differences were significant (α = 0.05). The increase in quantization from six bits to eight bits also increased classification accuracy over the range from 3% to 8% and all differences were significantly greater than zero. However the increase in spatial resolution from 80m to 30m had mixed effects on the classification accuracy within the range of $\pm 2\%$ and none of the differences were significant.

These results strongly suggest that the quantization level improvements and the addition of new spectral bands in the visible and middle IR regions (both afforded by the TM sensor design) will result in improved capabilities to accurately delineate land cover categories using a per-point Gaussian maximum likelihood classifier. On the other hand, results indicate that the increase in spatial resolution to 30m does not significantly enhance classification accuracy. The spatial result points to an inherent limitation of a per-point classifier and to the need to improve data analysis techniques to handle high spatial resolution data.

A more in-depth discussion of the methodology used and results obtained, can be found, under the same title, in:

a. Proceedings of the Landsat-4 Early Results Symposium held at NASA/Goddard Space Flight Center, February 22-24, 1983; and

b. Proceedings of the 1983 International Geoscience and Remote Sensing Symposium (IGARSS '83) held in San Francisco, California, August 31 - September 2, 1983.

TABLE 1

Characteristics of Data Set Treatments Required for a Complete Two Level (TM, MSS) by Three Factor (Spectral, Spatial, Radiometric) Analysis-of-Variance (ANOVA) Experiment.

NUMBER OF SPECTRAL BANDS	RADIOMETRIC QUANTIZATION	SPATIAL RESOLUTION	
		30 METERS	80 METERS
6 bands (thermal band excluded)	8 bit	A 30 meter/8 bit/6 bands	B 80 meter/8 bit/6 bands
	6 bit	C 30 meter/6 bit/6 bands	D 80 meter/6 bit/6 bands
3 bands (TM bands 2, 3 and 4)	8 bit	E 30 meter/8 bit/3 bands	F 80 meter/8 bit/3 bands
	6 bit	G 30 meter/6 bit/3 bands	H 80 meter/6 bit/3 bands

TABLE 2

OVERALL CLASSIFICATION ACCURACY AS A FUNCTION OF
SENSOR/DATA CHARACTERISTICS AND THE NUMBER
OF LAND COVER CLASSES BEING DELINEATED

Treatment	Characteristics	Case I [†] Mean (%)	S.D.	Change Relative to Treatment "A"	Case II [#] Mean (%)
A	30 meter/8 bit/6 bands	36.7(62)*	0.73	N.A	71.7
B	80 meter/8 bit/6 bands	37.9	1.13	+1.2	71.5
C	30 meter/6 bit/6 bands	31.2	1.27	-5.5	68.4
D	80 meter/6 bit/6 bands	29.9	1.05	-6.8	63.0
E	30 meter/8 bit/3 bands	29.0	0.39	-7.7	65.1
F	80 meter/8 bit/3 bands	30.9	1.50	-5.8	64.4
G	30 meter/6 bit/3 bands	25.7	0.57	-11.0	59.5
H	80 meter/6 bit/3 bands	26.7	0.98	-10.0	62.2
I	Real MSS - Band 1, 2, 4	20.6	0.37	-16.2	54.9

(NOTE: Items underlined are those factors changing relative to A, i.e., Actual TM Data)

* Accuracy obtained when analyst interaction was permitted to edit training statistics.
† Case I   Accuracies based upon use of 17 detailed land cover/land use classes.
# Case II Accuracies based upon use of 5 aggregated land cover classes.

CHARACTERIZATION OF LANDSAT-4 TM AND MSS IMAGE QUALITY FOR INTERPRETATION OF AGRICULTURAL AND FOREST RESOURCES

S. D. DEGLORIA AND R. N. COLWELL
UNIVERSITY OF CALIFORNIA/BERKELEY

The performance of both the Landsat-4 MSS and TM sensors is being evaluated through the systematic evaluation of image products generated from computer compatible tape data and commerically available film products from the EROS Data Center. Natural targets are used to evaluate spectral variability, spatial resolution, radiometric sensitivity, and geometric fidelity of these tape and image data. Spectral characteristics are being evaluated through the interpretation of image tone and texture variability of known features. Spatial characteristics are being evaluated through the analysis of residual errors derived from the least squares regression analysis of image and map coordinates.

Our focus during the early phase of our research was to evaluate the quality of TM and MSS data for the interpretation of agricultural and forest resources. The methodology employed for accomplishing our objectives were as follows: (1) Acquire the first available Landsat-4 scenes covering our agricultural and forestry test sites; (2) Acquire, process, and catalog small format, low altitude color oblique aerial photography of selected areas within the scenes to document major agronomic conditions prevalent at the time of the Landsat-4 overpass; (3) Compile the available ground data for the area imaged to relate the spectral data to crop and cover conditions; and (4) Produce TM and MSS image products for interpretation, and extract digital count values (Radiance Numbers, RN) from the CCT's for tabulating and plotting the field means and variances for each spectral band.

Systematic analysis of both image and numeric data for the agricultural and forestry study area have yielded the following results: (1)

The overall spectral, spatial, and radiometric quality of the TM data are excellent. Spectral variations in fallow fields are due to the variability in soil moisture and surface roughness resulting from the various stages of field preparation for small grains production. (2) Spectrally, the addition of the first TM short-wave infrared band (Band 5) has significantly enhanced our ability to discriminate different crop types. In Figure 1 the spectral plots indicate there is no significant difference between the sugar beet and alfalfa spectra in the visible and near reflectance infrared bands (1-4). In the short-wave region we see a significant difference in the spectral values between these two crop types which can be attributed to differences in leaf water content. This and other significant spectral crossovers between the red, near-infrared, and short-wave infrared bands are shown in Figure 2. Table 2 and 3 provide summary statistics for our forestry study area. Bands 1, 5 and 6 contain saturated pixels due to high albedo effects, low moisture conditions, and high radiant temperatures of granite and dry, bare soil on south facing slopes, respectively. (3) Spatially, the two-fold decrease in interpixel distance and four-fold decrease in area per pixel between the TM and MSS allow for improved discrimination of small fields, boundary conditions, road and stream networks in rough terrain, and small forest clearings resulting from various forest management practices.

	SUGAR BEETS		ALFALFA		MIXED PASTURE		ORCHARD		VINEYARD		GRAIN STUBBLE		BARE SOIL		NATIVE VEGETATION	
	$\bar{x}$	CV	$\bar{x}$	CV	$\bar{x}$	CV	$\bar{x}$	CV	$\bar{x}$	CV	$\bar{x}$	CV	$\bar{x}$	CV	$\bar{x}$	CV
TM1	50.4	2.5	50.1	2.3	53.8	2.8	51.4	2.6	52.5	3.1	65.2	2.6	56.4	2.5	50.6	3.2
TM2	20.3	3.9	20.5	3.6	22.5	4.1	20.2	3.8	21.3	3.8	29.9	4.3	23.4	4.0	18.9	3.9
MSS 1	13.8	7.4	14.4	7.5	15.1	7.8	14.1	8.3	14.7	6.8	21.4	7.1	16.1	7.5	13.4	9.2
TM3	16.9	4.0	17.1	3.7	22.4	5.4	19.4	4.4	21.5	5.4	36.3	4.4	24.9	3.8	18.0	6.1
MSS 2	8.8	12.0	9.3	11.5	12.0	8.5	10.4	8.6	11.8	8.3	21.6	6.7	14.2	9.1	9.5	11.4
TM4	60.4	3.9	58.8	3.8	46.2	5.6	30.4	3.5	33.3	5.1	38.6	4.9	28.2	7.1	25.4	11.1
MSS 3	37.2	7.3	38.4	7.0	30.4	1.8	20.1	5.9	22.4	8.9	30.3	5.6	20.8	8.6	15.7	14.7
MSS 4	34.4	7.5	35.4	2.9	28.0	1.8	18.5	5.6	18.9	1.6	22.8	6.8	16.2	8.8	13.4	18.7
TM5	28.0	5.0	44.8	2.8	53.9	4.8	37.5	4.6	46.4	6.7	65.8	4.2	43.8	4.5	33.7	13.2
TM7	9.1	11.1	15.2	9.1	21.5	8.2	17.5	10.6	23.8	7.8	43.7	5.4	25.7	6.4	16.2	18.2
TM6	91.8	0.5	92.7	0.7	93.4	0.6	92.1	0.6	92.7	0.7	91.8	0.6	90.9	1.0	92.0	0.7

Table 1. TM and MSS spectral statistics for the agricultural study area. Values tabulated are Radiance Numbers (RN) extracted from the CCT-PT and CCT-AM tapes.
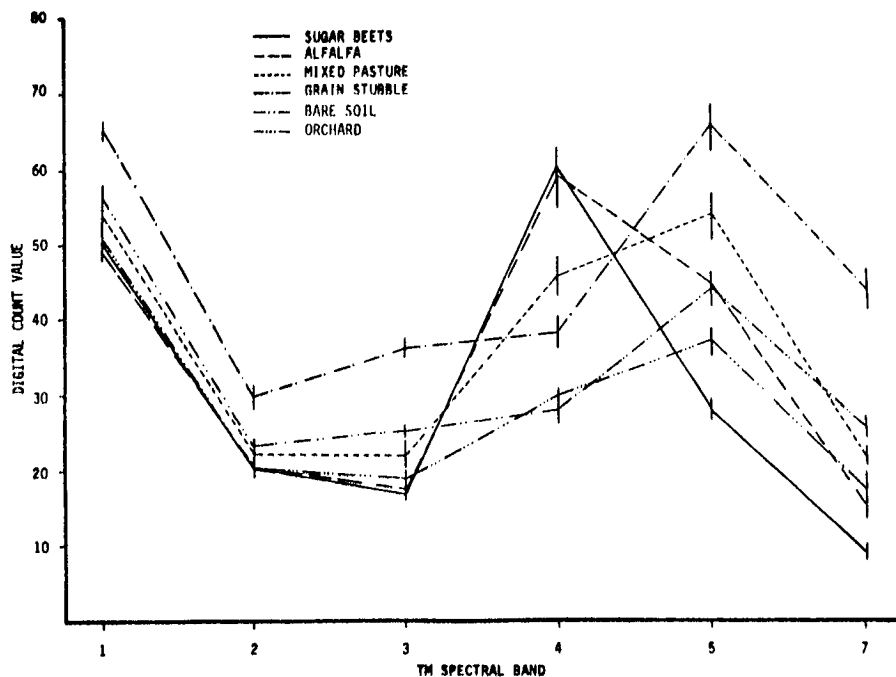
Figure 1. Plot of the RN values for each of the reflective TM bands. Data values represent field means ($\pm$ 1 s.d.) using one or more fields per cover condition. Values are tabulated in Table 1.
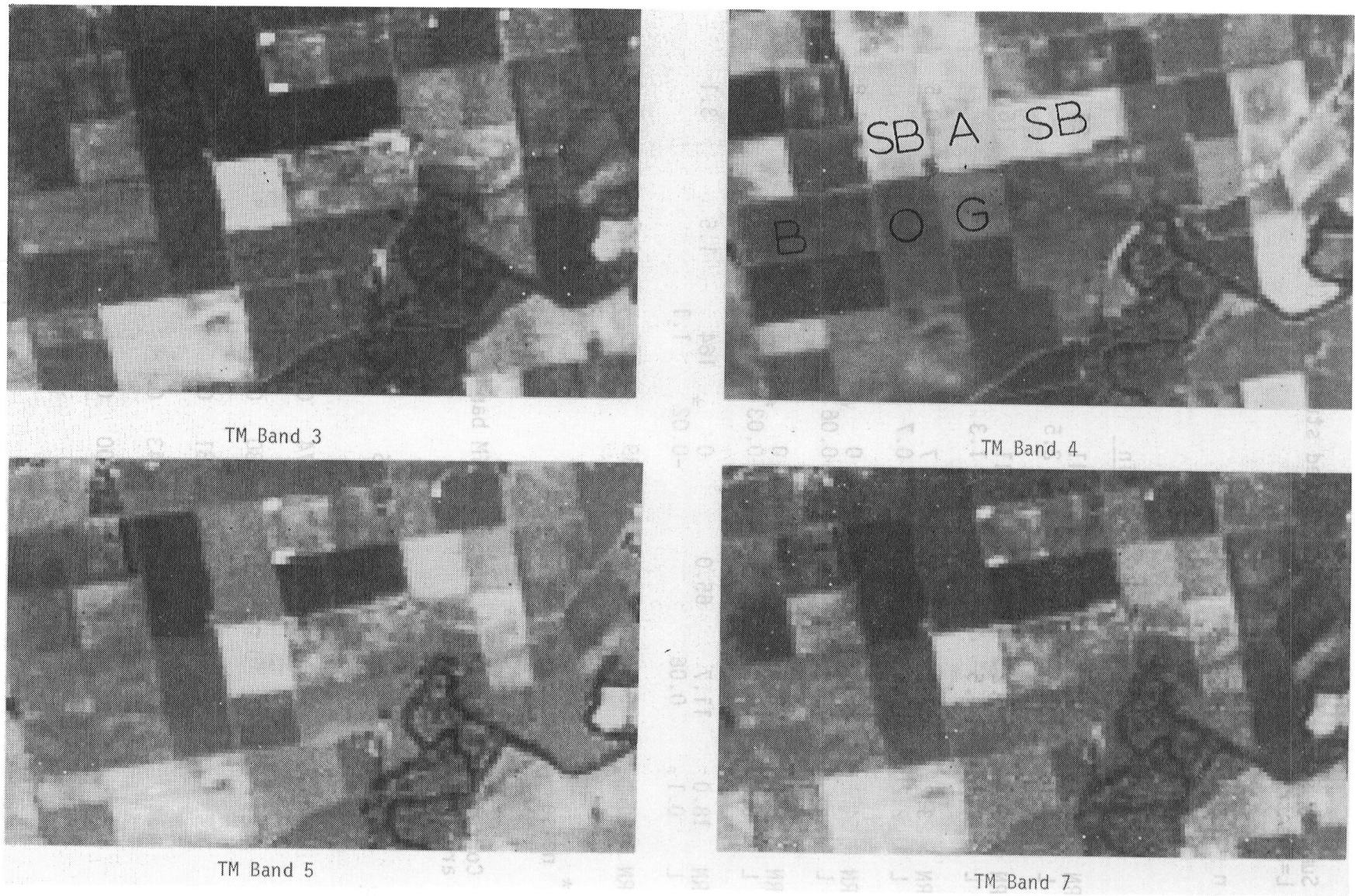
Figure 2. Visual representation of the data displayed in Figure 1 showing the differential reflectance of various cover types as a result of leaf structure and moisture content. (A=alfalfa, SB=sugar beets, O=orchard, B =bare soil, G =grain stubble)

Table 2. Summary statistics for the forested study area (RN=Radiance Number, L=Spectral Radiance).

n = 1,440,000 pixels

TM BAND		$\bar{x}$	s	CV	Min	Max	Skew	Kurtosis
1	RN	66.1	8.1	12.3	41	255	3.1	25.0
	L	4.1	0.5		2.5	16.1		
2	RN	23.7	5.2	21.9	11	166	2.5	16.8
	L	2.8	0.5		1.3	20.6		
3	RN	23.2	8.2	35.3	7	214	2.4	10.5
	L	2.2	0.8		0.7	20.2		
4	RN	64.1	16.1	25.1	0	172	0.2	1.8
	L	5.8	1.4		-0.06*	15.8		
5	RN	46.7	22.5	48.2	0	255	1.1	1.5
	L	0.6	0.2		-0.03*	3.2		
7	RN	18.0	11.7	65.0	0	164	1.5	3.1
	L	0.1	0.06		-0.02*	1.1		
6	RN	190.1	15.1	7.9	139	255	1.1	1.6

* noise

Table 3. Correlation matrix for the seven TM bands for the forested study area (n=40,000 pixels).

BAND	1	2	3	4	5	7	6
1	1.00	0.94	0.96	0.15	0.74	0.84	0.30
2		1.00	0.96	0.24	0.80	0.87	0.77
3			1.00	0.18	0.81	0.90	0.81
4				1.00	0.43	0.18	0.06
5					1.00	0.93	0.85
7						1.00	0.97
6							1.00

EVALUATION OF LANDSAT-4 THEMATIC MAPPER DATA AS APPLIED
TO GEOLOGIC EXPLORATION: SUMMARY OF RESULTS

JON D. DYKSTRA, CHARLES A. SHEFFIELD, AND JOHN R. EVERETT
EARTH SATELLITE CORP.

INTRODUCTION

The purpose of our experiment is to evaluate the applicability of Thematic Mapper (TM) data to geologic exploration. This includes both testing various data products for applicability and assessing the effect of various engineering characteristics on geologic applications. Early in this program, it became clear to us that investigators were thoroughly evaluating all engineering aspects and anything we did would likely be redundant. Thus, we have focused on the geologic aspect of our original purpose. Several parts of our study are not complete, so this truly is a progress report.

The broader spread, narrower band width and better resolution of the new bands and the improved sharpness of the image as a result of the higher resolution all expand the application of Landsat Thematic Mapper (TM) data to geologic exploration. The new data are extraordinarily powerful in themselves. However, their true power is realized when they are imaginatively combined with careful field work and other geological, geochemical and geophysical data in the context of perceptive, creative geologic thinking.

In a general sense, Landsat MSS data has made its major contribution to hydrocarbon exploration in the spatial domain. It appears that this also will be true for TM data. However, the much greater spectral power of TM data dictates that the balance between "spectral" and "spatial" contributions will be much more nearly equal. The increased spectral resolution of TM allows geologists to map altered zones associated with mineralization or microseepage based not only on iron oxides, but on the basis of recognizing rocks and soils rich in hydroxyl groups, such as many of the clays formed as a product of the mineralization process. The increased spectral sensitivity also promises the ability to detect some types of vegetation changes that are associated with anomalous mineralization. This will be particularly helpful where soil and

plants obscure the bedrock. This capability is not definitely proven, but it is theoretically possible and highly anticipated.

All of the above implies that digital processing techniques will play a much greater role in the application of TM data to exploration than it has in the application of MSS data. One of the lessons we relearned many times while using MSS data is that there is no single process that is appropriate to all areas or to all applications. Processing must suit the application and the area. One aspect of our experiment was to devise a method of selecting the three band combination that yields the most information. This method involves using the variance-covariance matrix to compute the volume of the "information" ellipsoid. In most areas, a 1, 4, 5 composite contains the most information (1, 2, 3 and 2, 3, 4 combinations are usually ranked very low). The question, "Is this maximum information the information I want for geology?" Is much more subjective. In some areas 4, 5, 7 composites seem better suited to geology but 1, 4, 5 is an excellent general purpose product.

We are currently in the midst of evaluating the desirability of using A-tapes to produce imagery for geologic evaluation. We cannot yet predict the outcome of this investigation.

In general, the value of the spatial data increases relative to the value of the spectral data as soil and vegetation cover increase. However, even in covered areas, the increased spectral sensitivity contributes to interpretation by making the spatial elements of terrain, fractures, geomorphology, etc., more easily recognizable. One factor that aids interpretation immensely is 30-metre resolution, so that the digitally processed images easily stand enlargement to 1:50,000 and, in some instances, larger scale - a capability that greatly reduces uncertainty, ambiguity and error in interpretations.

DEATH VALLEY, CALIFORNIA

In arid areas with good exposure, such as Death Valley, California, it is possible, with careful digital processing and inventive color compositing, to produce enough spectral differentiation of rock types so that

it is possible, using standard photo interpretation techniques, to produce facsimilies of standard geologic maps with a minimum of field work or reference to existing maps. We found that using an intensity-hue-saturation (IHS) image, we could closely match units mapped on the 1:250,000 scale geologic map of Death Valley (1977) produced by the California Division of Mines. Through the use of two ratios to control hue and saturation, and the first eigenband as the intensity, the resulting IHS image possesses the spectral information of a ratio image and the spatial integrity of the first eigenband. The hue of the image is controlled by the ratio of TM5 (1.6 microns) over TM2 (0.56 microns). The color assignments are such that high ratio values are red with decreasing values passing through the spectrum ending with the lowest values in blue. The saturation of the image is controlled by the ratio of TM5 (1.6 microns) over TM7 (2.2 microns).

TM2 was chosen for its sensitivity to ferric iron oxides; TM7 for its sensitivity to hydroxyl bands and TM5 for its high variance and broad information content. The 5/2 ratio will have high value (red hue) over areas of high ferric iron content, vegetation, as well as an assortment of other surface materials. The 5/7 ratio will have particularly high values (high saturation on the output image) over areas with contain hydroxyl bearing minerals or surface materials containing free water (e.g., clays, hydrated salts and vegetation). The first eigenband presents a positively weighted sum of the seven TM bands and thus provides excellent geomorphologic information allowing for precise geographic locations of the image's spectral information.

FOUR CORNERS AREA

In a slightly less arid area, such as the Paradox Basin of Utah and Colorado, soil cover and vegetation are much better developed than in the Death Valley. We are currently processing but have not yet had an opportunity to extensively examine TM data from this area. We know from Thematic Mapper simulator (TMS) data that digital processing can enhance spectral signatures even where the surface is 20-50% covered with vegetation. Of particular interest are the well known "bleached" red beds associated with uranium deposits and hydrocarbon accumulations. Probably the best known examples are on the southwest flank of Lisbon anticline where the Triassic Wingate

sandstone, which is normally a warm rosy brown cliff-forming rock unit in the area, is bleached almost white in the vicinity of uranium and hydrocarbon deposits. Uranium explorationists have used this bleaching of red beds as an exploration indicator for many years.

Several processing techniques highlight these color differences in TMS imagery. The differences are visible in "natural" color composites (TMS bands 1, 2, 3) and in other more exotic processes, particularly those involving ratios (e.g., 4/3, 1/3, 7/5).

SPANISH PEAKS, COLORADO

The Spanish Peaks area of south central Colorado is not one of our test sites but offers a striking example of the contribution that TM data can make to exploration. The area is a Cretaceous to early Tertiary basin that was the locus of several episodes of intrusive activity during Miocene time that produced the spectacular volcanic necks that form the Spanish Peaks and the complext dike pattern. Interpretation of a color composite composed of TM bands 1, 4, 5 enlarged to 1:48,000 revealed more than twice as many dikes as 1:60,000 scale black-and-white aerial photography. The number, location and distribution of the dikes compare very favorably to detailed field mapping of the area. In particular, a few more dikes are mapped on the TM imagery and they tend to be longer than those on the field map. The field map reveals a few dikes not seen on the TM imagery. This type of information is useful if you are trying to avoid drilling volcanic rock in the course of petroleum exploration. Spectral differentiation, color format, regional perspective and image continuity and low angle of illumination all probably contributed to recognition of the dikes in the area.

BIG HORN AND WIND RIVER BASINS, WYOMING

The Big Horn/Wind River Basin area of Wyoming lies just east of the Overthrust Belt in the area of foreland deformation. The area has more soil development and vegetation than the previous three areas. The light dusting of snow over the area in available TM data effectively frustrates spectral work.

Regional interpretation of the Overthrust Belt reveals several recurrent patterns of structural features. These same patterns extend into the foreland in a less compressed form.

A color composite of TM bands 1, 4, 5 reveals many of the structural and stratigraphic features better than either natural color (1, 2, 3) or false color infrared (2, 3, 4) versions. Despite the snow, one can see some peculiar coloration over the Madden gas field and the Copper Mountain uranium deposits.

Based on a quick interpretation, the structure in the Owl Creek area looks like some of the structures to the west. The major thrust on the south side of the Own Creek Range is well known and parallels the thrust in front of the Wind River Range to the south. The strike-slip faults are less well known.

CEMENT-VELMA, OKLAHOMA

In the more humid and agriculturally stirred areas, the role of spectral data tends to diminish. Just as Goldfield, Nevada is the Olympic training grounds for MSS spectral signatures of hydrothermal alteration, the area around Cement, Oklahoma is possibly the best documented instance of surficial alteration related to microseepage of hydrocarbons. Terry Donovan (1974) found a variety of chemical anomalies at and near the surface and Jerry Furgeson (1979) found anomalous amounts of pyrite in the Permian rocks of the subsurface. Vegetation is relatively dense, though much of it was dead at the time TM data were acquired. On the ground, alteration in the form of bleached red beds, anomalous calcite cement, ironstone concretions, etc., is obvious. To date, none of the digital approaches we have tested (ratios, compound ratios, principal components, IHS, etc.) has reliably indicated a credible anomaly. There are a few areas that show a bit of a bluish tinge in the 1, 4, 5 imagery. Some of these areas do correspond with structural culminations and some of Donovan's geochemical highs, but they are subtle, feeble, and open to a wide variety of interpretation.

In contrast to the spectral data, the structural data are mildly spectacular. Leo Herrmann's 1961 version of the structure on the Deese group at 5,000+ feet and beneath the Permian unconformity matches rather well with a simplified version of the features that can be interpreted from a 1, 4, 5 image of the TM data. Again, there is the same "Z" shaped configuration of WNW trending left-slip faults and north trending thrust faults we saw in Wyoming. Cement Field is located on a "flower" structure along a left-slip fault and Chickasha Field in on the related thrust fault. The Velma Field is located further to the southeast along the same left-slip fault that controls Chickasha field. Examination of the image reveals several similar but untested structures. These, of course, should be examined in detail. In addition, we need to spend more time looking for subtle geochemical and geobotanical effects.

SUMMARY AND CONCLUSIONS

As with any tool applied to geologic exploration, maximum value results from the innovative integration of optimally processed TM data with existing pertinent information and perceptive geologic thinking. The synoptic view of the satellite images and the relatively high resolution of TM data allows us to recognize regional tectonic patterns and map them in substantial detail. The refined spatial and spectral characteristics and digital nature of the Thematic Mapper data permit detection and enhancement of signs of surface alterations associated with hydrothermal activity and microseepage of hydrocarbons that have previously eluded us.

In general, as vegetation and soil cover increase, the value of spectral components of TM data decreases with respect to the value of the spatial component of the data. This observation reinforces the experience from working with MSS data that digital processing must be optimized both for the area and for the application.

PRELIMINARY GEOLOGIC/SPECTRAL ANALYSIS OF LANDSAT-4 THEMATIC MAPPER DATA, WIND RIVER/BIGHORN BASIN AREA, WYOMING

HAROLD R. LANG, JAMES E. CONEL AND EARNEST D. PAYLOR
JET PROPULSION LABORATORY

SUMMARY

A LIDQA evaluation of a Landsat-4 TM scene covering the Wind River/Bighorn Basin area, Wyoming, is currently underway at JPL. The major objective of the study is to evaluate Landsat-4 TM data for geologic applications. The involves a quantitative assessment of data quality including spatial and spectral characteristics. Analysis has concentrated on the 6 visible, near-infrared, and short wavelength infrared bands.

The scene (path 36, row 30, ID #40128-17232) was acquired on November 21, 1982. Data were provided to JPL by GSFC in SCROUNGE-processed, P-tape format. Image products developed include composites, ratio composites, unsupervised classifications, and principal components images.

Preliminary analysis demonstrates that: (1) principal component images derived from the correlation matrix provide the most useful geologic information. Components so produced represent linear transformations based on ground reflectance. The separation of unique spectral classes, therefore is largely independent of non-random atmospheric and instrumental factors. Co-registered TM and aircraft acquired TM simulator (TMS) PC images demonstrate that conclusions reached in TMS studies are for the most part directly applicable to TM data. (2) To extract surface spectral reflectance, the TM radiance data must be calibrated. Reflectance measurements were not acquired during the overflight, but an empirical calibration, based on scatterplots of DN vs. reflectance for natural and cultural targets, measured in situ during the period October 27 - November 3, 1983, was carried out. These scatterplots (Figure 1) demonstrate that TM data can be calibrated and sensor response is essentially linear. (3) Low instrumental offset and gain settings result in spectral data that do not utilize the full dynamic range

(i.e. 255 DN) of the Thematic Mapper System. Calibration data from Figure 1 were used to calculate gain and offset increase (Figure 2) which should optimize scanner response for earth science applications.
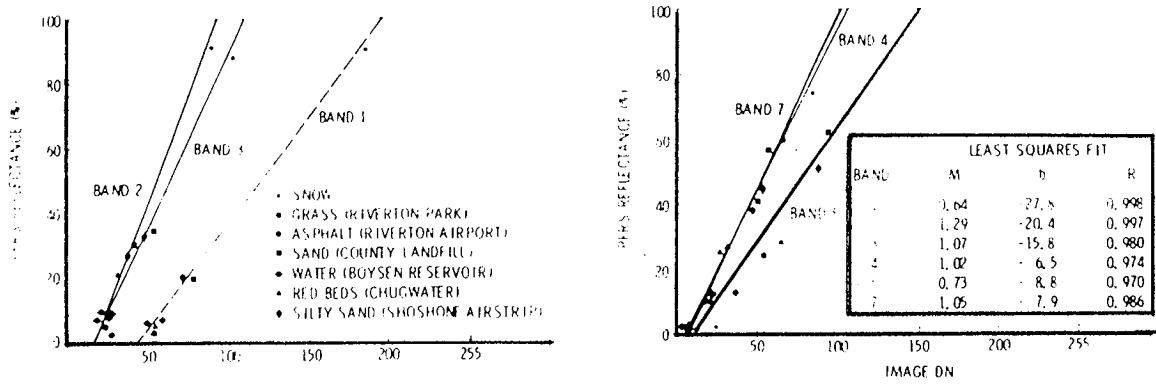
FIGURE 1. CALIBRATION CURVES FOR LANDSAT-4 TM DATA BASED
ON FIELD (PFRS) REFLECTANCE MEASUREMENTS,
WIND RIVER/BIGHORN BASIN AREA, WYOMING

BAND	OFFSET (IN LANDSAT 4 DN)	GAIN
— 1	44	1.63
— 2	16	3.29
— 3	15	2.73
— 4	6	2.60
— 5	12	1.86
— 7	8	2.68
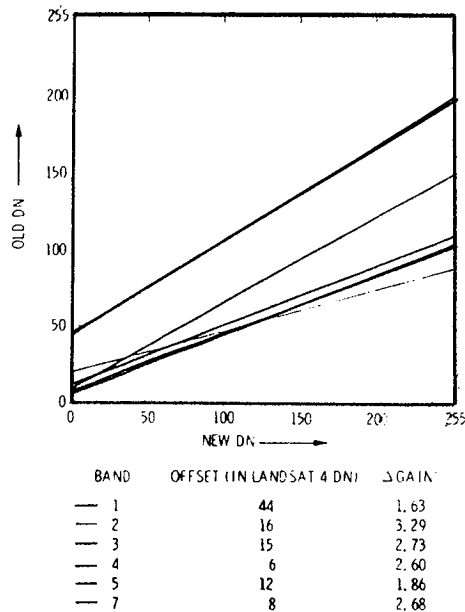
FIGURE 2. A GAIN AND OFFSET INCREASE FOR THE TM SENSOR
CALCULATED FROM CALIBRATION RESULTS,
WIND RIVER/BIGHORN BASIN AREA, WYOMING

110

AN INITIAL ANALYSIS OF LANDSAT-4 THEMATIC MAPPER DATA FOR THE DISCRIMINATION OF AGRICULTURAL, FORESTED WETLAND, AND URBAN LAND COVERS

DALE A. QUATTROCHI

NASA/NATIONAL SPACE TECHNOLOGY LABORATORIES

An initial analysis of Landsat-4 Thematic Mapper (TM) data for the discrimination of agricultural, forested wetland, and urban land covers has been conducted using a scene of data collected over Arkansas and Tennessee on August 22, 1982. A study area in Poinsett County, Arkansas was used to evaluate a classification of agricultural lands derived from multitemporal Landsat Multispectral Scanner (MSS) data in comparison with a classification of TM data for the same area. Results from this comparative analysis showed that the multitemporal MSS classification produced an overall accuracy of 80.91% while the single-date TM classification yielded an overall classification accuracy of 97.06% correct.

Data over Reelfoot Lake in northwestern Tennessee were used to evaluate the TM's capabilities for delineating forested wetland land covers. Sixty spectral signatures were driven from the data utilizing information from channels 2, 3, 4, 5 and 7. These 60 signatures were ultimately grouped into five primary wetland cover types: cypress; mixed hardwoods; willow and cypress; brush, grasses, and emergents; and floating acquatic vegetation. From an accuracy assessment of the classification, it was determined that the five wetland categories had an overall percent correct classification of 95.36%, based on a comparative evaluation with ground truth information.

Additionally, the TM data were used to identify urban features within a small city in northwestern Tennessee. Data over Union City, a town with a population of about 15,000 people, were classified and evaluated for accuracy in discriminating urban land covers. Six specific land covers were identified from the classified data product: roads and inert materials; commercial and industrial development; residential development; agriculture and bare soil; transitional or grassland areas; and forested areas. In a comparative assessement with ground truth information, the classification derived for the

study area yielded an overall accuracy of approximately 90% correct. An assessment of digitally enhanced TM data was also performed using principal components analysis to facilitate photointerpretation of urban features within Union City. These transformed data were used to illustrate the potential of the TM for providing detailed information on the location of individual structures, and for the discrimination of discrete features in the urban milieu.

PRELIMINARY EVALUATION OF THEMATIC MAPPER
IMAGE DATA QUALITY

R. B. MACDONALD, F. G. HALL, D. E. PITTS, R. M. BIZZELL
NASA/LYNDON B. JOHNSON SPACE CENTER

S. YAO, C. SORENSEN, E. REYNA AND J. CARNES
LOCKHEED ENGINEERING AND MANAGEMENT SERVICES COMPANY INC.

Thematic Mapper (TM) data from Mississippi County, Arkansas, and Webster County, Iowa, were examined for the purpose of evaluating the image data quality of the TM which was launched on board the Landsat-4 spacecraft in July 1983. Expectations based upon field research data, helicopter spectrometer data, and Thematic Simulator data collected and analyzed over the last 5 years at the Johnson Space Center appear as though they may be fulfilled. However, the results reported here are based on only a few scenes of data and must be placed in the context of other investigations for other geographic and climatic regimes before general conclusions can be reached.

Preliminary clustering and principal component analysis indicates that the middle infrared and thermal infrared data of TM appear to add significant information over that of the near IR and visible bands of the multispectral scanner data. Moreover, the higher spatial resolution of TM appears to provide better definition of the edges and the within variability of agricultural fields. Quantifications of these improvements are now underway and will be available in the near future. The geometric performance of TM data, without ground control correction, was found to exceed our expectations (1/10 pixel rms under an affine transformation to a 7-1/2 minute USGS map). The modulation transfer function for the 1.65 m band was found to agree with prelaunch specifications when the effects of the GSFC cubic convolution and the atmosphere were removed. The band-to-band registration for the bands within the non-cooled focal plane was found to be better than specified. However, the middle infrared and thermal infrared, which are on a separate cooled focal plane were found to be misregistered and were significantly worse than prelaunch specifications.

ASSESSMENT OF COMPUTER-BASED GEOLOGIC MAPPING OF ROCK UNITS IN THE LANDSAT-4 SCENE OF NORTHERN DEATH VALLEY, CALIFORNIA

NICHOLAS M. SHORT
NASA/GODDARD SPACE FLIGHT CENTER

Geologic mapping of stratigraphic units by use of aerial-photointerpretation methods has been the established practice for nearly four decades. Mapping by means of multispectral remote sensors on aircraft and, since the first Landsat in 1972, on spacecraft should in principle be a more efficient procedure. Classification mapping of stratigraphic units within Landsat scenes by computer-based statistical analysis of spectral data has achieved relatively low and generally unacceptable accuracies of typically 40-60% in semi-arid mountainous terrains. Rock unit identification by ratio and principal components analysis may reach higher accuracies in terrains dominated by good exposures of rock materials and sparsity of vegetation. However, none of these methods is likely to attain consistently high accuracy in any favorable terrain because of two fundamental differences between conventional geologic maps and those derived from remote sensing data. These are:

1. only spectral categories of rock materials can be separated by remote sensing, allowing some rock units to be specified, but geologic maps depend on stratigraphic discrimination in which relative ages must be recognized by some time criterion that normally requires close examination, and

2. much of the area represented by a stratigraphic unit is actually covered by soil, debris, vegetation, etc. and is mapped by extrapolation whereas a remote sensing map shows only what is at the immediate surface.

Improved classification accuracies have been predicted for Landsat-4 because of the four additional spectral bands, higher resolution, and greater sensitivity of the Thematic Mapper (TM). This has now been verified for land use and agricultural classifications but has not been fully tested for geologic classes. This paper reports results from a series of classifications conducted on a subscene of the northern Death Valley, California, acquired by the TM on November 17, 1982. These are summarized as follows:

TYPE OF CLASSIFICATION	IMAGE SIZE (pixels)	BANDS USED	NO. OF CLASSES
Supervised (subsampled)	300 x 320	1,2,3,4,5,7	21 (19)
Supervised (full size)	1500 x 1600	1,2,3,4,5,7	18
Unsupervised (32 cluster)	300 x 320	1,2,3,4,5,7	17
Supervised	"	1,5,7	19
"	"	2,3,4	18
Unsupervised (16 cluster)	"	1,2,3,4,5,7	11 (8)
"	"	2,3,4	9 (7)

(Vertical axis label at left: Increasing Apparent Accuracy ↑)

Measurements of accuracy are made through comparison with the 1977 edition of the Death Valley geologic sheet. This employs a simplified map version which is registered by computer to the image data base, allowing a pixel by pixel match with the classified scene. The results from this study show accuracy ranges from 36 to 79% depending on the type of classifier used and the statistical adjustments made to the data. Accuracy values in identifying geologic units were 2 to 3 times higher for those in the relatively flat valleys than for units in the rugged mountainous terrain. Improvements in accuracy will be sought by correcting for slope/aspect variations in mountainous terrain using topographic data recorded in Defense Mapping Agency (DMA) tapes. The above classification results will also be compared with ratio and principal component image classifications made from the same scene.

[EXERPTED FROM LANDSAT-4 EARLY RESULTS SYMPOSIUM PAPER]

A CONCEPT FOR THE PROCESSING AND DISPLAY OF
THEMATIC MAPPER DATA

RUPERT HAYDN
UNIVERSITY OF MUNICH

INTRODUCTION

With the successful launch of the Thematic Mapper on Landsat-4, NASA has implemented a system which will have tremendous impact on the future of spaceborne remote sensing. The improved capabilities of this scanner in comparison to the Landsat-MSS form an important basis for evaluating the operational aspects of remote sensing from space and also for exploring its implications to the earth sciences, especially in terms of information acquired within the so called short-wave infrared regions (SWIR) of the electromagnetic spectrum.

In keeping with the overall goals of this program, it is essential to improve data availability not only to the existing remote sensing community but also to potential users with new applications. Therefore, topics such as image distribution networks and image formats in terms of optimizing the data content and extractable information within commonly available standard products should be emphasized. The purpose of this paper is to discuss this concept of optimization and to show ways in which preliminary Thematic Mapper image products might represent a feasible approach towards the above cited "commonly available standards".

User Requirements Versus Landsat Thematic Mapper Data

With respect to the availability of Thematic Mapper image products, one must specifically consider the needs of the large potential earth-science user community, which is not necessarily interested in remote sensing research per se, but in the utilization of remote sensing products as one of many tools. For the near future, the link between remote sensing technology and the potential user community has to be established on a level which adequately

meets its requirements on a non-experimental or operational basis. This can probably be best fulfilled through addressing existing and well established capabilities for interpretive analysis of image data.

The Landsat-4 Thematic Mapper system represents an ideal platform from which to promote the establishment of such a link. The high resolution capability of TM brings spaceborne remote sensing into the realm of high altitude aerial photography. Therefore, the traditional methods in photointerpretation can now be applied more directly than was possible with lower resolution data. This poses a challenge for the potential user community which has to be met. The spectral information acquired by multispectral scanners is a feature unique to remote sensing technology. The diversity of spectral bands on TM offers new capabilities for identifying and classifying earth materials that must be considered in any utilization scheme.

Generallly, it can be stated that multispectral information can best be accessed and evaluated through digital interactive image processing techniques. The potential user community, however, has not reached the level where image processing is being used routinely as a standard tool. Therefore, for the time being, special effort must be put into development of strategies that will guarantee optimal utilization of the spectral information contained in remote sensing data acquired under the varying conditions affecting each scene. The Thematic Mapper system provides spectral information in seven carefully selected spectral bands, covering the visible, near IR, short-wave IR and thermal IR region of the electromagnetic spectrum. The challenge is to devise the best approach for presenting this complex spectral information in a pictorial format which can be understood and accepted as a standard by the growing user community.

Currently, natural and false color images are the standard display products with which the user community has become familiar. But, if we incorporate one or both of the TM (bands 5, 7) into the production of a color image, that community should be willing to accept this as another new standard which supplements rather than replaces the imagery already in use.

The mere display of individual TM-bands in form of black and white renditions cannot be regarded as an optimum standard product because the actual recorded spectral information is not easily assessed by visual means. Thus, unique spectral characteristics recorded in one band are most effectively displayed and identified when considered in combination with or contrast to other spectral bands. Therefore, the generation of improved standard products requires a certain amount of image processing in order to take full advantage of the multispectral information recorded. Taking advantage of the spectral information means also to generate pictorial presentations which can be readily understood and "spectrally deciphered" by the interpreter.

[EXERPTED FROM LANDSAT-4 EARLY RESULTS SYMPOSIUM PAPER]

QUICK LOOK ANALYSIS OF TM DATA OF THE WASHINGTON, D.C. AREA

DARREL L. WILLIAMS, JAMES R. IRONS, BRIAN L. MARKHAM,
ROSS F. NELSON AND DAVID L. TOLL
NASA/GODDARD SPACE FLIGHT CENTER

RICHARD S. LATTY
UNIVERSITY OF MARYLAND

MARK L. STAUFFER
COMPUTER SCIENCES CORPORATION

With the launch of Landsat-4 on July 16, 1982, and the successful operation of its primary payload, the Thematic Mapper (TM), a significantly new source of data became available to the remote sensing community. Relative to the familiar Multispectral Scanner (MSS), the TM offers: improved spatial resolution (30m versus 80m), new and more optimally placed spectral bands, and improved radiometric sensitivity quantized over eight bits rather than six bits. All of these improvements in sensor capability were justified from the standpoint that they would significantly improve data quality and information content, and, thereby increase digital classification accuracies. Post-launch verification of these expected improvements is of great interest to NASA and the remote sensing community.

Researchers within the Earth Resources Branch at NASA's Goddard Space Flight Center in Greenbelt, Maryland, have developed a fixed factor analysis-of-variance (ANOVA) approach to quantify the impact of each TM sensor characteristic (spectral, spatial, and radiometric resolutions) on classification accuracy. All assessments are made relative to MSS sensor characteristics, and the impact of each characteristic is assessed individually, and in all possible combinations. Thematic Mapper data acquired over the Washington, D.C., area on November 2, 1982, are being utilized to conduct the experiment. To date, four of the eight data sets required to fulfill the ANOVA design have been created and analyzed. These consisted of: the original data (28.5 meter pixel, eight bits, six channels); the original

data degraded to six bit quantization; a three channel subset of the original data (TM bands 2, 3, and 4 which are similar to MSS bands 1, 2 and 4); and the original data degraded to MSS spatial resolution. [The thermal data (band 6) were excluded from this study due to the difference in spatial resolution (120 meters.)] Nine different study sites, 256 by 256 pixels in size, were randomly selected from the full scene for analysis. Recent aerial photography was available and all sites were visited during the last week of October to collect ground reference data. All nine study areas for each of the four data sets were classified using a per-point Gaussian maximum likelihood classifier.

The following results were obtained: the reduction of quantization level from eight bits to six bits caused a decrease in overall accuracy (7%); the use of only three bands (TM 2, 3 and 4) covering the visible and near infrared portion of the spectrum caused a decrease in overall accuracy (7%); and the decrease in spatial resolution resulted in an increase in overall accuracy (4%). Results indicate that the increased radiometric and spectral resolution of the TM instrument do provide increased information content. The result of the spatial resolution degradation is somewhat misleading, in that the result is more a function of the type of classifier used (i.e., per-point), rather than a function of spatial resolution. This result points to the need for new classifiers, such as contextual classifiers, which take into account the increased spectral heterogeneity in higher resolution data.

ABOVEGROUND BIOMASS ESTIMATION IN A TIDAL BRACKISH MARSH USING SIMULATED THEMATIC MAPPER SPECTRAL DATA

MICHAEL HARDISKY AND V. KLEMAS
UNIVERSITY OF DELAWARE

A series of experiments have been intiated to determine the feasibility of using Thematic Mapper spectral data to estimate wetlands biomass. To date, actual Thematic Mapper data have not been available for our Delaware test site. However a number of experiments have been conducted using hand-held radiometers simulating Thematic Mapper wavebands 3, 4 and 5. Spectral radiance data have been collected from the ground and from a low altitude aircraft in an attempt to gain some insight into the potential utility of actual Thematic Mapper data for biomass estimation in wetland plant communities.

The study described herein does not attempt to distinguish individual plant species within brackish marsh plant associations. Rather, we have chosen to lump plant species with similar canopy morphologies and then estimate from spectral radiance data the biomass of the group. The rationale for such an approach is that plants with a similar morphology will produce a similar reflecting or absorbing surface (i.e. canopy) for incoming electromagnetic radiation. Variations in observed reflectance from different plant communities with a similar canopy morphology are more likely to be a result of biomass differences than a result of differences in canopy architecture. If the hypothesis that plants with a similar morphology exhibit similar reflectance characteristics is true, then biomass can be estimated based on a model for the dominant plant morphology within a plant association and the need for species discrimination has effectively been eliminated.

Modeling the relationship between spectral radiance indices and live aerial biomass in brackish marsh plant communities required consideration of diverse morphologic characteristics among plants residing in the same community. Figure 1 shows the linear relationship between vegetation index
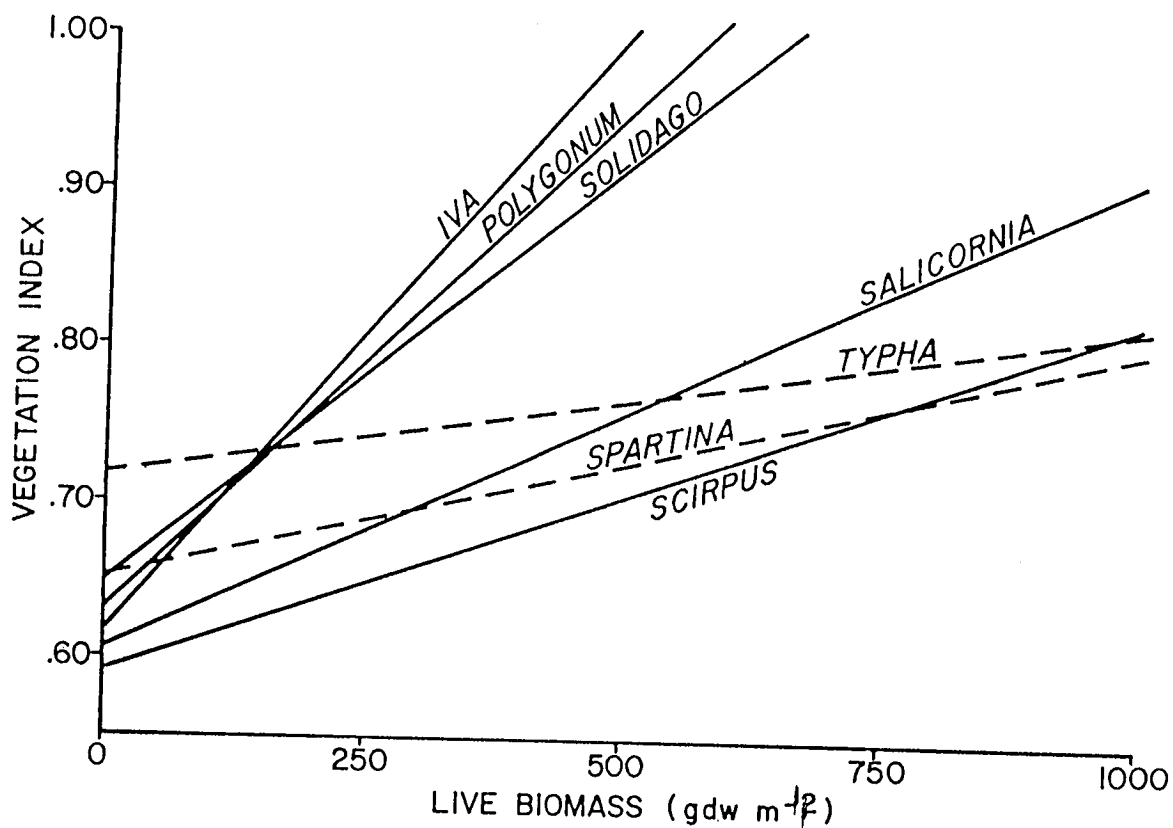
Figure 1. Relationship between live biomass of a variety of wetland
plants and the canopy spectral radiance expressed as the
vegetation index. Iva, Polygonum and Solidago represent
broadleaf canopies. Typha and Spartina represent
gramineous canopies. Saliconia and Scirpus represent
leafless canopies.

and total live biomass for a variety of wetland plants. Iva Polygonum, and Solidago represent broadleaf canopies and exhibit rapid increases in vegetation index for relatively small changes in biomass. This characteristic suggests that the spectral index can become saturated rapidly. Structurally, these canopies maintain most leaf surfaces in the horizontal plane and generally form a complete canopy cover, reducing or eliminating exposure of dead components or soil background to solar irradiance. This combination of canopy characteristics yields a very absorptive canopy in the red region and a very reflective canopy in the near infrared region, thus the high vegetation index relative to the amount of live biomass present.

The opposite extreme to the broadleaf canopy would be the leafless canopies represented by Salicornia and Scirpus. Both Salicornia virginica and Scirpus olneyi possess erect, leafless stems with most green tissue in the vertical plane and primarily soil background and dead plant material in the horizontal plane. Normally these canopies are very open with soil surface characteristics potentially contributing greatly to the observed spectral radiance.

The third canopy type represented in Figure 1 is the gramineous canopy type of Spartina and Typha. Spartina alterniflora exhibits alternate leaves along the length of the stem, whereas Typha angustifolia has basal leaves. Both plants form canopies with portions of leaves in the horizontal and in the vertical plane. S. alterniflora exhibits a broad range of canopy configurations as a result of its wide environmental tolerance limits. Both plant canopies can maintain substantial quantities of dead material within the canopy. The amount of live leaf tissue determines to what degree dead material and soil background will influence spectral reflectance. Theoretically, the occurrence of flat leaves (portions of which may be horizontal) in the gramineous canopy would place them somewhere between the broadleaf and leafless canopies in terms of an increase in vegetation index value for an increase in biomass (i.e. an intermediate slope). In practice this does not occur because the measured vegetation index represents the composite of reflectance from vegetation (live and dead) and the soil. In the case of the gramineous canopy, the dead vegetation and soil are oftentimes

123

well illuminated and contribute significantly to the measured vegetation index. The net effect is an attenuation of vegetation index increases with increasing biomass amount, when compared to the other canopy types.

Based on the three morphologic canopy types, simple regression models were developed equating the vegetation index and the infrared index with biomass. Spectral data were collected with the hand-held radiometer from the ground and from a low altitude aircraft. Sampling points were arranged on a 30 m grid with actual harvesting of vegetation conducted after the radiance data were collected.

Table 1 compares the biomass estimates for the brackish marsh computed from ground gathered spectral radiance data and estimated from harvesting. Included in Table 1 are total live biomass estimates computed from MSS vegetation index values. With the vast majority of spectral radiance index and model combinations, the spectral radiance index estimates of total live biomass were not significantly different from the harvest biomass estimates. The species combination models for the vegetation and infrared indices were particularly good, with the all species models being the best models for use with all three spectral radiance indices. The MSS vegetation index estimates were very similar to the vegetation index estimates. This is not surprising considering both indices contain essentially the same spectral information.

Total live biomass estimates from airplane gathered spectral radiance indices converted for use in models developed with ground spectral data are presented in Table 2 for each of the three spectral transformations. Infrared index estimates of total live biomass were not significantly different from harvest estimates of total live biomass for the single species and species combination models. These same models yielded biomass estimates from the MSS vegetation index and the vegetation index, which were usually significantly lower than the harvest estimates of total live biomass. Both forms of the grasses/Scirpus models and the linear form of the all species model used with the two vegetation indices provided total live biomass estimates, which were very similar to harvest biomass estimates (all were not significantly different). The log form of the all species model yielded the best estimates of total live biomass when used with the infrared index.

TABLE 1

OLD MILL CREEK BRACKISH MARSH BIOMASS
PREDICTIONS, AUGUST 1982 (GROUND DATA)

Model	Form	Vegetation Index Predicted Biomass	Diff.	Infrared Index Predicted Biomass	Diff.	MSS Vegetation Index Predicted Biomass	Diff.
Single species[a]	L	794(12)	- 61(92)	836(44)	- 19(74)	792(60)	- 63(84)
	LN	700(69)	-155(88)	772(53)	- 83(84)	704(61)	-151(84)
Species combination[b]	L	877(75)	22(90)	858(64)	3(81)	732(105)	-123(105)
	LN	868(72)	13(96)	925(68)	70(97)	673(103)	-182(105)
Grasses & Scirpus	L	1065(54)	210(95)*	1042(58)	187(94)	1063(49)	208(91)*
	LN	1060(77)	205(115)	1000(79)	145(110)	1039(71)	183(110)
All species	L	952(63)	97(102)	1014(63)	159(98)	964(55)	109(96)
	LN	1020(96)	165(132)	968(86)	113(116)	970(82)	115(120)
All species	L	695(29)	-160(74)*	553(21)	-302(66)*	---	---
(equal weight)	LN	997(83)	142(120)	703(49)	-152(85)	---	---

Values are means with one standard error of the mean in parentheses. Biomass units are gdw m^{-2}.

a - Single species model for broadleaf was Acnida / Hibiscus for gramineous, S. alterniflora (both height forms) and for leafless Scirpus.

b - Species combination model for broadleaf species was the all broadleaf species, for gramineous S. alterniflora Typha and for leafless Scirpus / Salicornia.

Form - L = linear, LN = natural log

Diff. = Difference between spectrally estimated and harvest estimated biomass means. A negative value indicates the spectrally estimated mean was less than the harvest estimate. An asterisk indicates that spectral and harvest estimates were statistically different at the 0.05 level according to a paired t-test.

TABLE 2

OLD MILL CREEK BRACKISH MARSH BIOMASS PREDICTIONS, AUGUST 1982 (AIRCRAFT DATA CONVERTED FOR USE IN GROUND DEVELOPED MODELS)

Model	Form	Vegetation Index Predicted Biomass	Diff.	Infrared Index Predicted Biomass	Diff.	MSS Vegetation Index Predicted Biomass	Diff.
Single species[a]	L	609(82)	-246(70)*	870(31)	15(49)	558(79)	-297(67)*
	LN	519(55)	-336(52)*	753(27)	-102(49)	498(55)	-357(53)*
Species combination[b]	L	764(49)	- 91(49)	931(54)	76(57)	577(85)	-278(73)*
	LN	661(35)	-194(44)*	927(24)	71(50)	500(74)	-355(65)*
Grasses & Scirpus	L	928(22)	73(55)	1075(11)	220(55)*	852(44)	- 3(59)
	LN	818(27)	- 37(55)	983(16)	128(56)*	750(47)	-105(61)
All species	L	794(25)	- 61(55)	1050(12)	195(55)*	728(49)	-127(62)
	LN	709(32)	-146(56)*	941(17)	86(56)	641(50)	-214(63)*
All species	L	622(12)	-233(53)*	565(4)	-290(54)*	---	---
(equal weight)	LN	732(28)	-123(55)*	697(10)	-158(55)*	---	---

Values are means with one standard error of the mean in parentheses. Biomass units are gdw m^{-2}

a - Single species model for broadleaf was Acnida / Hibiscus for gramineous, S. alterniflora (both height forms and for leafless Scirpus.

b - Species combination model for broadleaf species was the all broadleaf species, for gramineous S. alterniflo Typha and for leafless Scirpus / Salicornia.

Form - L = linear, LN = natural log

Diff. = Difference between spectrally estimated and harvest estimated biomass means. A negative value indicat the spectrally estimated mean was less than the harvest estimate. An asterisk indicates that spectral and harvest estimates were statistically different at the 0.05 level according to a paired t-test.

Airplane gathered spectral radiance index values were used directly in models using airplane gathered spectral data for predicting total live biomass (Table 3). The MSS vegetation index and the vegetation index values provided estimates of total live biomass, which were not significantly different from harvest estimates of total live biomass. Infrared index values produced significantly higher estimates of total live biomass then were estimated by harvest techniques. Of the three spectral radiance indices tested, the vegetation index yielded the best overall estimates of total live biomass.

TABLE 3

OLD MILL CREEK BRACKISH MARSH BIOMASS PREDICTIONS
AUGUST 1982 (AIRCRAFT DATA WITH MODELS FOR AIRCRAFT DATA)

Model	Form	Harvest Biomass	Predicted Biomass	Difference
Vegetation	L	855(54)	924(41)	69(62)
Index	LN	855(54)	802(49)	- 53(64)
Infrared	L	855(54)	1214(18)	359(57)*
Index	LN	855(54)	1346(38.)	490(65)*
MSS Vegetation	L	855(54)	603(126)	-252(122)
Index	LN	855(54)	697(94)	-158(96)

Models correspond to the type D models in Table 5.15.

Values are means of 21 plots with one standard error in parentheses.

Biomass units are gdw m^{-2}.

Difference = Difference between spectrally estimated and harvest estimated biomass means. A negative value indicates the spectrally estimated mean was less than the harvest estimate. An asterisk indicates that spectral and harvest estimates were statistically different at the 0.05 level according to a paired t-test.

COMPARISON OF THE INFORMATION CONTENT OF DATA FROM THE LANDSAT-4 THEMATIC MAPPER AND THE MULTISPECTRAL SCANNER

JOHN C. PRICE

USDA HYDROLOGY LABORATORY

Simultaneous data acquisition by the Landsat-4 Thematic Mapper (TM) and the Multispectral Scanner (MSS) permits the comparison of the two types of image data with respect to engineering performance and data applications. In this paper the "information" contained in five matching scenes in agricultural areas is evaluated for the visible and near-IR channels, leading to the conclusion that the TM provides a significant advance in information gathering capability as expressed in terms of either bits per pixel or bits per unit area.

Because the MSS lacks a thermal IR channel the 10-12 micrometer data of the TM at 120 m resolution are analyzed theoretically using methods developed for the Heat Capacity Mapping Mission, which produced data at 481 meter resolution, but with a more favorable orbital acquisition strategy. It appears that the TM thermal IR data are of interest mainly for mapping water bodies, which do not change temperature during the day, and for monitoring thermal features associated with human activity. Interpretation for surface moistness is also possible, but use of thermal data for agricultural purposes would require a broader swath width to increase coverage frequency, and possibly a paired "night" satellite in order to assure day-night coverage, which is needed for accurate quantitative analysis of the thermal IR data.

For large scale agricultural assessment both the cost and frequency of data acquisition are very important. Despite the excellent quality of the TM data, a pair of lower cost (MSS) satellites must be considered as a viable option for applications such as for national or international production forecasting. For studies of localized areas the superior TM spatial and spectral resolution is clearly an overwhelming advantage.

STUDY OF THEMATIC MAPPER AND MULTISPECTRAL
SCANNER DATA APPLICATIONS

F. G. SADOWSKI, R. H. HAAS, J. A. STURDEVANT, W. H. ANDERSON, P. M. SEEVERS,
J. W. FEUQUAY, L. K. BALICK, F. A. WALTZ
TECHNICOLOR GOVERNMENT SERVICES, INC./EROS DATA CENTER

AND

D. T. LAUER
U.S. GEOLOGICAL SURVEY/EROS DATA CENTER

The U.S. Geological Survey EROS Data Center evaluated the utility of
Landsat Multispectral Scanner (MSS) and Thematic Mapper (TM) data for natural
resource assessment and land cover information, emphasizing manual
interpretation and digital classification of the data for U.S. Department of
the Interior applications. In most cases, substantially more information was
derived from TM data than from MSS data.

Studies were conducted to evaluate the capability of TM data for
providing improved land cover information using data taken over the
Washington, D.C. area. The results were derived from TM and coincident MSS
data that were acquired by Landsat-4 on November 2, 1982. Characteristics of
TM digital data that were observed for several broad classes of land cover
were analyzed and comparisons were drawn between TM data and the data of the
coincident Landsat-4 MSS scene. Also the TM data were visually evaluated as
single-band, black-and-white images, and in several three-band combinations as
color composite images. Finally, demonstrations were made of TM data
transformations which can be used to present the data in a manner that is
potentially more useful for analysis or display. These transformations enable
generating (a) hue, intensity, and saturation data space from red, green, and
blue color space, and (b) perspective view images.

The digital data analyses of the Washington, D.C. scene suggested the potential for TM data to provide improved land cover information due to the addition of new spectral data channels. The mid-IR bands (5 and/or 7) may be especially useful because of (a) the large range of variability for digital values in five separate land cover classes and (b) low correlations with other spectal bands for vegetated land cover and water. The mid-IR bands may also play a role in increasing the dimensionality of data space that has been transformed into its principal components. Low correlations between the blue band (band 1) and other spectral bands suggest its utility for studying variations within areas of water as well as vegetated land areas.

The mean data values of five land cover classes occurring in the Washington, D.C. area were shown to be more widely separated in TM spectral bands 2, 3 and 4 than for the equivalent MSS bands 1, 2 and 4. In addition, the relative variances associated with the classes were more often lower for the TM bands than for the corresponding MSS bands. These observations could indicate better multispectral discrimination of land cover classes by TM bands 2, 3 and 4. However, an artifact in the MSS data may have contributed substantially to the greater relative variances observed in the MSS spectral bands.

The large variability noted for the digital values in the mid-IR bands (5 and 7) likely contributed to the results of a study of black-and-white images of the six reflective TM bands, in which interpreters indicated a preference for images of bands 5 and/or 7 over other bands for making distinctions in 8 out of 11 of the interpretation categories that were addressed. Results of interpreting six color composite images of the Washington, D.C. scene showed highest interpreter preferences for a standard color-infrared composite (bands 2, 3 and 4), or a color composite consisting of bands 3, 5 and 4 in 8 out of 11 categories. A natural color composite image (bands 1, 2 and 3) showed high interpreter preferences for three interpretation categories involving distinctions within predominantly nonvegetated areas.

Two additional studies were conducted in native prairie areas of South Dakota (Scene ID 40070-16444 and 16451; September 24, 1982) and Kansas (Scene ID 40049-16275; September 3, 1982). One study emphasized manual interpretation by field personnel while the second study evaluated the new spectral and spatial data via digital analysis.

When the TM data taken of central South Dakota were reproduced as 1:100,000 scale color composite images, field personnel were able to use the TM data efficiently for a variety of discipline-related tasks. Scientists and technicians were able to locate roads, small stock ponds, and many other land features. They were also able to identify resource types and assess the ecological status of natural vegetation within management units. These tasks were best accomplished with visual interpretation using a false-color composite of TM bands 3, 4 and 5. TM data also provided a new source of spectral information that was useful for natural resource assessment. Now mid-infrared spectral bands, TM band 5 and band 7, aided in distinguishing water resources, wetland vegetation resources, and other important terrain features. The added information was useful for both manual interpretation and digital data classification of vegetation resources and land features.

Results from the analyses of both TM and TM Simulator spectral data suggest that the coefficient of variation for major land cover types is generally less for TM data than for MSS data taken from the same area. This reduction in variance contributes to an improved multispectral classification of land cover types. The TM bands 5 and 7 also add a new dimension to multispectral analysis, contributing new information about vegetation in natural ecosystems. Although the amount of new information in TM bands 5 and 7 is small, it is unique in that the same information cannot be derived from four-band Landsat MSS spectral data (Fig. 1).

Digital data analyses of the South Dakota scene indicate that the effect of the dynamic range of TM band 5 data and the unique interaction of reflectance in TM bands 4 and 5 were important in digital classification of vegetation and land cover. Furthermore, the greater resolution and information content of TM data provide several alternatives for habitat assessment.
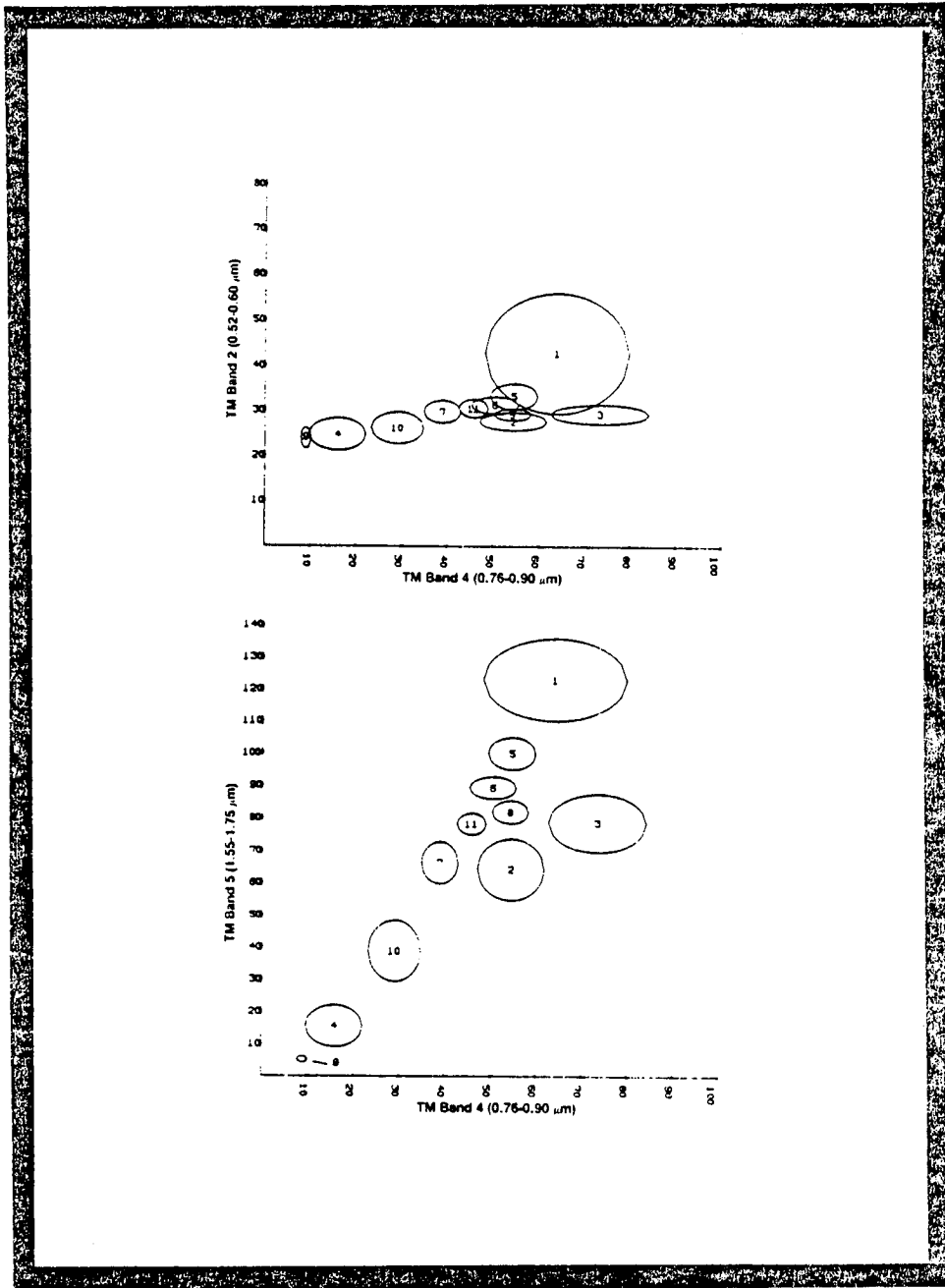
Figure 1. Comparison of ISOCLASS clustering showing mean TM spectral values (scaled brightness) for TM band 2 vs. TM band 4 and TM band 5 vs. TM band 4

132

THEMATIC MAPPER DATA QUALITY AND PERFORMANCE ASSESSMENT
IN RENEWABLE RESOURCES/AGRICULTURE REMOTE SENSING

ROBERT M. BIZZELL AND HAROLD L. PRIOR
NASA/LYNDON B. JOHNSON SPACE CENTER

For the past decade the Johnson Space Center has been involved in the research and development of technology that utilizes satellite based remotely sensed data to perform global crop inventories. The Large Area Crop Inventory Experiment (LACIE) established the proof-of-concept with the Landsat MSS. The fundamental understanding gained with the LACIE formed the basis for the development of these techniques in the framework of a systems approach that has been evaluated in the Agriculture and Resources Inventory Surveys Through Aerospace Remote Sensing (AgRISTARS) project. The successes with these joint projects have been manifest by the installation and periodic upgrade by the Foreign Agriculture Service (FAS) of the USDA within their ongoing operational forecasting system.

The limits reached with the MSS emphasized the need for the Thematic Mapper (TM) to further expand the progress made to date. It is believed that the increased spatial resolution will provide solutions to proportion estimation error due to mixed pixels, and the increased spectral resolution will provide for the identification of important agricultural features such as crop stage, and condition.

This paper will describe the results of analyses conducted relative to these hypothesis from sample segments (approximately 30 sq. miles) extracted from the 4-band Detroit scene and the 7-band Mississippi County, Arkansas engineering test scene. Several studies were conducted to evaluate the geometric and radiometric performance of the TM to determine data viability for the more pertinent investigations of TM utility. In most cases this requirement was more than sufficiently satisified. This allowed the opportunity to take advantage of detailed ground observations for several of the sample segments to assess class separability and detection of other important features with TM.

The results presented regarding these TM characteristics show that not only is the increased definition of the within scene variance captured by the increased spatial and spectral resolution, but that the mid-IR bands (5 and 7) are necessary for optimum crop type classification. Both qualitative and quantitative results are presented that describe the improvements gained with the TM both relative to the MSS and on its own merit.

PRELIMINARY COMPARISONS OF THE INFORMATION CONTENT AND
UTILITY OF TM VERSUS MSS DATA

BRIAN L. MARKHAM
NASA/GODDARD SPACE FLIGHT CENTER

Comparisons were made between subscenes from the first TM scene acquired of the Washington, DC area (July 29, 1982 - 4 bands only) and a MSS scene acquired approximately one year earlier (July 11, 1981). Three types of analyses were conducted to compare TM and MSS data: a water body analysis, a principal components analysis and a spectral clustering analysis.

The water body analysis compared the capability of the TM to the MSS for detecting small uniform targets. All water bodies (>10 meters) were located on aerial photographs collected July 13, 1982 and categorized by the size of the maximum inscribable circle. Each scene was independently clustered and the clusters assigned to water or non-water. Each water body was said to be detected for the MSS or the TM if a minimum of one pixel at its location was classified into a water cluster. Of the 59 ponds located on the aerial photographs 34 (58%) were detected by the TM with six commission errors (15%) and 13 (22%) were detected by the MSS with three commission errors (19%). The smallest water body "detected" by the TM was 16 meters; the smallest "detected" by the MSS was 40 meters.

For the principal components analysis, means and covariance matrices were calculated for each subscene, and principal components images generated and characterized. The 4-band TM image had slightly higher dimensionality than the MSS in this rural-suburban area, with 2.6% of the variance in the third component as compared to 1.2%. The first two principal components of the TM and MSS were similar, containing brightness-like and greenness-like features. The MSS third and fourth principal components were dominated by noise and striping whereas the third TM principal component (a red to blue-green contrast) was less noisy and appeared to contain information useful for separating built-up features from bare soil. This third component detected the spectral flatness of construction materials in the visible spectrum as opposed to the sloping response of bare soils.

In the spectral clustering comparison each scene was independently clustered and the clusters were assigned to informational classes. The clusters were assignable to the same classes on the 4-band TM as on the MSS data with the exception that the TM data provided separation of bare soil areas from areas of buildings that MSS data did not provide. The TM band 1 contributed to this improved separation.

The preliminary comparisons indicated that TM data provides enhancements over MSS in terms of (1) small target detection and (2) data dimensionality (even with 4-band data). The extra dimension, partially resultant from TM band 1, appears useful for built-up/non-built-up area separation.

PARAMETRIC AND NONPARAMETRIC ANALYSIS OF LANDSAT TM AND MSS IMAGERY FOR DETECTING SUBMERGED PLANT COMMUNITIES

STEVEN G. ACKLESON AND VYTAUTAS KLEMAS
UNIVERSITY OF DELAWARE

INTRODUCTION

This research is concerned with assessing the spatial, spectral and radiometric characteristics of Landsat TM and MSS imagery for detecting submerged aquatic vegetation. We approach the problem from two perspectives; purely stochastic or nonparametric in a radiative sense and theoretical in which we use radiative transfer equations to predict upwelling radiance at satellite altitude. In a previous report, we addressed only the spectral aspect of the theoretical approach in which a submerged plant canopy was to be distinguished from a surrounding bottom of sand or mud. In this paper, we continue this line of approach, concentrating on the radiometric characteristics of selected TM and MSS bands.

BACKGROUND

The vast majority of satellite remote sensing of surface features addresses the problem from a purely stochastic perspective. We refer to this approach as nonparametric in the sense that no assumptions are made about the optical nature of the surface feature. Typically, a computer is used to generate categories within the digital multi-band data based upon the variation in spectral signatures. The categories may be derived either manually be selecting subregions or training sites within the image that correlate with ground observations or by instructing the computer to group the data into some finite number of categories of similar signatures. If the nonparametric approach is to be successful, the image must contain large homogeneous surface features relative to the spatial resolution of the data and the researcher must have an ample amount of ground observations with which to correlate each category. If either of these conditions are not met the approach breaks down. Nonparametric techniques have proved quite successful in the past, especially when applied to terrestrial problems.

Recent advances in physical modeling of radiative transfer have greatly improved our ability to understand the optical nature of both terrestrial and marine features. With the development of high quality field radiometers the researcher can now attempt to predict upwelling radiance at satellite altitude with a high degree of confidence. We refer to this approach to the remote sensing problem as parametric because now assumptions are made about the optical nature of the surface feature. Although the problem becomes significantly more complicated the parametric approach does not fall prey to the constraints imposed upon nonparametric techniques. Extensive ground observations are replaced with relatively few surface measurements and the size of the feature can be much smaller, so long as at least one pixel of data is represented. An interesting byproduct of the parameteric approach is one of increased appreciation for the optical nature of the surface feature. The researcher is better able to interpret changes in radiance within imagery for which there are no surface measurements or ground observations.

METHODOLOGY

Parametric Approach

Spectral Assessment. Radiative transfer theory is used to model upwelling radiance that would be received by Landsat TM and MSS viewing a hypothetical estuarine environment. The environment is composed of a clear maritime atmosphere, an optically shallow estuary of either clear or turbid water, and three possible bottom types: vegetation, sand or mud.

Radiometric Assessment. The radiometric resolutions of TM bands 1, 2 and 3 and MSS bands 4 and 5 are compared for the same cases discussed in the previous section. Upwelling radiance at satellite altitude calculated for each band is converted to count values using calibrations taken from the literature. Apparent contrast is then calculated between target and background signals as:

$$\Delta C = C_T - C_B$$

where

C_T = count value calculated from target signal, and

C_B = count value calculated from background signal.

Nonparametric Approach

As a test of the nonparametric approach an ERDAS 400 microcomputer is used to enhance and classify TM imagery of Broad Creek, Maryland. The image is a 256 pixel by 240 line sub-scene generated on November 2, 1982 and centered at latitude $38^{o}44'20"N$, longitude $76^{o}15'25"W$. The full 7-band data set is classified using an unsupervised clustering routine in which a maximum of 27 catagories are generated. Of primary interest in the scene is a medium size SAV bed known to exist on the west bank of Broad Creek.

Ground truth in the form of low altitude, aerial photography was collected at Broad Creek on August 2, 1982, three months prior to the TM overpass. The photos were taken from a Cessna 174 using a handheld 35mm camera using Kodak Pan-x film.

RESULTS

The effectiveness of an orbiting sensor in discriminating spectrally between submerged features is a function of the inherent contrast between the submerged features and how strongly the bottom signal is attenuated by the water column. In optically shallow water the inherent contrast is the controlling factor. Thus, the optimum sensor band is that which correlates with the greatest inherent contrast between adjacent bottom types. In optically deeper water, the optimum sensor band is that for which the water column is most transparent.

In the clear ocean water the optimum band for detecting vegetation on a sand or mud bottom is shown to change with the optical depth of the water. In the turbid San Vicente water the optimum band in optically shallow water remains the optimum band in optically deeper water.

Under certain conditions the contrast between a submerged feature and the surrounding bottom will decrease to zero for some intermediate depth and then increase for yet deeper depths. This could have a significant impact upon how changes in water reflectance should be interpreted and can only be predicted with detailed knowledge of the spectral variation of optical parameters across the sensor band.

Radiometric calibration is shown to be a dominant factor in determining which TM or MSS band will be optimum for detecting a submerged feature such as SAV. Sensors with higher gain settings in general produce data with more information. The gain built into the TM sensors are significantly higher than those of the MSS. This gives TM data a clear advantage in detecting submerged features. In several cases, a band is found to be optimum for detecting SAV in a radiometric sense and yet sub-optimal in a spectral context.

A nonparametric analysis of Thematic Mapper data appears to be useful for detecting SAV in the case of Broad Creek, Maryland. An unsupervised clustering classification of a November 2, 1982 image clearly discriminated between SAV and the surrounding unvegetated bottom. The results were found to agree well with aerial photography collected two months prior to the TM image.

A FIRST EVALUATION OF LANDSAT TM DATA TO MONITOR
SUSPENDED SEDIMENTS IN LAKES

F. R. SCHIEBE, J. C. RITCHIE AND G. O. BOATWRIGHT
U.S. DEPARTMENT OF AGRICULTURE

A comparison was made between ground data collected from Lake Chicot, Arkansas, and Thematic Mapper (TM) data collected on September 23, 1982. A preliminary analysis of limited data indicate that Thematic Mapper data may be useful in monitoring suspended sediment and chlorophyll in a lake with high suspended sediment loads. Total suspended loads ranged from 168 to 508 mg/l. TM Band 3 appears to be most useful with Bands 1, 2 and 4 also containing useful information relative to suspended sediments. Considering water data only, Bands 1, 2 and 3 appear to provide similar information. Bands 3 and 4 are also significantly related. Bands 5 and 7 appear to have independent information content relative to the presence or absence of water. Insufficient range of water temperature ground truth data made an evaluation of TM Band 6 difficult.

SNOW REFLECTANCE FROM LANDSAT-4 THEMATIC MAPPER

JEFF DOZIER
UNIVERSITY OF CALIFORNIA/SANTA BARBARA

ABSTRACT

In California 75% of the agricultural water supply comes from the melting Sierra Nevada snowpack. Basin-wide albedo measurements from the Landsat-4 Thematic Mapper could be used to better forecast the timing of the spring runoff, because these data can be combined with solar radiation calculations to estimate the net radiation budget. The TM is better-suited for this purpose than the MSS because of its larger dynamic range. Saturation still occurs in bands 1-4, but is severe only in band 1. Differentiation of snow optical grain size is possible with TM band 4 through a moderately clear atmosphere. TM band 5 can discriminate clouds from snow, and the combination of bands 2 and 5 appears best for snow mapping.

INTRODUCTION

In California 75% of the agricultural water supply comes from the melting Sierra Nevada snowpack. The California Cooperative Snow Survey uses measurements of snow water equivalent from snow courses, snow depth from aerial survey markers, and snowcovered area from satellite data to estimate the amount and the timing of the spring runoff.

Our work on snow reflectance from the TM should lead to improved use of satellites in snow hydrology. Basin-wide albedo measurements from the TM could be used to better forecast the timing of the spring runoff, because these data can be combined with solar radiation calculations to estimate the next radiation budget. The TM is better-suited for this purpose than the MSS because of its larger dynamic range. Saturation still occurs in bands 1-4, but is only severe in band 1. Moreover, TM band 5 can discriminate clouds from snow.

Calculations of snow reflectance in all 6 TM reflective bands (i.e. 1, 2, 3, 4, 5 and 7), using a delta-Eddington model[5], show that snow reflectance in bands 4, 5 and 7 is sensitive to grain size. An objective in our investigation is to interpret surface optical grain size of snow, for spectral extension of albedo. Our results so far are encouraging.

Table 1 shows calculations of integrated reflectance for snow over all reflective TM bands, and water and ice clouds with thickness of 1mm water equivalent over TM bands 5 and 7. In the blue and green bands (1-2) snow reflectance is not sensitive to grain size, so measurements in these wavelengths will show the extent to which snow albedo is degraded by contamination from atmospheric aerosols, dust, pine pollen, etc. In the red and near-infrared, snow reflectance is sensitive to grain size but not to contaminants, so grain size estimates in these wavelengths can be used to spectrally extend albedo measurements.

The reason that snow reflectance in bands 1 and 2 is not sensitive to grain size is that ice is so transparent in these wavelengths that increasing the size of a snow crystal does not significantly change the probability that a photon impinging on the crystal will be absorbed. Impurities are much more absorptive than ice in these wavelengths, however, so small amounts of contaminants will affect reflectance[4]. In the near-infrared, bands 3 and 4, ice is slightly absorptive, so an incident photon is more likely to be absorbed if the crystal is larger, and snow reflectance is therefore sensitive to grain size. Impurities are not so important in these wavelengths because their absorption coefficients are not much larger than those of ice.

DYNAMIC RANGE

Table 2 gives characteristics of the Thematic Mapper, and, for background information, the Landsat-4 Multispectral Scanner and NOAA-7 Advanced Very High Resolution Radiometer. Bands are listed in spectral order. In the radiance columns of the table, quantization and saturation radiances of the sensor bands are compared with the solar constant, integrated

through the sensor response functions. Solar constant spectral distributions are from the NASA standard[3] adjusted to fit the integrated values measured from the Nimbus-7 cavity radiometer of the earth radiation budget experiment[1]. The last column in the table expresses the sensor saturation radiance as a percentage of the solar constant, integrated through the band response function.

Snow will frequently saturate in band 1, but in bands 2, 3 and 4 the saturation problem is not nearly as severe as with the MSS, so the TM can be used to measure snow albedo and thus allow basin-wide energy budget snowmelt calculations. Bands 5 and 7 will not saturate over snow.

ATMOSPHERIC CORRECTION

Figure 1 shows spectral planetary albedo over snow surfaces of optical grain radiai r=50 m, 200 m and 1000 m, for an Eltermann atmosphere with surface visibility 23km. The absorption and scattering characteristics of the atmosphere were generated with LOWTRAN5[2]. Planetary reflectance was then calculated with a delta-Eddington model, using snow reflectance as the bottom boundary condition. The distinction between reflectance of snow of different grain sizes in TM band 4 is not appreciably degraded by the atmosphere.

REGISTRATION TO TERRAIN DATA

The remaining task required to estimate spectral albedo from the TM over alpine terrain is registration of the TM data to digital terrain data. This task is proving difficult, because the TM data are so much more detailed than the topographic data. Currently, only 3" data (~100m resolution) are available for the Sierra Nevada, but 30m data are in preparation within USGS.

CONCLUSION

Landsat-4 Thematic Mapper data include spectral channels suitable for snow/cloud discrimination and for snow albedo measurements that can be extended throughout the solar spectrum. Except for band 1, the dynamic range is large enough that saturation occurs only occasionally.

REFERENCES

1. Hickey, J. R., L. L. Stowe, H. Jacobowitz, P. Pellegrino, R. H. Maschoff, F. House, and T. H. VonderHaar, 1980, Initial solar irradiance determinations from Nimbus 7 cavity radiometer measurements, Science, 208, 281-283.

2. Kneizys, F. X., E. P. Shettle, L. W. Abreu, J. H. Chetwynd Jr., J. E. A. Selby, W. O. Gallery, R. W. Fenn, and R. A. McClatchey, 1980, Atmospheric transmittance from 0.25 to 28.5μm: Computer Code LOWTRAN5, Air Force Geophysics Laboratory Report AFGL-TR-80-0067.

3. Thekaekara, M. P., ed., 1970, The solar constant and the solar spectrum measured from a research aircraft, NASA TR-R-351.

4. Warren, S. G., and W. J. Wiscombe, 1980, A model for the spectral albedo of snow, 2, Snow containing atmospheric aerosols, Journal of the Atmospheric Sciences, 37, 2734-2745

5. Wiscombe, W. J., and S. G. Warren, 1980, A model for the spectral albedo of snow, 1, Pure snow, Journal of the Atmospheric Sciences, 37, 2712-2733.

Table 1
TM Band Integrated Reflectances, $\mu_0 = \cos 60°$

band	clean semi-infinite snow optical grain radius (μm)				
	50	100	200	500	1000
1	.992	.988	.983	.974	.963
2	.988	.983	.977	.964	.949
3	.978	.969	.957	.932	.906
4	.934	.909	.873	.809	.741
5	.223	.130	.067	.024	.011
7	.197	.106	.056	.019	.010

band	water cloud, 1mm water optical droplet radius (μm)				
	1	2	5	10	20
5	.891	.866	.769	.661	.547
7	.784	.750	.650	.481	.345

band	ice cloud, 1mm water equivalent optical crystal radius (μm)				
	1	2	5	10	20
5	.817	.780	.665	.513	.383
7	.765	.730	.642	.478	.341

Table 2
Landsat-4 TM, Landsat-4 MSS, and NOAA-7 AVHRR Spectral Characteristics

band	μm		radiances ($Wm^{-2}\,\mu m^{-1}\,sr^{-1}$)			
			NEΔL	sat.	solar	%
TM1	.45	.52	.63	161	621	26
MSS4	.50	.61	4.0	259	574	45
TM2	.53	.61	1.24	316	540	58
AVHRR1	.56	.72	.51	518	485	107
MSS5	.60	.70	2.8	179	491	36
TM3	.62	.69	.95	241	468	52
MSS6	.70	.81	2.3	149	401	37
AVHRR2	.71	.98	.33	341	364	94
TM4	.78	.90	.92	234	320	73
MSS7	.81	1.02	3.0	192	285	67
TM5	1.57	1.78	.13	32	66	48
TM7	2.10	2.35	.07	17	24	69
AVHRR3	3.53	3.94	(thermal bands)			
AVHRR4	10.32	11.36				
TM6	10.42	11.66				
AVHRR5	11.45	12.42				
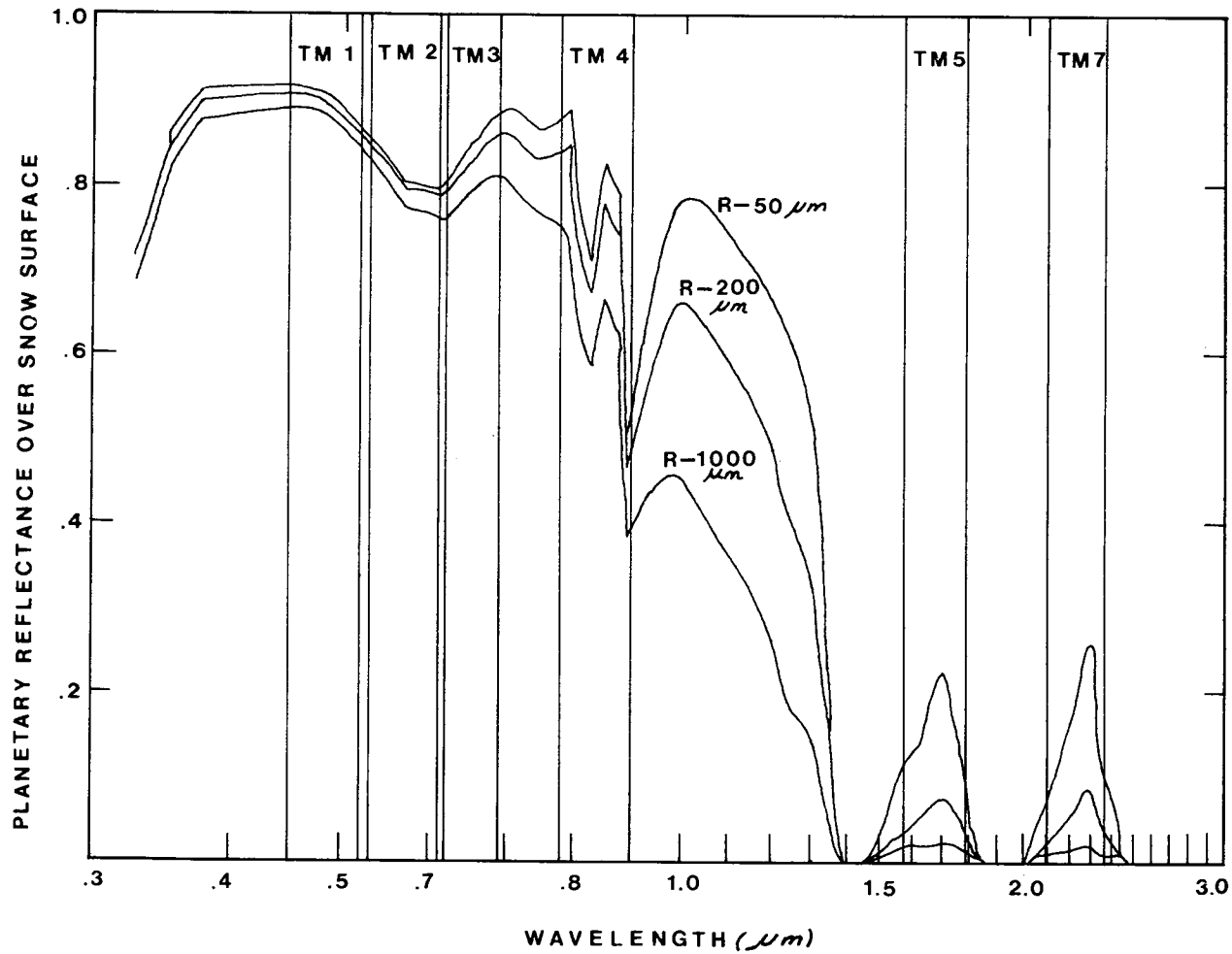
Figure 1. Planetary reflectance over a snow surface, at illumination angle 60°
and grain radii from 50 to 1000μm, for the reflective bands (1-5, 7) of the
Landsat-4 Thematic Mapper, through an Eltermann atmosphere with 23km surface
visibility.

PRELIMINARY EVALUATION OF TM FOR SOILS INFORMATION

DAVID R. THOMPSON, KEITH E. HENDERSON,
A. GLEN HOUSTON AND DAVID E. PITTS
NASA/LYNDON B. JOHNSON SPACE CENTER

Thematic mapper data acquired over Mississippi County, Arkansas, were examined for utility in separating soil associations within generally level alluvium deposited by the Mississippi River. The 0.76-0.90 μm (Band 4) and the 1.55-1.75 μm (Band 5) were found to separate the different soil associations fairly well when compared to the USDA-SCS general soil map. The thermal channel also appeared to provide information at this level. A detailed soil survey was available at the field level along with ground observations of crop type, plant height, percent cover and growth stage. Soils within the fields ranged from uniform to soils that occur as patches of sand that stand out strongly against the intermingled areas of dark soil. Examination of the digital values of individual TM bands at the field level indicates that the influence of the soil is greater in TM than it was in MSS bands. TM appears to provide greater deail of within field variability caused by soils than MSS and thus should provide improved information relating to crop and soil properties. However, this soil influence may cause crop identification classification procedures to have to account for the soil in their algorithms.

THE USE OF THEMATIC MAPPER DATA FOR LAND COVER DISCRIMINATION -- PRELIMINARY RESULTS FROM THE UK SATMaP PROGRAMME

M. J. JACKSON, J. R. BAKER
NATURAL ENVIRONMENT RESEARCH COUNCIL, UK

J. R. G. TOWNSHEND, J. E. GAYLER AND J. R. HARDY
READING UNIVERSITY, UK

The principal objectives of the UK SATMaP programme are to determine Thematic Mapper (TM) performance with particular reference to spatial resolution properties and geometric characteristics of the data. Since no data of the UK test sites have been received so far, analysis has been restricted to images from the U.S. and has concentrated on spectral and radiometric properties.

Examination of selected sub-scenes reveals that the visible bands display a narrow range of digital values. For example, for band 2 over 95% of the pixels are found within 25 out of 255 digital counts. The histograms are better balanced for bands 4, 5 and 6. For example for band 4 the 95% limit covers 120 digital counts. For classification purposes it is not considered that the eight-bit quantization available is being effectively utilized, even if one takes account of the limited data set analysed.

In assessing the accuracy of classification techniques for Thematic Mapper data the consistency of the detector-to-detector response is critical. Preliminary studies were undertaken, therefore, to assess the significance of this factor for the TM. The results obtained suggest the existance of striping especially in band 4 for the Detroit scene. This is related to differences in forward and backward scans of the sensor. The average difference is approximately two digital counts and is clearly present from the eastern edge of the Detroit scene to the lake shore near the centre of the image. Examination of Reelfoot Lake in the eastern portion of the Arkansas scene fails to reveal a similar response, nor is it apparent in any part of the Mississippi. Either a change in response of the sensor or a difference in the data processing is therefore indicated.

For all three sub-scenes analysed there are strong correlations between the three visible bands, the coefficients exceeding 0.9 in all cases. Of the other band combinations only bands 4 and 5, 5 and 6, and 6 and 7 show any strong relationships. Negative correlations are found consistently between band 4 in the near infrared and the visible bands though the strength of these relationships varies substantially between the sub-scenes.

The overall structure of the relationships can be examined by principal component analysis. For the first two sub-scenes there are apparently three basic dimensions of variability whereas for the third this is reduced to two dimensions, since band 5, 6 and 7 are missing.

In order to examine the utility of the Thematic Mapper data more carefully, six different land cover classes approximately Anderson level 1 were selected. These included an area of water from the sediment-laden Mississippi, woodland, agricultural land and urban land. A "plume" class was also selected which includes the plume of smoke emanating from the power station and drifting over the Mississippi river.

For the first three bands the overall form of the spectral response is remarkably similar for all classes, whereas for the near and middle infrared bands considerable differences in overall response are found. For the thermal infrared band, the means of the classes are very similar but is worth noting that the standard deviations are also very low suggesting this band may have some discriminatory power.

Considerable differences can be seen between the correlation structure of the different categories and that of the whole sub-scene. For example for water and woodland the correlations between the three visible bands are much weaker; the usual weak to moderate negative relationship between the visible bands and the near infrared band 4 is replaced by strong positive correlations for the industrial and plume categories. For the agricultural and urban land categories bands 5 and 6 have moderate to strong relationships with the other bands except for band 4, whereas the first two sub-scenes as a whole and the water and woodland classes of one sub-scene show much weaker relationships.

If the Eigenvectors of the first two principal components are examined, it is apparent that although the dimensionality of the data is similar for the whole sub-scene and several of the individual land cover categories, the principal components are orientated very differently within the seven dimensional feature space. In other words different bands contribute to very varying degrees to these first two components. Relatively speaking bands 2 and 3 contribute least to the first two principal components, and bands 4, 1 and 5 the most. The results strongly suggest that although there may be only three dimensions within the data, if we wish to depict the variability within as well as between broad cover categories then more than three bands will have to be used.

The classification potential of the Thematic Mapper has been examined by calculating the divergence between the classes.

It is notable that except for band 2 all the bands are indicated as having significant discriminatory potential for at least two of the classes. Overall the results indicate the particular significance of bands 3, 4 and 5 in discrimination between the classes. Additionally it is interesting that the thermal band, band 7, is of independent value in discrimination despite its low spatial resolution and a less than optimal time for sensing with this band.

Advanced classificatory algorithms are being explored to improve information extraction from TM data. Specifically the use of cartographic digital vector data and other remote sensing data in registered formats is being investigated to develop classification techniques which exploit per-pixel, textural and contextual algorithms within the framework of a probabalistic tree classifier and an integrated multi-level and multi-parameter data set.

The first TM image of the UK was received via X-band transmission to Fucino, Italy and was processed by ESRIN, Frascati. Qualitative analysis of the image clearly shows that in rural areas, there is a very significant improvement over the MSS, whereas in urban areas the improvement is much less marked, probably as a result of the high density of English urban development (Figure 1).
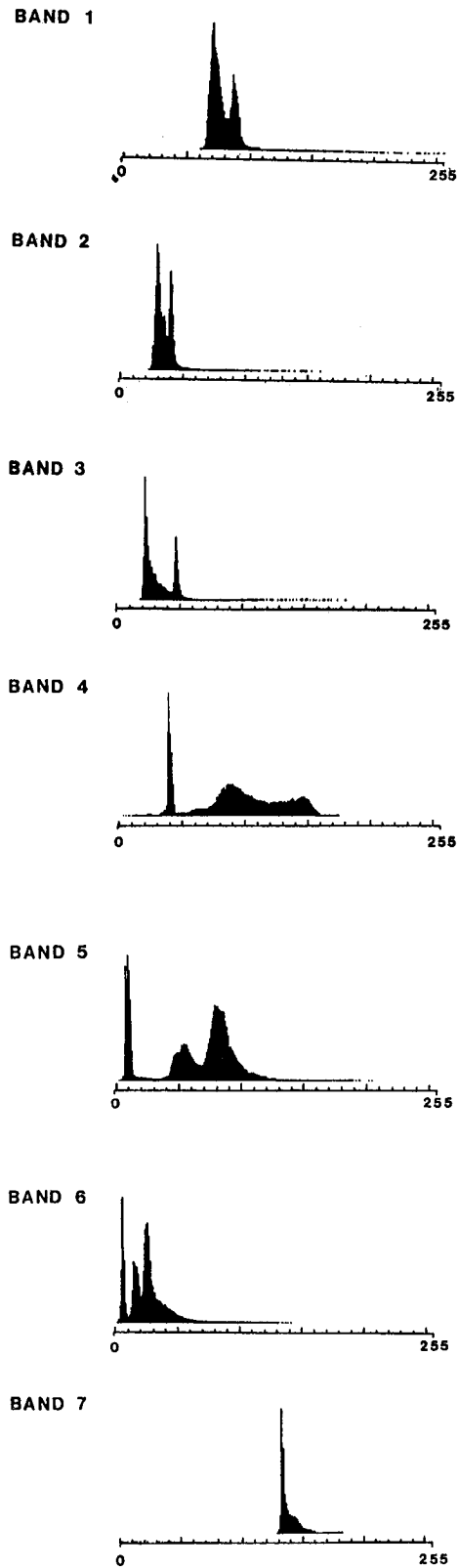
Figure 1. Histograms For Each Spectral Band For Sub-scene 1.
Note that band 7 is the thermal band.

152

LANDSAT-4 THEMATIC MAPPER SCENE CHARACTERISTICS FOR A SUBURBAN AND REGIONAL TEST SITE

DAVID L. TOLL
NASA/GODDARD SPACE FLIGHT CENTER

OBJECTIVES

The primary objective of this effort is to study the Landsat Thematic Mapper land use/land cover discrimination performance from a spatial resolution, spectral region and radiometric perspective. Selected methods to improve the land use/land cover performance are also evaluated.

STUDY SITE AND DATA DESCRIPTION

An area encompassing a wide variety of land use/land cover types was selected for analysis. The area includes the Beltsville and Laurel, Maryland region occurring within the Baltimore-Washington, D.C. corridor. The major land use/land cover types are water, forest, agriculture, excavated sites, major transportation routes, commercial and industrial sites, and residential neighborhoods. The study site was chosen to include a 500^2 TM pixel size $(28.5^2$ m), yielding a 14^2 km study site. Selected Landsat TM and MSS scenes were evaluated (Table 1). To assist all evaluations, color infrared photography at 1:40,000 scale flown on July 13, 1982 was used.

TABLE 1.
LANDSAT DATA COLLECTION SUMMARY

DATA	Date	Bands	Ground IFOV	Quantization	Tape Format
Landsat-4 TM	July 29, 1982	1-4	30 m	256	P
Landsat-4 TM	Nov. 2, 1982	1-7	30m (120 m for TM6)	256	P
Landsat-2 MSS	July 11, 1981	4-7	80 m	64	P
Landsat-4 MSS	Nov. 2, 1982	4-7	80 m	64	P

Classification of the Landsat-4 TM scene in comparison to MSS for the Nov. 2, 1982 date yielded an improvement in accuracy from 74.81 (range 70.8% - 78.4% at α = 0.05) to 83.2% (79.8% - 86.2%). In order to study the possible causes for the change in classification accuracy between TM and MSS, key sensor parameter differences between TM and MSS were evaluated. The July 29 and Nov. 2 TM data sets were processed to simulate the MSS parameters: 1) 80 m spatial resolution; 2) six bit quantization; and 3) three spectral bands[1]. An all possible configuration of the sensor parameters yielded eight data set combinations for each date. One of the eight combinations was the simulation of the MSS (6 bits, 80 m resolution, and 3 spectral bands). A comparison of the real three band MSS overall classification accuracy with the MSS simulation indicated a similar classification accuracy of 69.1% versus 70.2%. The nonsignificant (α= 0.05) difference in classification accuracy indicated the procedures implemented to simulate the MSS sensor parameters from TM were successful. Results of the three factor (i.e., 3 sensor parameters), 2 level (TM and MSS) sensor specification are given in Table 2. ANOVA results are given in Table 3. With the exception of the ANOVA results, a more detailed description may be found in Toll (1983). Williams, et al. (1983) reports on a sensor parameter investigation with a more extensive study area.

Results indicate for both the July 29 and Nov. 2 dates the improvements in TM accuracy over MSS were attributed to the TM spectral region additions of TM 1(0.45 - 0.52 μm), TM 5(1.55 - 1.75 μm) and TM 7(2.08 - 2.35 μm) and to a smaller degree the increased quantization to 256 bits. The spectral band additions and increased quantization compensated for the decrease in classification accuracy from the higher 30 m spatial resolution. At the higher spatial resolution the within class variance for the per pixel classification was large. The added class variation resulted in an increase in spectral class overlap. On the other side, one factor not assessed was the

---

[1] On TM there is no MSS band 6 (0.70 - 0.80 μm) equivalent. Hence only MSS bands 4(0.50 - 0.60 μm), 5(0.60 - 0.70 μm) and 7(0.80 - 1.10 μm) were simulated.

TABLE 2

OVERALL CLASSIFICATION ACCURACY (%) AND AVERAGE PAIRWISE TRANSFORMED
DIVERGENCE (T) OF TM SPECTRAL BANDS, QUANTIZATION LEVELS AND
SPATIAL RESOLUTION.

	Spectral Bands (#)							
	6*				3			
	Quantization Levels (bits)							
	8		6		8		6	
	Spatial Resolution (m)							
Measurement Criteria	30	80	30	80	30	80	30	80
Nov. 2, 1982	78.7%	85.1%	73.7%	77.9%	69.3%	74.7%	66.5%	69.1%
	1876 T	1952 T	1781 T	1882 T	1576 T	1729 T	1544 T	1648 T
July 29, 1982	81.7%	85.3%	81.1%	84.2%	74.5%	80.0%	74.8%	68.9%
	1876 T	1889 T	1730 T	1739 T	1761 T	1797 T	1730 T	1739 T

* 4 bands used with the July 29, 1982 data set.

TABLE 3

ANOVA RESULTS OF SENSOR PARAMETER MODEL

| | Nov. 2, 1982 | | July 29, 1982 | |
SOURCE	SUMS OF SQUARES	F-VALUE	SUMS OF SQUARES	F-VALUE
Spatial (A)	20.5	1024#	16.2	361#
Spectral (B)	70.8	3540#	37.8	841#
Quantization (C)	25.2	1260#	0.6	13
AB Interaction	0.7	36	0.2	4
AC Interaction	1.6	81	0.3	7
BC Interaction	1.4	72	0.1	2
Error	0.02		0.045	

significant at 0.05 confidence level

effect of boundary pixels. At the higher spatial resolution of TM, the number of class boundaries of mixed class pixels is lower in comparison to the total pixels. Mixed class pixels typically result in an increase in spectral class overlap.

WAVEBAND ANALYSIS

TM waveband performance for discriminating land use/land cover was studied for the Nov. 2, seven band data set. Overall classification accuracy results are given in Table 4 for the one band case and the ten best two band and three band combinations. Results from the one band study indicated the middle infrared bands, TM 5(1.55 - 1.75 μm) and TM 7(2.08 - 2.35 μm) provides the most spectral information to discriminate among the studied classes. The discrimination of the classes for the middle infrared bands may be attributed to the difference in moisture concentrations between cover. The visible bands TM 2(0.52 - 0.60 μm) and TM 3(0.63 - 0.69 μm) provided the next best spectral discrimination. The use of near infrared band, TM 4(0.76 - 0.90 μm) yielded a low classification accuracy, particularly for agriculture, commercial and industrial and residential classes. The coarse spatial resolution of 120 m contributed to a lower classification accuracy for the thermal band, TM 6(10.4 - 12.5 μm).

TABLE 4

OVERALL CLASSIFICATION ACCURACIES FOR NOV. 2, 1982 LANDSAT TM SCENE

ONE BAND ANALYSIS	TWO BAND COMBINATION (10 BEST)	THREE BAND COMBINATION (10 BEST)
TM 5 - 53.5%	TM 2 & 4 - 68.6%	TM 2, 4 & 6 - 72.9%
TM 7 - 52.6%	TM 3 & 4 - 67.2%	TM 1, 4 & 5 - 72.6%
TM 3 - 50.5%	TM 1 & 4 - 66.8%	TM 2, 4 & 5 - 72.4%
TM 2 - 46.7%	TM 1 & 5 - 66.0%	TM 3, 4 & 6 - 71.2%
TM 4 - 45.9%	TM 2 & 5 - 65.9%	TM 1, 4 & 6 - 71.0%
TM 1 - 42.0%	TM 3 & 5 - 65.5%	TM 1, 3 & 4 - 70.9%
TM 6 - 39.3%	TM 5 & 6 - 65.3%	TM 1, 2 & 4 - 70.7%
	TM 4 & 6 - 64.0%	TM 2, 3 & 4 - 70.3%
	TM 3 & 6 - 60.7%	TM 3, 5 & 6 - 70.1%
	TM 1 & 6 - 58.7%	TM 3, 4 & 5 - 69.7%

Analysis of two band and three band combinations indicated representation from the three spectral regions, visible, near infrared and middle infrared yielded the highest classification accuracies. TM 4(0.76 - 0.90μm) was usually associated with the highest ranking as a result of low intraband correlations. Hence, an addition of a band from another spectral region with TM 4 would maximize spectral information content for cover class discrimination. Conversely, the lowest classification accuracies were typically associated with band groupings from the same spectral region.

Table 5 shows the increase in classification accuracy with consecutively increasing the number of spectral bands. However, as the number of spectral bands increased the degree of improvement decreased. For example, after five bands were included the subsequent additions yielded a negligible increase of 0.06%. Hence, for many TM applications the inclusion of only five bands is all the number of bands that is necessary.

TABLE 5

OVERALL CLASSIFICATION ACCURACY AS A FUNCTION OF BAND NUMBER, N=525

NUMBER OF BANDS (TM#)	OVERALL CLASSIFICATION ACCURACY (%)	CHANGE(%)
1 (5)	53.5	--
2 (2 4)	68.6	15.1
3 (2 4 6)	72.9	4.3
4 (3 4 5 7)	75.0	2.1
5 (1 3 4 5 7)	78.1	3.1
6 (1 2 3 4 5 7)	78.7	0.6
7 (1 2 3 4 5 6 7)	79.2	0.5

SPECTRAL CLASS DISCRIMINATION IMPROVEMENT STUDY

Selected procedures were evaluated in order to assess the improvement in TM spectral separability between land use/land cover classes. For a base line data set the November 2, 1982 TM scene was used. Overall classification

accuracy results are summarized in Table 6. Each procedure yielded a significant (α= 0.05) increase in classification accuracy over the untransformed TM data set. Both smoothing and median filtering reduced the within class variation while maintaining the spectral distance between classes. The increase in accuracy was from 79.2% for the untransformed data to 89.1% for median filtering and 90.5% for smoothing. The capture of phenology variations by adding the July 29th TM scene improved the accuracy to 87.2%. To a lesser degree the principal component and canonical transformations increased classification accuracy to 83.2% and 83.4% respectively. Clustering of subclasses yielded an increase to 83.2%.

TABLE 6

OVERALL CLASSIFICATION ACCURACY RESULTS FOR LANDSAT TM CLASSIFICATION
IMPROVEMENT STUDY

Data (Nov. 2, 1982 - 7 band TM)	Overall Classification Accuracy (%), n=525	Range (a=0.05)
Untransformed	79.2	75.5 - 82.5
Median filtering (5 x 5 pixel window)	89.1	86.1 - 91.5
Smoothing (5 x 5 pixel window)	90.5	87.7 - 92.7
Two date classification (July 29, 1982, 4 band)	87.2	84.2 - 89.7
Principal Component Transformation	83.2	79.8 - 86.2
Canonical Transformation	83.4	80.0 - 86.3
Training Class Clustering	83.2	79.8 - 86.2

REFERENCES

1. Toll, D. L., 1983. Preliminary Study of Information Extraction of
    Landsat TM Data for a Suburban/Regional Test Site, Landsat-4
    Scientific Characterization Early Results Symposium, NASA/GSFC, Feb.
    22-24.

2. Williams, D. L., J. Irons, B. Markham, R. Nelson, D. Toll, R. Latty
    and M. Stauffer, 1983. Impact of Thematic Mapper Sensor
    Characteristics on Classification Accuracy, International Geoscience
    and Remote Sensing Symposium, San Francisco, CA, Aug. 31 - Sept. 2,
    IEEE Digest.

FINAL COMPARISON OF TM AND MSS DATA FOR SURFACE MINE ASSESSMENT
IN LOGAN COUNTY, WEST VIRGINIA

R. G. WITT, H. W. BLODGET
NASA/GODDARD SPACE FLIGHT CENTER

R. M. MARCELL
SCIENTIFIC APPLICATIONS RESEARCH

INTRODUCTION AND REVIEW

There are many applications areas for which the Landsat-4 Thematic Mapper (TM), with its upgraded spectral, spatial, and radiometric performance, was expected to provide improvements in feature detection and delineation relative to the Multispectral Scanner (MSS). In the past, the successful use of remotely sensed satellite data for mapping and monitoring surface mines has been generally dependent on the size, shape, and extent of mine features. The nature of Appalachia's coal strip mines, most of which follow narrow serpentine contours in mountainous terrain, previously has made them difficult to detect and delineate. Thus the objectives of the current research were two-fold: to compare the mapping accuracies of TM with MSS for surface mine assessment; and to compare a variety of digital data processing techniques, including principal components, canonical analysis, and band selection for this purpose. Signature extension was also attempted in the final stage of the project.

Earlier results for a small intensely mined area of Logan County indicate that such data reduction techniques offer results equal or superior to the processing of full data sets[1], a fact which is particularly important when working with a large volume of TM data. Also, the data transformation procedures were useful in removing systematic noise from the data sets. In the comparison of same-date TM and MSS data sets for Holden Quadrangle, the intensely mined portion of Logan County, the TM gave overall results that were approximately 9% better than the MSS equivalent classifications (85% vs. 75%).[2] Finally, an attempt was made to extend the unsupervised signatures

developed from Holden Quadrangle to all of Logan County[3], and compare county-wide TM and MSS classifications. Results of this work are presented herein.

PROCEDURES

The classification methods which produced the best results in terms of map accuracy for the intensely mined portion of Logan County were selected for extension to the entire county. These were as follows: four canonical axes, four principal components, and four selected raw bands (TM); three canonical axes and three principal components (MSS); and baseline raw seven-band (TM) and four-band (MSS) classifications. The county-wide data sets were subjected to the transformations, and then classified using the unsupervised signatures previously obtained from the Holden Quadrangle subset. A point-by-point accuracy assessment was conducted on each of the classifications for urban, mines, and agriculture/grass land cover categories. Estimates were made for the accuracy of the predominant category forest (>90% of area on all classifications) and water (<.5%) by visual comparison with the 12 October 1980 aerial photographs.

TABLE 1

MSS AND TM ACCURACIES FOR LOGAN COUNTY

(PERCENT CORRECT AND ACREAGE)

MSS/TM CLASSIFICATIONS (4 Sept. 1982 data sets)	LAND USE/LAND COVER CATEGORIES					
	Mines	Urban	Ag/Grass	Forest (est.)	Water (est.)	TOTAL
ALL 4	14.1 872	17.8 1707	6.7 1644	99.0	33.0	34.4%
PC 3	23.7 1238	22.2 2002	9.6 1090	99.0	33.0	38.6%
CAN 3	26.0 1800	32.6 1745	9.6 1717	99.0	33.0	41.8%

TABLE 1
MSS AND TM ACCURACIES FOR LOGAN COUNTY
(PERCENT CORRECT AND ACREAGE)
(CONTINUED)

MSS/TM CLASSIFICATIONS (4 Sept. 1982 data sets)	LAND USE/LAND COVER CATEGORIES					
	Mines	Urban	Ag/Grass	Forest (est.)	Water (est.)	TOTAL
ALL 7	37.6	41.9	53.9	95.0	75.0	57.1%
	1237	3048	14826			
PC 4	46.4	21.6	57.9	95.0	75.0	55.2%
	2406	1954	14936			
CAN 4	61.1	37.9	60.8	95.0	75.0	63.7%
	2273	2251	16476			
BNDS	40.3	38.9	37.9	95.0	75.0	53.0%
	1320	3172	9678			
MSS AVG.	21.3	24.2	8.6	99.0	33.0	38.3%
TM AVG.	46.4	35.1	52.6	95.0	75.0	57.3%
Factor of Improvement (TM over MSS)	1.2	.45	5.1			.5

The classification results for Logan County demonstrate great improvements in map accuracy for TM relative to the MSS in delineating small, irregular surface features such as narrow contour strip mines. There exists nearly 20% difference when the average overall accuracies of the TM classifications (57.3%) and the MSS classifications (38.3%) are compared. This average increase in classification accuracy (MSS vs. TM) is even greater when only the three land use categories covering small areas (<5%) of the county are considered. For mines, urban, and agriculture/grass, the average difference between the MSS results and TM results increases to nearly 27% (see Table on previous page).

The average improvement for the mines category was 25%, or a 1.2 factor of improvement for TM relative to MSS. Some problems associated with the low absolute accuracies for this category, both MSS and TM, are the spectral heterogeneity of the target features, their spatial irregularity and diverse sizes, and the temporal incongruence between the satellite data set used and the photography used as ground verification data. Two advantages offered by the TM for mapping surface mines were as follows: improved spectral separability of mines vs. urban areas due to additional bands; and, improved spatial discrimination of contour mine features as narrow as one (TM) pixel. Because of the dynmaic nature of surface mine expansion and revegetation, however, accuracies relative to air photos were substantially reduced below probable levels.

The average improvement for the urban category was 11% (TM relative to MSS), or a .45 factor of improvement. Here the problem with low absolute accuracies was one of definition. Most of the so-called "urban" areas in Logan County are towns characterized by low density residential land use, located along narrow floodplains of stream valleys. The typical low density of these housing units makes such development difficult to identify by means of the TM, and even harder to detect with the MSS. This problem may be partly related to the signature extension from Holden Quadrangle to the rest of the county. The agriculture/grass category had the greatest average difference in accuracy between the MSS and TM classifications of 44%. This translates into

a factor of improvement for TM relative to MSS of 5.1. Due to the narrow nature of stream valleys and the general lack of open land, it was difficult to select multi-pixel test sites for this category. Several of the sites chosen were actually revegetated surface mines, which classified as a mix of land covers.

In terms of overall classification performance, the TM four-axis canonical classification clearly gave the best result at 64%, followed by the TM seven-band classification (57%), TM four principal components image (55%), and TM band selected classification (53%). The TM canonical classification also had the highest accuracies for the mines and agriculture/grass categories. None of the MSS classifications had overall accuracies greater than 40%, and they do little more than delineate the general valley structure within Logan County.

CONCLUSIONS AND SUMMARY

A variety of classifications using both raw and transformed MSS and TM data sets from 4 September 1982 were performed for the Logan County, West Virginia study area. The object was to compare the utility of TM and MSS data for delineating small, irregular ground features, particularly surface mines, and also to test data reduction/transformation techniques (band selection, canonical analysis, and principal components) in relation to a traditional means of unsupervised classification.

Statistical results demonstrate that, on the average, the TM classifications yielded an overall .53 factor of improvement relative to the MSS classifications. When the accuracies for only three minor (in terms of areal extent) land use categories are examined, the factor of improvement for TM over MSS increases to 1.48; i.e., the TM is nearly one and one-half times better than the MSS for delineating small and irregular ground features such as contour strip mines.

While the absence of timely ground truth information kept accuracies below anticipated levels, the TM provided good site-specific information on surface mines in Logan County. It appears that the TM can be used not only to

locate and identify contour strip mines in various stages of expansion and revegetation, but that the extent and configuration of individual surface mines can be accurately mapped as well. This represents a major advance over the MSS that seems mostly attributable to the improved spatial resolution of the TM.

Comparing the data reduction/transformation techniques with the standard unsupervised classifications of raw MSS and TM data, the results show that canonical analysis in this case is a superior procedure for delineating spectrally heterogeneous land uses that cover a small area within a scene. Canonical analysis gave the best overall results for both the TM and MSS data sets, and also proved to be the most accurate technique for mapping surface mines. This is probably due to the elimination of noise in the transformed data sets, leading to increased separability of urban and mine areas, which are spectrally confused to a high degree in the raw MSS and TM data set classifications.

It is worth noting that all of the county-wide classifications were derived from unsupervised signatures and data transformations originally developed for the Holden Quadrangle area. Signature extension over large areas with remotely sensed satellite data has typically not worked well in the past, but the transformation matrices used herein produced adequate classification results when applied to the county-wide data sets. The use of a reduced number of bands (or axes, or components) represents a significant CPU time/cost savings when compared with the classification of the full MSS and (especially) TM data sets. Because of the higher accuracies achieved at lower cost, it is recommended that canonical analysis be considered as a standard procedure for processing TM and MSS data when the delineation of unique ground features like surface mines is necessary or important.

REFERENCES

1.   Brumfield, et al. 1983. Comparative techniques used to evaluate Thematic Mapper data for land cover classification in Logan County, West Virginia. Landsat-4 Scientific Characterization Early Results Symposium, NASA/Goddard Space Flight Center, Greenbelt, MD, February 22-24, 1983, Proceedings (to be published).

2.   Witt, et al. 1983. Relative accuracies of TM and MSS data for surface mine assessment in Logan County, West Virginia. National Conference on Resource Management Applications, San Francisco, CA, August 23-27, 1983, Proceedings (to be published).

3.   Blodget, et al. 1983. Preliminary technique assessment for Thematic Mapper data land cover classification in Logan County, West Virginia. American Society of Photogrammetry Fall Technical Meeting, Salt Lake City, Utah, September 19-23, 1983, Proceedings: pp. 607-615.

COMPARISON OF LAND COVER INFORMATION FROM LANDSAT MULTISPECTRAL SCANNER (MSS) AND AIRBORNE THEMATIC MAPPER SIMULATOR (TMS) DATA FOR HYDROLOGIC APPLICATIONS

J.C. GERVIN

NASA/GODDARD SPACE FLIGHT CENTER

Y.C. LU AND R.F. MARCELL

COMPUTER SCIENCES CORPORATION

In a cooperative program with the US Army Corps of Engineers (Corps), NASA is evaluating the capabilities of Landsat-4 Thematic Mapper (TM) data for environmental and hydrologic applications. Both NASA and the Corps are interested in assessing the relative effectiveness of TM, MSS and conventional data for land cover classification, particularly in urban/suburban areas, and for developing parameters for input to hydrologic (flood forecasting) and economic (flood damage) models. In addition, it would be particularly desirable to establish a set of optimal TM band combinations for land cover classification and related data analysis which could reduce processing time and cost while preserving accuracy and reliability.

Several sites already under study by the Corps were selected for this program. This paper will report results for one of these sites, the Clinton River Basin in Michigan. Moreover, the data examined here were gathered by the TMS, an airborne sensor designed to simulate TM spatial and spectral resolution prior to launch.

APPROACH

Detailed land cover classifications were performed on TMS and MSS data of the Clinton River Basin (acquired on August 19, 1981, and June 28, 1980, respectively) using supervised classification techniques. Differences in interclass separability were compared to select several promising TMS band combinations, selected from the 27 covering the Clinton River Basin.

Supervised classifications for those band combinations were completed for three 7.5 minute (1:24,000 scale) US Geological Survey (USGS) topographic maps, Mt. Clemens West, Utica and Waldenburg, including Bands 2, 3 and 4 (MSS-comparable); 3, 4 and 7; 3, 4, 5 and 7; and all bands (where Band 7 is thermal).

The three USGS maps used in the accuracy assessment included the primarily residential Mt. Clemens West map, the agricultural Waldenburg map and the Utica map, which represents a variety of land cover types. The watershed contains many small heterogeneous land cover areas, including industrial plants, commercial buildings along major roadways, small ponds, isolated residential developments, golf courses, narrow woodlands along streams and small agricultural fields.

Conventional land cover maps at a scale of 1:24,000 were prepared by the Southeast Michigan Council of Governments (SEMCOG) using 1978 aerial photography for Mt. Clemens West, Utica and Waldenburg for use in verification and accuracy assessment of the TMS and MSS classifications. A pixel-by-pixel comparison was performed between the digitized ground truth maps and each corresponding Landsat MSS and TMS classification map.

RESULTS AND DISCUSSION

The resulting accuracy comparisons, in terms of percent of pixels correctly identified in each land cover category on the ground verification data, are summarized by land cover category and MSS and TMS band combination for all three maps in Table 1. The bottom row indicates the percent occupied by each of the land cover types examined, based on the ground verification data.

The overall accuracies for the land cover classifications of the Clinton River Basin are somewhat lower than those often reported in the literature. This can be attributed to the heterogeneity of this largely suburban area, the rigorous accuracy assessment applied, inconsistencies in the ground verification data, due in part to the passage of time between the photointerpretation and TMS data acquisition, and the separation of developed into commercial/industrial and residential.

TABLE 1

CLASSIFICATION ACCURACY SUMMARY FOR MT. CLEMENS WEST, UTICA, AND WALDENBURG

PERCENT CORRECT

Sensor	Water	Agriculture and Grass	Woodland	Commercial/ Industrial	Residential	Total
MSS	19	43	50	41	59	48
TMS						
(2, 3, 4)	42	58	38	49	72	57
(3, 4, 7)	42	55	42	49	69	56
(3, 4, 5, 7)	45	64	41	50	80	63
All Bands	44	61	43	51	83	63
Percent Cover	1	45	18	8	28	

Although these accuracy figures could probably be improved through revised ground verification data or the use of multitemporal data, contextual classification, or other more advanced digital techniques, this might obscure the results of greatest interest: a comparison of the per point accuracy of land cover classification results between MSS and TMS and between various TMS band combinations.

For all three maps, the spectral band combination comparable to the MSS (Bands 2, 3 and 4) produced an overall accuracy of 57 percent, an increase of 9 percent over the MSS. The optimum 3-band combination selected by the transformed divergence technique provided similar results. This is largely attributable to the substantially (approximately 20 percent) higher accuracies for residential, water and agriculture/grass.

The selected 4-band combination provided nearly as good a discrimination of land cover as all seven TMS bands. The 4- and 7-band classifications did show considerable improvement in accuracy over the 3-band combinations (63 percent versus 57 and 56 percent), particularly in residential (80 and 83 percent versus 72 and 69 percent) and agriculture/grass (64 and 61 percent versus 58 and 55 percent).

CONCLUSIONS

TMS data produced a more accurate and spatially contiguous classification than MSS for this study site. While the accuracy of the 4-band TMS data set was as good as the 7-band, the 3-band TMS data sets were also better than the MSS. These results indicate that both the increased spectral discrimination and spatial resolution contribute to improved classification accuracy. The possibility of reducing the data analysis burden associated with large TM data volumes through effective band selection therefore appears promising.

The combination of bands selected based on the transformed divergence technique provided one band in each of the major regions of the spectrum: visible (Band 3), near IR (Band 4), middle IR (Band 5) and thermal IR (Band 7). This selection agrees reasonably well with results obtained by other investigators.

These results should be viewed with some caution, however. The data are from a TMS rather than the actual TM. Moreover, the MSS data were obtained in early summer while the TMS was flown in late summer; therefore, some of the differences noted could be due to seasonal, atmospheric and sun angle effects rather than sensor differences.

The implications of the improved classification accuracy of TMS data are important for Corps hydrologic and economic modeling. In particular, the higher accuracies for the developed categories (residential and commercial) should improve the predictions of runoff in flood forecasting models and of flood damage for damage calculation models appreciably. Moreover, the promising results with band selection will permit users of the data to benefit from the improved classification capability without having to deal with the entire data volume.

RELATIVE ACCURACY ASSESSMENT OF LANDSAT-4 MSS AND TM DATA
FOR LEVEL I LAND COVER INVENTORY

E. M. MIDDLETON, R. G. WITT
NASA/GODDARD SPACE FLIGHT CENTER

Y.C. LU and R. S. SEKHON
COMPUTER SCIENCES CORPORATION

A study was undertaken to compare digital data for the Washington, DC scene from the Landsat-4 Multispectral Scanner (MSS) and the Landsat-4 Thematic Mapper (TM), simultaneously acquired on November 2, 1982 (Scene IDs: 40109-15140). Classification success for the TM and MSS data sets was determined by a per pixel comparison with digitized ground verification data (GVD). These GVD were comprised of Level I land cover (developed, agriculture, forest, water, wetlands, and barren) for four USGS 7.5-minute topographic quadrangle maps. The GVD were spatially resampled to 60m for comparison with the 60m resampled MSS pixels and 30m for comparison with the 30m resampled TM pixels. The acreages per cell from the contingency tables from the quads were combined producing one data set each for TM/GVD and MSS/GVD. This corresponds to a total of 655,890 TM pixels, 163,434 MSS pixels and 72,755 hectares.

Classification accuracy was computed as an average value and for each cover type. Accuracy was expressed two ways: 1) as the percent correspondence with GVD (% "correct") and 2) as the percent correspondence relative to both the GVD and Landsat classification schemes. Errors of omission and commission associated with the Landsat classifications were also computed. Approach (1) considers errors of omission only whereas approach (2) considers errors of omission and commission.

The comparative classification success for the TM and MSS was 79.2 versus 68.2 percent overall using approach (1) and 65.7 versus 51.8 percent using the more rigorous approach (2). This represents an overall accuracy improvement for TM between 11 and 14%, or a factor of about 1.3, for these data. This overall improvement also was seen in the individual cover

categories where TM out-performed MSS in all cover categories in terms of correspondence to the GVD, and performed as well or better in terms of errors of omission and commission. The greatest overall gain in accuracy (+20%) was observed for the developed category (computed using approach 2) and was due largely to a 34% or factor of 3.5 reduction in the error of commission. A notable gain in correspondence to GVD also was seen for agriculture (+16.4%) and forest (+7.5%), both due to reductions in the errors of omission. In summary, a substantial improvement in accuracy for Level I land cover categorization, equal to 13.8%, was shown for TM relative to MSS when both errors of omission and commission were considered.

TM VS. MSS: COMPARATIVE CLASSIFICATION SUCCESS

	Classification Accuracy (Correspondence to GVD)				Classification Error (Noncorrespondence to GVD)			
	Accuracy (Approach 1)		Accuracy (Approach 2)		Omission		Commission	
Land Cover Type	%Diff. TM-MSS	Ratio $\frac{TM}{MSS}$	%Diff. TM-MSS	Ratio $\frac{TM}{MSS}$	%Diff. TM-MSS	Ratio $\frac{MSS}{TM}$	%Diff. TM-MSS	Ratio $\frac{MSS}{TM}$
D	+4.92	1.08	+20.08	1.52	-4.92	1.14	-33.74	3.43
A/G	+16.37	1.25	+16.13	1.28	-16.37	1.85	-5.59	1.47
F	+7.55	1.09	+3.33	1.06	-7.55	1.61	+0.82	0.97
W	+3.20	1.04	+0.92	1.01	-3.20	1.20	+2.86	0.75
Wt	+2.70	1.05	+1.09	1.61	-2.70	1.06	-1.14	1.01
B	0	0	0	0	0	0	0	0
Over All Types	+11.03	1.16	+13.84	1.27	RATIO (MSS/TM) Total Error = $\frac{31.77}{20.74}$ = 1.53			

KEY   D = Developed; A/G = Agriculture/Grasslands; F = Forests; W = Water; Wt = Wetlands; B = Extractive/Barren

LIST OF AFFILIATIONS

1. ATMOSPHERIC SCIENCES LABORATORY
   White Sands Missile Range
   New Mexico 88002

2. CANADA CENTRE FOR REMOTE SENSING
   2464 Sheffield Road
   Ottawa, Ontario, Canada K1A 0Y7

3. CENTRE d'ETUDES ET DE RECHERCHES
      DE TOULOUSE
   2, Avenue Edouard Belin
   31055 Toulouse, France

4. COMMISSION OF THE EUROPEAN
      COMMUNITIES
   Joint Research Centre
   Ispra, Italy

5. COMPUTER SCIENCE CORPORATION
   8728 Colesville Road
   Silver Spring, Maryland 20910

6. DEPARTMENT ETUDES THEMATIQUES
   CNES/OT/T1
   18, Avenue Edouard Belin
   31055 Toulouse, France

7. EARTH SATELLITE CORPORATION
   (EarthSat)
   7222 47th Street
   Chevy Chase, Maryland 20815

8. ENVIRONMENTAL RESEARCH INSTITUTE
      OF MICHIGAN
   P.O. Box 8618
   Ann Arbor, Michigan 48107

9. EUROPEAN SPACE AGENCY
   Earthnet Programme Office
   Via Galilio Galilei
   ESRIN - Frascati 00044 Italy

10. GENERAL ELECTRIC COMPANY
    P.O. Box 8555
    Valley Forge, Pennsylvania 19101

11. GENERAL ELECTRIC SPACE DIVISION
    Lanham Center Operations
    4701 Forbes Boulevard
    Lanham, Maryland 20706

12. IBM CORPORATION
    Palo Alto Scientific Center
    1530 Page Mill Road
    Palo Alto, California 94304

13. JET PROPULSION LABORATORY
    California Institute of Technology
    4800 Oak Grove Drive
    Pasadena, California 91109

14. LABORATOIRE DE METEOROLOGIE DYNAMIQUE
    Atmospheric Science Foundation
       de France
    Ecole Normale Superieure
    24 Rue Lhomond
    75231 Paris, France

15. LOCKHEED ENGINEERING AND MANAGEMENT
       SERVICES COMPANY, INC.
    1830 NASA Road 1
    Houston, Texas 77058

16. NASA/AMES RESEARCH CENTER
    Moffett Field, California 94035

17. NASA/GODDARD SPACE FLIGHT CENTER
    Greenbelt Road
    Greenbelt, Maryland 20770

18. NASA/LYNDON B. JOHNSON SPACE CENTER
    Houston, Texas 77058

19. NASA/NATIONAL SPACE TECHNOLOGY
       LABORATORIES
    NSTL Station, Mississippi 39529

20. NATURAL ENVIRONMENT RESEARCH COUNCIL
    NERC Scientific Services
    Holbrook House, Station Road
    Swindon, Wilts, SN1 1DE
    United Kingdom

21. NOAA/NATIONAL ENVIRONMENTAL SATELLITE,
       DATA, AND INFORMATION SERVICE
    Federal Office Building 4
    Washington, DC 20233

22. PURDUE UNIVERSITY
    Laboratory for Applications of
      Remote Sensing
    12201 Potter Drive
    West Lafayette, Indiana 47906-1399

23. READING UNIVERSITY
    Department of Geography
    Reading, RG6 2AU
    United Kingdom

24. RESEARCH & DATA SYSTEMS, INC.
    10300 Greenbelt Road
    Lanham, Maryland 20706

25. ROCHESTER INSTITUTE OF TECHNOLOGY
    School of Photographic Arts and
      Sciences
    One Lomb Memorial Drive
    Rochester, New York 14623

26. SANTA BARBARA RESEARCH CENTER
    75 Coromar Drive
    Goleta, California 93117

27. SCIENTIFIC APPLICATIONS RESEARCH
    Riverdale, Maryland 20737

28. STATE UNIVERSITY OF NEW YORK
    College of Environmental Science &
      Forestry
    308 Bray Hall
    Syracuse, New York 13210

29. SYSTEMS AND APPLIED SCIENCES
      CORPORATION
    5809 Annapolis Road
    Hyattsville, Maryland 20784

30. TECHNICOLOR GOVERNMENT SERVICES, INC.
    Ames Research Center
    Moffett Field, California 94035

31. TECHNICOLOR GOVERNMENT SERVICES, INC.
    EROS Data Center
    Sioux Falls, South Dakota 57198

32. USDA/HYDROLOGY LABORATORY
    Beltsville Agricultural Research
      Center, West
    Beltsville, Maryland 20705

33. U.S. GEOLOGICAL SURVEY
    2255 No. Gemini Drive
    Flagstaff, Arizona 86001

34. U.S. GEOLOGICAL SURVEY
    EROS Data Center
    Sioux Falls, South Dakota 57198

35. U.S. GEOLOGICAL SURVEY
    12201 Sunrise Valley Drive
    Reston, Virginia 22092

36. UNIVERSITY OF ARIZONA
    Arizona Remote Sensing Center
    Tucson, Arizona 85721

37. UNIVERSITY OF CALIFORNIA/BERKELEY
    Remote Sensing Research Program
    Berkeley, California 94720

38. UNIVERSITY OF CALIFORNIA/SANTA BARBARA
    Santa Barbara, California 93016

39. UNIVERSITY OF DELAWARE
    College of Marine Studies
    Newark, Delaware 19716

40. UNIVERSITY OF GEORGIA
    Department of Geography
    Athens, Georgia 30602

41. UNIVERSITY OF MARYLAND
    Department of Civil Engineering
    College Park, Maryland 20742

42. UNIVERSITY OF MUNICH
    Faculty for Geosciences
    Luisenstr. 37 D-8000 Munchen
    West Germany

43. VIRGINIA POLYTECHNIC INSTITUTE
    Blacksburg, Virginia 24061

1. Report No. NASA CP-2326	2. Government Accession No.	3. Recipient's Catalog No.
4. Title and Subtitle LANDSAT-4 SCIENCE INVESTIGATIONS SUMMARY Including December 1983 Workshop Results VOLUME II		5. Report Date July 1984
		6. Performing Organization Code 923
7. Author(s) John Barker, Editor		8. Performing Organization Report No.
		10. Work Unit No.
9. Performing Organization Name and Address NASA Goddard Space Flight Center Greenbelt, Maryland 20771		
		11. Contract or Grant No. NAS5-28033
		13. Type of Report and Period Covered Conference Publication
12. Sponsoring Agency Name and Address National Aeronautics and Space Administration Washington, D.C. 20546		
		14. Sponsoring Agency Code

15. Supplementary Notes

16. Abstract

This document presents a series of brief summaries of the results of individual investigations of Landsat-4 image data characteristics. The results were reported at the Landsat-4 Early Results Symposium, February 1983, and at the Landsat Science Characterization Workshop held in December 1983.

17. Key Words (Suggested by Author(s)) Landsat-4, imagery, results, radiometry, geometry, remote sensing, Multispectral Scanner, Thematic Mapper, applications	18. Distribution Statement Unclassified-Unlimited STAR Category 42

19. Security Classif. (of this report) Unclassified	20. Security Classif. (of this page) Unclassified	21. No. of Pages 185	22. Price A09

National Aeronautics and
Space Administration

Washington, D.C.
20546

SPECIAL FOURTH CLASS MAIL
BOOK

U.S.MAIL

NASA

POSTMASTER: If Undeliverable (Section 158
Postal Manual) Do Not Return